Magnetorheological properties of the suspensions based on modified magnetic filler

Bc. Martin Cvek

Master thesis
2014

Tomas Bata University in Zlín
Faculty of Technology

Univerzita Tomáše Bati ve Zlíně
Fakulta technologická
Ústav fyziky a mater. inženýrství
akademický rok: 2013/2014

ZADÁNÍ DIPLOMOVÉ PRÁCE

(PROJEKTU, UMĚLECKÉHO DÍLA, UMĚLECKÉHO VÝKONU)

Jméno a příjmení:	**Bc. Martin Cvek**
Osobní číslo:	**T12378**
Studijní program:	**N2808 Chemie a technologie materiálů**
Studijní obor:	**Materiálové inženýrství**
Forma studia:	**prezenční**
Téma práce:	**Magnetoreologické vlastnosti suspenzí na bázi modifikovaného magnetického plniva**

Zásady pro vypracování:

Diplomová práce se v literární rešerši bude zabývat problematikou magnetoreologie obecně a magnetickými plnivy a jejich možnou modifikací různými typy materiálů pro jejich efektivní využití. Dále pak bude zahrnovat principy měření magnetických, reologických vlastností a možností hodnotit stabilitu částic a také jejich suspenzí. V experimentální části bude student kovalentně modifikovat povrch magnetických částic polymerem. Poté zhodnotí vliv modifikace na magnetické vlastnosti a také chemickou odolnost v kyselém prostředí. Z těchto částic připraví suspenze, na kterých bude sledovat reologické vlastnosti pod vlivem různě intenzivního magnetického pole. Nakonec bude hodnotit vliv modifikace na sedimentační stabilitu připravených suspenzí.

Rozsah diplomové práce:

Rozsah příloh:

Forma zpracování diplomové práce: **tištěná**

Seznam odborné literatury:

1. **De Vicente J, Klingenberg DJ, Hidalgo-Alvarez R, Magnetorheological Fluids: a review, Soft Matter, 7, 2011, 3701.**
2. **Hu B, Fuchs A, Huseyin S, Grodaninejad F, Evrensel C, Atom transfer radical polymerized MR fluids, Polymer, 47, 2006, 7653.**
3. **Park BJ, Fang FF, Choi HJ, Magnetorheology: materials and application, Soft Matter, 6, 2010, 5246.**

Vedoucí diplomové práce: **Ing. Miroslav Mrlík**
Centrum polymerních materiálů

Datum zadání diplomové práce: **7. února 2014**

Termín odevzdání diplomové práce: **30. května 2014**

Ve Zlíně dne 7. února 2014

doc. Ing. Roman Čermák, Ph.D.
děkan

L.S.

UNIVERZITA TOMÁŠE BATI VE ZLÍNĚ
Fakulta technologická

doc. Mgr. Aleš Mráček, Ph.D.
ředitel ústavu

Příjmení a jméno: Cvek Martin Obor: Materiálové inženýrství

P R O H L Á Š E N Í

Prohlašuji, že

- beru na vědomí, že odevzdáním diplomové/bakalářské práce souhlasím se zveřejněním své práce podle zákona č. 111/1998 Sb. o vysokých školách a o změně a doplnění dalších zákonů (zákon o vysokých školách), ve znění pozdějších právních předpisů, bez ohledu na výsledek obhajoby [1)];
- beru na vědomí, že diplomová/bakalářská práce bude uložena v elektronické podobě v univerzitním informačním systému dostupná k nahlédnutí, že jeden výtisk diplomové/bakalářské práce bude uložen na příslušném ústavu Fakulty technologické UTB ve Zlíně a jeden výtisk bude uložen u vedoucího práce;
- byl/a jsem seznámen/a s tím, že na moji diplomovou/bakalářskou práci se plně vztahuje zákon č. 121/2000 Sb. o právu autorském, o právech souvisejících s právem autorským a o změně některých zákonů (autorský zákon) ve znění pozdějších právních předpisů, zejm. § 35 odst. 3 [2)];
- beru na vědomí, že podle § 60 [3)] odst. 1 autorského zákona má UTB ve Zlíně právo na uzavření licenční smlouvy o užití školního díla v rozsahu § 12 odst. 4 autorského zákona;
- beru na vědomí, že podle § 60 [3)] odst. 2 a 3 mohu užít své dílo – diplomovou/bakalářskou práci nebo poskytnout licenci k jejímu využití jen s předchozím písemným souhlasem Univerzity Tomáše Bati ve Zlíně, která je oprávněna v takovém případě ode mne požadovat přiměřený příspěvek na úhradu nákladů, které byly Univerzitou Tomáše Bati ve Zlíně na vytvoření díla vynaloženy (až do jejich skutečné výše);
- beru na vědomí, že pokud bylo k vypracování diplomové/bakalářské práce využito softwaru poskytnutého Univerzitou Tomáše Bati ve Zlíně nebo jinými subjekty pouze ke studijním a výzkumným účelům (tedy pouze k nekomerčnímu využití), nelze výsledky diplomové/bakalářské práce využít ke komerčním účelům;
- beru na vědomí, že pokud je výstupem diplomové/bakalářské práce jakýkoliv softwarový produkt, považují se za součást práce rovněž i zdrojové kódy, popř. soubory, ze kterých se projekt skládá. Neodevzdání této součásti může být důvodem k neobhájení práce.

Ve Zlíně .....

.....

[1] *zákon č. 111/1998 Sb. o vysokých školách a o změně a doplnění dalších zákonů (zákon o vysokých školách), ve znění pozdějších právních předpisů, § 47 Zveřejňování závěrečných prací:*

(1) Vysoká škola nevýdělečně zveřejňuje disertační, diplomové, bakalářské a rigorózní práce, u kterých proběhla obhajoba, včetně posudků oponentů a výsledku obhajoby prostřednictvím databáze kvalifikačních prací, kterou spravuje. Způsob zveřejnění stanoví vnitřní předpis vysoké školy.

(2) Disertační, diplomové, bakalářské a rigorózní práce odevzdané uchazečem k obhajobě musí být též nejméně pět pracovních dnů před konáním obhajoby zveřejněny k nahlížení veřejnosti v místě určeném vnitřním předpisem vysoké školy nebo není-li tak určeno, v místě pracoviště vysoké školy, kde se má konat obhajoba práce. Každý si může ze zveřejněné práce pořizovat na své náklady výpisy, opisy nebo rozmnoženiny.

(3) Platí, že odevzdáním práce autor souhlasí se zveřejněním své práce podle tohoto zákona, bez ohledu na výsledek obhajoby.

[2] *zákon č. 121/2000 Sb. o právu autorském, o právech souvisejících s právem autorským a o změně některých zákonů (autorský zákon) ve znění pozdějších právních předpisů, § 35 odst. 3:*

(3) Do práva autorského také nezasahuje škola nebo školské či vzdělávací zařízení, užije-li nikoli za účelem přímého nebo nepřímého hospodářského nebo obchodního prospěchu k výuce nebo k vlastní potřebě dílo vytvořené žákem nebo studentem ke splnění školních nebo studijních povinností vyplývajících z jeho právního vztahu ke škole nebo školskému či vzdělávacího zařízení (školní dílo).

[3] *zákon č. 121/2000 Sb. o právu autorském, o právech souvisejících s právem autorským a o změně některých zákonů (autorský zákon) ve znění pozdějších právních předpisů, § 60 Školní dílo:*

(1) Škola nebo školské či vzdělávací zařízení mají za obvyklých podmínek právo na uzavření licenční smlouvy o užití školního díla (§ 35 odst. 3). Odpírá-li autor takového díla udělit svolení bez vážného důvodu, mohou se tyto osoby domáhat nahrazení chybějícího projevu jeho vůle u soudu. Ustanovení § 35 odst. 3 zůstává nedotčeno.

(2) Není-li sjednáno jinak, může autor školního díla své dílo užít či poskytnout jinému licenci, není-li to v rozporu s oprávněnými zájmy školy nebo školského či vzdělávacího zařízení.

(3) Škola nebo školské či vzdělávací zařízení jsou oprávněny požadovat, aby jim autor školního díla z výdělku jím dosaženého v souvislosti s užitím díla či poskytnutím licence podle odstavce 2 přiměřeně přispěl na úhradu nákladů, které na vytvoření díla vynaložily, a to podle okolností až do jejich skutečné výše; přitom se přihlédne k výši výdělku dosaženého školou nebo školským či vzdělávacím zařízením z užití školního díla podle odstavce 1.

ABSTRAKT

Tato diplomová práce se zabývá přípravou kompozitních částic typu jádro-slupka za účelem zvýšení stability magnetoreologických (MR) suspenzí. Jádro těchto kompozitních struktur bylo tvořeno karbonylovým železem (CI), na které byly naroubovány polymerní řetězce poly(glycidyl methakrylátu) (PGMA) pomocí radikálové polymerace s přenosem atomu (ATRP) polymerace. ATRP technika byla použita s cílem získat polymerní řetězce s kontrolovanou strukturou, řízenou molekulovou hmotností a úzkou polydisperzitou a tím upravit MR vlastnosti CI/PGMA částic. Na povrch čistých částic CI byly nejdříve zavedeny funkční skupiny pomocí funkčního organosilanu, poté následovala amidační reakce s ATRP iniciátorem a roubování PGMA polymerních větví. Úspěšná modifikace částic polymerem byla ověřena pomocí spektrálních metod, poté byl měřen vliv PGMA polymerní vrstvy na magnetické vlastnosti, chemickou a termo-oxidační stabilitu částic. Polymerem modifikované částice byly dispergovány v silikonovém oleji a u připravených suspenzí byla provedena magnetoreologická měření v ustáleném smykovém toku a v oscilačním režimu, na závěr byla sledována jejich sedimentační stabilita.

Klíčová slova: magnetoreologie, karbonylové železo, poly(glycidyl methakrylát), silikonový olej, magnetoreologická suspenze, stabilita suspenzí, kontrolovaná radikálová polymerace (ATRP)

ABSTRACT

This master thesis deals with the preparation of composite core-shell particles in order to enhance stability of magnetorheological (MR) suspensions. The core of these composite structures was formed with carbonyl iron (CI) and poly(glycidyl methacrylate) (PGMA) polymer chains were grafted *via* atom transfer radical polymerization (ATRP) as a shell. ATRP technique was employed in order to obtain polymer chains with controllable structure, molecular weight and narrow polydispersity index (PDI) and thus be able to adjust the MR properties of CI/PGMA particles. Surface of the CI particles was firstly functionalized with silane agent followed by amidation reaction with ATRP initiator and by grafting of PGMA polymer chains. Successful modification of the particles with the polymer was verified with the use of spectral methods, then the influence of PGMA polymer layer on magnetic properties, chemical and thermo-oxidative stability of the particles was measured. Particles modified with polymer were dispersed in silicone oil and the sedimentation stability and magnetorheological measurements in both steady shear flow and oscillatory shear mode were performed.

Keywords: magnetorheology, carbonyl iron, poly(glycidyl methacrylate), silicone oil, magnetorheological suspension, stability of suspensions, atom transfer radical polymerization (ATRP)

ACKNOWLEDGEMENTS

First of all, I wish to thank my supervisor Miroslav Mrlík, Ph.D. He was an excellent support and gave me a lot of vocational advice and constant help during this research.

I am grateful to Assoc. Prof. Dr. Vladimír Pavlínek for the possibility of collaboration with his research team at Centre of Polymer Systems in Zlín.

Further, I would like to thank Michal Sedlačík, Ph.D. for consultations, literary sources and constructive suggestion of innovative sedimentation measurement method.

Another thanks are directed to M.Sc. Tomáš Plachý for his time when he helped me with rheology measurements and spectral analysis.

I also thank to scientific researchers of Centre of Polymer Systems, namely Michal Machovský, Ph.D., M.Sc. Pavel Bažant and Vladimír Babayan, Ph.D. for their help during measurements.

Further, I would like to thank Centre of Polymer Systems in Zlín and Slovak Academy of Sciences for the possibility of using measuring devices.

I also wish to thank the Internal Grant Agency of the Czech Republic (project no. IGA/FT/2014/017) for financial support.

My final thank is directed to my family for supporting me during my studies.

I hereby declare that the print version of my Master's thesis and the electronic version of my thesis deposited in the IS/STAG system are identical.

CONTENTS

INTRODUCTION

Magnetorheological (MR) suspensions are technically and commercially interesting intelligent systems which play an important role in technology and material sciences. MR suspensions are composed of soft magnetic particles with micron-size diameter dispersed in a non-magnetic carrier liquid. The main feature of these smart systems is the MR effect, which is the ability to rapidly change the viscosity (in order of ms) in the presence of external magnetic field [1, 2]. This behavior is caused due to the arrangement of dispersed particles to column-like structures in a flow domain. The MR effect is almost completely reversible when the external magnetic field is removed [3].

MR suspensions offer solutions to many technical problems. Various research papers dealing with these smart materials have been published which allowed a wider commercial utilization of these systems. Successful implementation of the MR suspensions into practice is obvious, especially in the automotive or building industry but also in biomedical engineering.

However, there are some challenges in fine-tuning of the overall MR performance. The MR suspensions, should exhibit well balanced properties such as thermo-oxidation, chemical and sedimentation stability, while the magnetic properties should sustain on the appropriate level. The mentioned properties of MR systems can be enhanced with the use of additives, but currently the development is moving to preparation of composite core-shell structures for this reason. The shell of the particles is usually polymeric. Various polymers have been used for the preparation of the new types of core-shell composite particles, which allowed modifying the properties of MR suspensions [4 – 9]. However, the presence of polymer shell on the particles can enhance sedimentation stability due to reduced density and better compatibility with carrier liquid or chemical stability, but the saturation magnetization which is responsible for MR effect inevitably reduces, which is undesirable.

In most studies the polymer coating was synthesized with the use of dispersion polymerization [4, 5]. This technique is not fully controllable, so the polymer coating does not have defined properties, such as molecular weight of the polymer, constitution, thickness of the polymer layer and others.

Therefore, in this study the preparation of the core-shell structured particles was carried out with the use of atom transfer radical polymerization (ATRP). This technique was selected as an effective tool to covalently graft the polymer onto the inorganic surface. This method seems to be superior for the preparation of core-shell structures prior to conventional dispersion polymerization. The polymers synthesized *via* ATRP exhibit controlled morphologies, functionality, composition, and narrow polydispersity index [10]. Therefore, the thickness of a shell layer can be controllably and precisely adjusted. Such particles have defined thickness of polymer shell which is required for chemical stability or sedimentation stability enhancement and moreover the reduction of MR effect appears to be almost negligible.

I. THEORY

1 MAGNETORHEOLOGICAL SUSPENSIONS

Magnetorheological (MR) suspensions are a kind of intelligent systems which are able to controllably change their rheological properties by an external magnetic field [11 – 13]. Conventional MR suspensions are two-phase systems containing magnetizable micron-sized particles dispersed in a non-magnetic carrier liquid. These smart materials were discovered in late 1940´s at the US National Bureau of Standards by Jacob Rabinow [14]. Since then magnetorheology has become multidisciplinary field whose importance has considerably increased in the last two decades [2].

In the absence of external magnetic field, the magnetizable particles are randomly dispersed in a carrier liquid and the system exhibits almost Newtonian behavior. When the magnetic field is applied the dispersed particles develop column-like clusters, due to induced magnetic dipole-dipole interactions [12]. These column-like (also called chain-like) structures are oriented in the direction of magnetic field strength, moreover they represent a spatial barrier in a flow domain and the suspension solidifies. The transformation of a MR suspension from a liquid-like to solid-like state is rapid (in order of ms) and it is almost completely reversible, when the external magnetic field is removed. This phenomenon is called MR effect. This kind of behavior can be effectively used in mechanical systems that require the active control of vibrations or the transmission of torque. Shock absorbers, brakes, clutches, seismic vibration dampers, control valves and artificial joints are some examples of usage MR suspensions [1].

1.1 Dispersed phase

MR suspensions usually include 20 – 40 vol% of the magnetic particles [1]. The particles used in MR systems are typically in the form of a metal powder, which can be prepared by various processes (e.g. reduction of metal oxides, grinding or attrition, electrolytic deposition, metal carbonyl decomposition or rapid solidification) [11].

In general dispersed particles in MR suspensions must have large saturation magnetization, small coercivity and remanent magnetization, which will be explained in Section 2.2. The properties such as activity over a wide temperature range and stability against settling, irreversible flocculation and chemical degradation (oxidation) are also desirable. The characteristics of the particles (chemical composition, particle size, shape and volume

fraction) have the tremendous impact on the field-dependent mechanic strength of MR suspension and will be discussed further (Section 4.1) [2].

1.1.1 Carbonyl iron (CI) particles

Carbonyl iron (CI) particles are frequently used in magnetorheology, due to its spherical shape and appropriate size in the range 2 – 10 μm. CI particles are also suitable candidates because the saturation magnetization of the iron is relatively high (M_S = 2.1 Tesla) and iron has low remanent magnetization [2]. Moreover, it is easy to magnetize and demagnetize the soft CI particles compared to hard magnetic materials such as alnico (iron alloys which in addition are composed of aluminium, nickel and cobalt) [4].

Considerably clean form of CI can be prepared from pentacarbonyl iron precursors by chemical vapor deposition (CVD). Pentacarbonyl iron $Fe(CO)_5$ is a liquid and its thermal decomposition on elementary iron is based on the equation:

$$Fe(CO)_5 \rightarrow Fe + 5\ CO \qquad (1)$$

Thermal energy at boiling point (103 °C) of $Fe(CO)_5$ is not enough to split the atomic bond, so the decomposition is ongoing according to Equation 1 at atmospheric pressure at optimum temperature 250 – 280 °C [15]. CI particles made by CVD exhibit optimal shape, high purity, therefore they are preferred for MR purposes compared to CI prepared by using electrolytic or spray atomization process [16].

a) Traditional manufacturing process of CI

Pentacarbonyl is precisely dosed to an evaporating device and its vapors go into a decomposition reactor from above. Decomposition reactor is a metal cylindrical container heated up to the decomposition temperature. In the upper part of the reactor primary iron nuclei and carbon monoxide (CO) are generated from the pentacarbonyl. The iron particles are growing during falling down through the reactor and they are settling in the container under the reactor. The finest particles are carried by the gas into the capture device. The average diameter of the particles is 3 – 5 microns [15].

The finite size of the iron particles depends on the amount of primary nuclei generated in the first section of the reactor. Also the retention time of the particles in the system, the

length of the reactor and the velocity of flowing gas are the factors which can affect the size of CI particles. The amount of generated primary nuclei depends on the temperature of the entrancing vapors, temperature of the reactor and on the dilution of the gases. More generated primary nuclei in the first stage of the process mean minor finite size of the particles, because the amount of pentacarbonyl vapors is minor attributable to one particle [15].

b) CI preparation based on photochemical reaction

Relatively new (2010) preparation method of CI production is based on photochemical reaction. The principle of this method is completely different from traditional manufacturing of CI. The solution containing the iron ions is mixed with formic acid (pH of the solution is 2.0 – 3.0) and the mixture is subsequently irradiated for 5 minutes by ultraviolet light. CI production is performed at ambient temperature and pressure. Compared to traditional production of CI, there is no need of high pressure or toxic and dangerous gases in this procedure [17].

Although magnetic properties of CI particles are very suitable for magnetorheology purposes, there are some limits of CI particles which should be overcomed for realizing full potential of this material. CI particles exhibit relatively high density, rather poor sedimentation, chemical, and thermo-oxidation stability. These properties are crucial for their practical use in MR suspensions. Therefore, materials such as magnetite or cobalt have been studied with the effort to overcome these possible problems.

1.1.2 Magnetite (Fe_3O_4) particles

Magnetite particles have nonzero resultant magnetic moment which stems from the imbalance of magnetic moments of Fe^{2+} and Fe^{3+} ions. This characteristic indicates that magnetite outwardly appears to be a small permanent magnet. Therefore, the use of magnetite microparticles in MR suspensions is limited because such particles would magnetically tie in operational parts of the device and thus they would not fulfill their function [18].

However the magnetic properties are dependent on the size of the particles. Therefore, colloidal dispersions of metal nanoparticles so called ferrofluids (FF) can be prepared. Nanoparticles of FF are single domain and possess a permanent magnetic dipole moment. Nevertheless, FFs exhibit only a small change in their viscosity and do not develop a sufficient yield stress, therefore their technical applications are very limited [19].

1.1.3 Cobalt particles

Also materials such as cobalt can be used as a dispersed phase in MR suspensions. Research has been carried out with cobalt spheres [20], cobalt fibers [21], iron cobalt oxides ($CoFe_2O_3$) [22] and ($CoFe_2O_4$) [23]. Study [22] revealed that the MR suspensions of cobalt ferrite exhibit larger yield stress than those containing the ferrite compound (Fe_3O_4) at the same concentrations. Recent study [23] describes the preparation of $CoFe_2O_4$ nanoparticles in laboratory conditions *via* sol-gel method, moreover deals with the influence of annealing temperature on resultant properties of the MR suspensions.

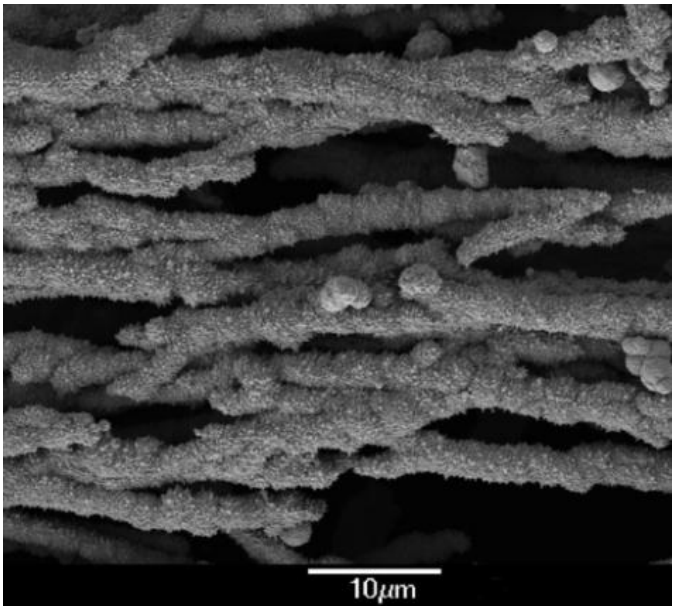

Figure 1. SEM image of the cobalt fibers [21]

1.1.4 Composite core-shell particles

Generally, bare metal particles used in MR suspensions do not achieve good results in practical use, mainly because of their settling due to gravitational forces. The other negative factors are poor oxidation and chemical stability. Therefore, current development is focused on the preparation of core-shell composite systems providing enhanced stability and tunable MR performance [4 – 9].

There are two types of core-shell structures. First, the magnetic material can be used as a shell layer, while the core of the composite particle consists of non-magnetic material [24]. In this case, the strong bonding between core and shell is required to prevent fragmentation during shearing. The other type, when the core of the particle consists of magnetic material and the shell is non-magnetic, is more often [16]. The use of both types of core-shell particles results in enhanced sedimentation stability due to reduced density. Variant with non-magnetic shell is a better choice, because besides sedimentation stability also improves chemical and oxidation stability [5]. Many polymers have already been used as a coating material. In the following section is a brief overview of the most interesting ones.

a) CI/PS particles

Polystyrene (PS) coated CI particles (CI/PS) were fabricated by Quan *et al.* [4] through a simple coating method of dispersion polymerization. Figure 2 shows the change in morphologies of CI particles before and after the polymerization. Result in [4] indicates that PS-coated CI particles improve sedimentation stability with only minor negative effect of MR performance – saturation magnetization decreased from 250 to 240 emu/g.

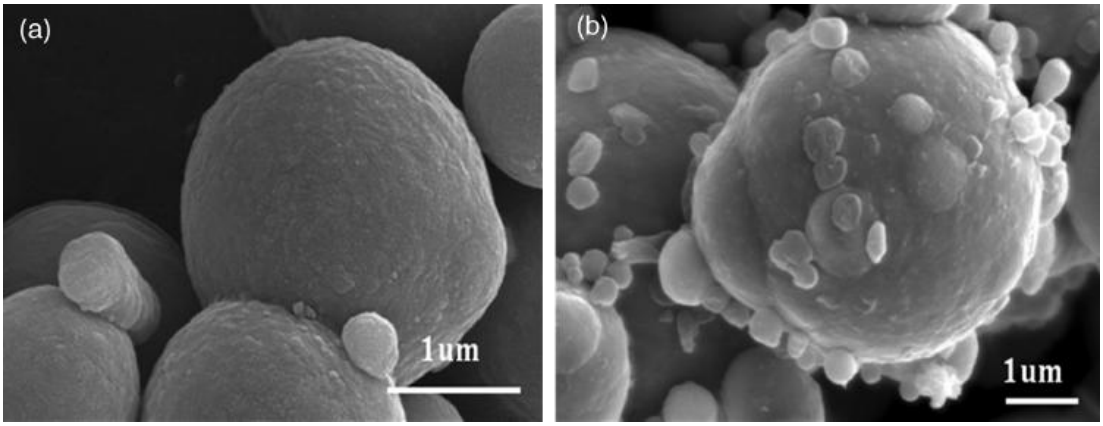

Figure 2. SEM image of (a) pure CI and (b) PS-coated CI particles [4]

b) CI/PPy particles

The other type of composite MR particles with modified properties can be core-shell structured polypyrrole(PPy)-coated carbonyl iron particles (CI/PPy). The preparation and characterization of such particles is described in the reference [5]. The suspensions with CI/PPy particles exhibit slightly lower magnetic properties as well as the yield stress, but significantly improved sedimentation stability [5, 25].

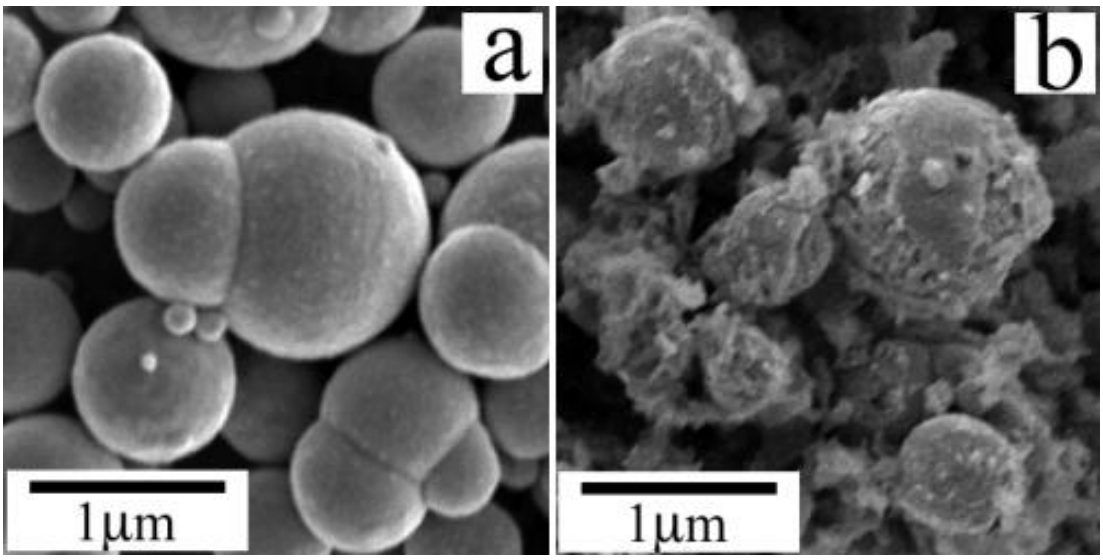

Figure 3. SEM images of (a) bare CI and (b) coated with PPy ribbon-like particles [25]

c) CI/PANI particles

Sedlacik *et al.* prepared CI particles coated with polyaniline (PANI) in order to enhance sedimentation stability of MR suspensions. Core-shell composite particles with a CI magnetic core and PANI conducting shell were prepared by using a PANI colloidal dispersion in chloroform. PANI coating contributes to enhanced overall suspension stability, and higher MR effect was also reported [7].

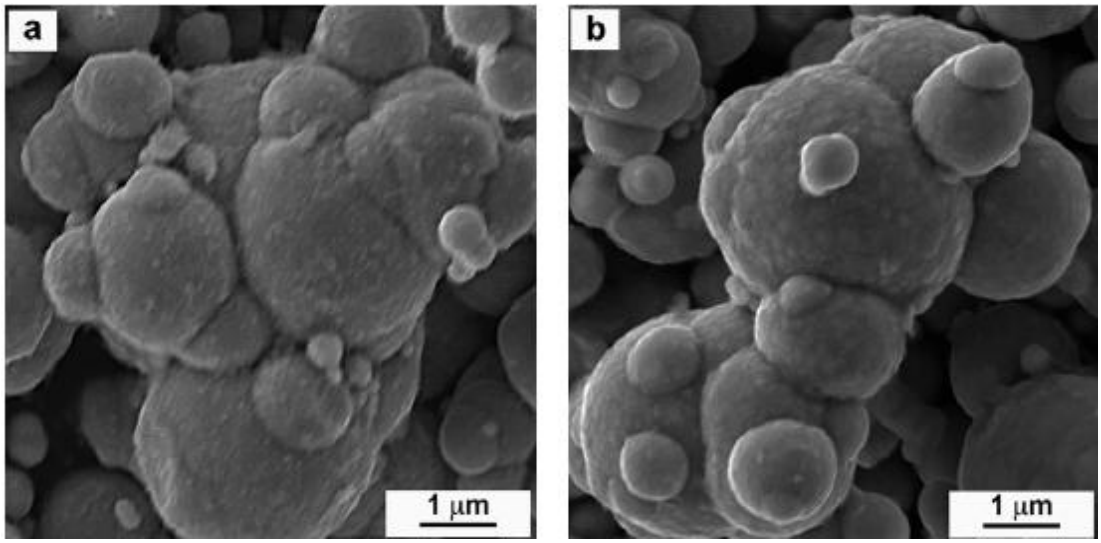

Figure 4. SEM image of (a) bare CI and (b) CI/PANI particles [7]

d) CI/Ni particles

Coatings of the MR particles may include not only polymer materials but also metals e.g. nickel (Ni). Ni-coated CI particles (CI/Ni) are core-shell composites, in which carbonyl iron is used as the core and the shell consists of nickel. Nickel appears to be very effective in reducing oxidation of the iron. However, the treatment process can lead to undesirable decrease in the saturation magnetization moreover material handling difficulties during preparation were also reported [26]. Nevertheless, these particles are appropriate candidates for applications where high oxidation stability is required.

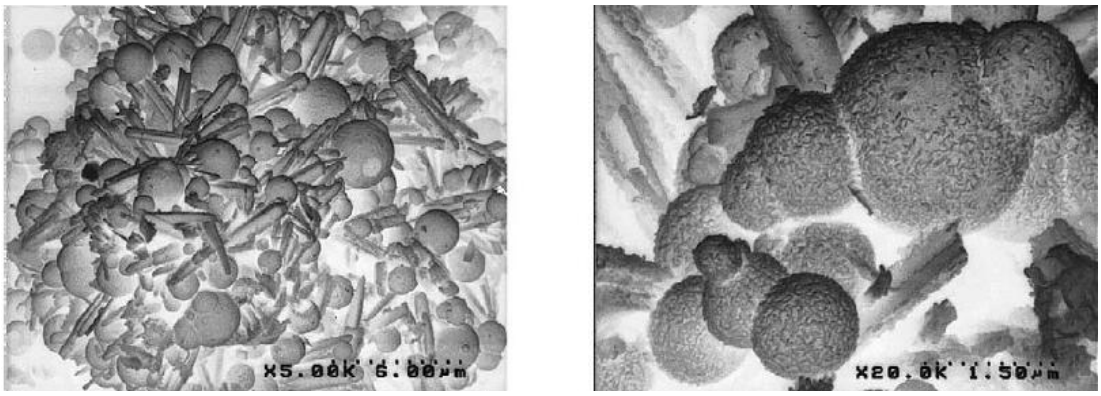

Figure 5. SEM micrographs of CI particles coated with nickel [26]

e) Other types of particles

Also nickel zinc ferrite-based MR suspensions were prepared but their applications are limited, since these materials exhibit much lower values of saturation magnetization [27]. The importance of saturation magnetization of the particles is discussed later in Section 4.2.

The other ferromagnetic materials used for preparation of MR suspensions are compounds of chromium. The addition of chromium dioxide can stabilize the conventional CI suspension due to lower density (5.22 g/cm^3) in comparison to iron (7.80 g/cm^3), which results in improved sedimentation stability; they also play an important role in steric repulsions between relatively large CI particles [1].

1.2 Carrier liquid

The function of the carrier liquid is the lubrication (in combination with additives) and damping features. The choice of the fluid may dramatically influence the MR effect. Higher MR effect can be reached with the carrier liquid with small viscosity and its small dependence on the temperature [28]. Various types of carrier liquids are usually used in order to create MR suspension. At the beginning of magnetorheology, water was the most used carrier liquid. However, devices using the MR suspensions based on water have a narrow temperature range of their applicability. Moreover, the water may speed up the corrosion of the uncoated particles and components of MR device. The major interest of water-based MR suspensions is for biological and medical applications [29].

In 2000, Park *et al.* [30] used water-oil emulsion as a continuous phase of MR suspension. The dispersed phase was formed by hydrophilic-treated CI particles. The aim of the study was to prepare new stable MR suspension. The main idea of this study was based on the interactions among the water droplets in continuous phase and hydrophilic magnetic particles (Figure 6) [30]. The enhancement of the overall stability and especially dispersion stability of the MR suspension was observed, but other studies using similar carrier liquid were not found in the literature.

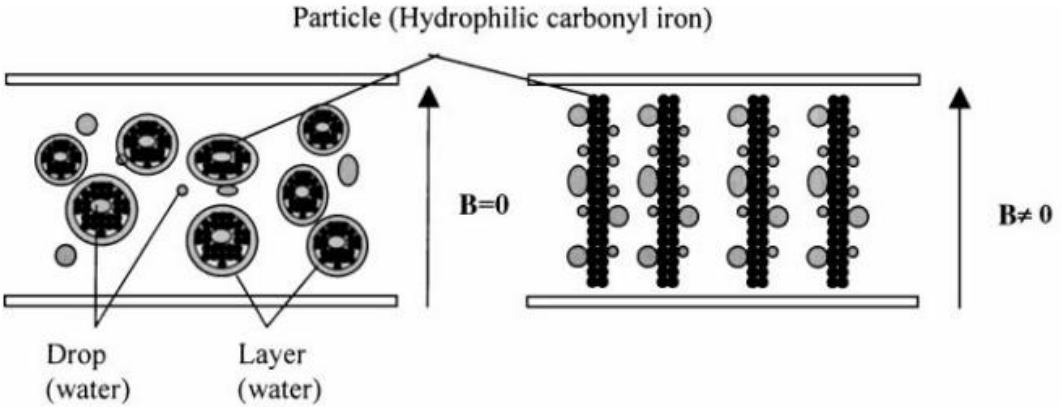

Figure 6. The water-oil emulsion with hydrophilic-treated CI particles according to Park [30]

Nowadays among the most common used carrier liquids belong various oils, such as the mineral oils, silicone oils and paraffin oils. Also silicon copolymers white oils, halogenated aromatic liquids, halogenated paraffins, diesters and many others can be used for this reason [11]. The selection of carrier liquids is based on their intrinsic viscosity, their temperature stability and compatibility with the surface treatment of components forming an MR device. Silicon oil has suitable properties like broad operating temperature range, and compatibility with other materials occurring in the MR device i.e. (rubber seals) [31].

Also ferrofluids (FF) which are stable colloidal dispersions of ferromagnetic nanoparticles were successfully investigated as possible carrier liquid for MR suspensions. FF carrier medium is the effective way how to enhance the sedimentation stability of the micron-sized particles used in conventional MR suspensions [19].

Recently (2012) Gómez *et al.* studied properties of ionic liquids used in magnetorheology as carrier fluids. Ionic liquids show special properties, such as very low vapor pressure, high thermal stability and non-corrosive nature. Moreover, the use of ionic liquids improves suspension redispersibility [32]. This was the first type of carrier liquid which helped to understand the wall slip effect in MR suspensions. However, full characterization (such as stabilization) of suspensions based on this carrier liquid is still missing in the literature.

2 FUNDAMENTALS OF MAGNETISM

The basis of all MR systems is the fact, that at least one their phases must be magnetic field responsive. In most cases, it is the dispersed phase, which responds to the field. But in some cases it can be the carrier liquid that is field-sensitive, i.e. (inverse FFs) [1].

The magnetic properties of matter have their origin in the electric charges moving inside the atoms and molecules. The movement of electrons creates current loops that can be considered as magnetic dipoles with magnetic moment *m*. Each electron in an atom has magnetic moments that originate from two sources [33]. The electrons orbiting around the nuclei and simultaneously they spin on their axes as described in the Figure 7.

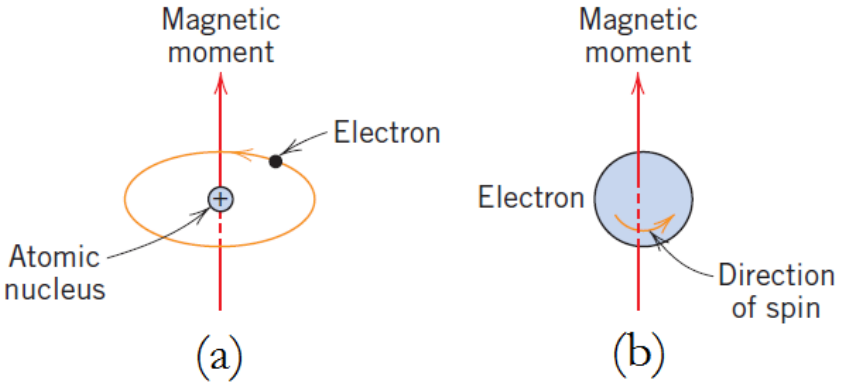

Figure 7. Demonstration of the magnetic moment associated with an orbiting electron (a) and a spinning electron (b); adopted from [33]

The relation between the current in an electron current loop *I* and the resulting magnetic field strength *H* is described by Ampere´s law.

$$\oint_C^0 \vec{H} \cdot \vec{dl} = I \tag{2}$$

This Equation 2 basically states, that the line integral of tangential component of the magnetic field strength around a closed path is equal to the total current enclosed by the path. The vector *H* is independent on the properties of the medium (e.g. water, iron, MR suspension etc.) [31]. Behavior of MR suspensions is commonly studied in the presence of external magnetic field which can be generated by a coil. The current in the coil is proportional to the magnetic field strength applied on the suspension.

2.1 Magnetic properties

The magnetic properties of materials can be described by many different quantities with different units. Table 1 summarizes the quantities and units utilized throughout this study, together with the conversion factors to SI units.

Table 1. Units for magnetic properties

Quantity	**Symbol**	**Gaussian**	**Conversion factor**	**SI & rationalized units**
Magnetic induction	*B*	gauss (G)	10^{-4}	tesla (T), Wb/m^2
Magnetic field strength	*H*	oersted (Oe)	$10^3/4\pi$	A/m
Mass magnetization	*M*	emu/g	1 $4\pi \times 10^{-7}$	$A{\cdot}m^2/kg$ Wb·m/kg
Magnetic moment	*m*	emu	10^{-3}	$A{\cdot}m^2$, J/T
Permeability	μ	dimensionless	$4\pi \times 10^{-7}$	H/m, Wb/(A·m)

The force effect of the magnetic field on the moving charged particles describes magnetic induction (*B*) (also called magnetic flux density). This quantity depends on the properties of the medium (unlike *H*). The relation between *B* and *H* is given by:

$$B = \mu_0(H + M) = \mu_0\mu_r H \quad (3)$$

where μ_0 is the permeability of free space ($4\pi \times 10^{-7}$ H/m), and μ_r is the relative magnetic permeability of the material. Symbol *M* is the magnetization of the matter, which is proportional to the number of magnetic moments and the dipole magnetic moment *m*, and *M* can be calculated according to following equation [1, 31].

$$M = \chi H \quad (4)$$

where χ is the magnetic susceptibility, which is given by the equation:

$$\chi = \mu_r - 1 \quad (5)$$

The types of magnetism include diamagnetism (μ_r < 1), paramagnetism (μ_r > 1) and ferromagnetism (μ_r >> 1). In addition, antiferromagnetism and ferrimagnetism are considered as subclasses of ferromagnetism [33]. In this study were utilized ferromagnetic CI particles, therefore following section is dedicated to ferromagnetic properties.

2.2 Ferromagnetism

Ferromagnetism is defined as a material phenomenon exhibited by materials like iron (nickel or cobalt) that become magnetized in a magnetic field and retain their magnetism when the field is removed. This mechanism is bound to a specific temperature range; ferromagnetic materials consist of domains and exhibit a hysteresis. These basic characteristics are discussed in following sections [34, 35].

2.2.1 The effect of temperature on magnetic behavior

Temperature affects the material characteristics including magnetic properties. Temperature increase results in enhancement of thermal vibrations magnitude of the atoms. Thermal motion of the atoms tends to randomize the directions of magnetic moments, which is reflected in different magnetic behavior.

Saturation magnetization (M_S) is not a constant, but its value is a function of temperature. M_S is a maximum at 0 K, at which thermal vibrations are non-existent. With increasing temperature M_S decreases gradually and then abruptly drops to zero at temperature which is called the Curie temperature (T_C). Above T_C the ferromagnetic and ferrimagnetic materials behave like paramagnetic. Each material has its own T_C. For instance, for iron particles T_C value is 768 °C [33].

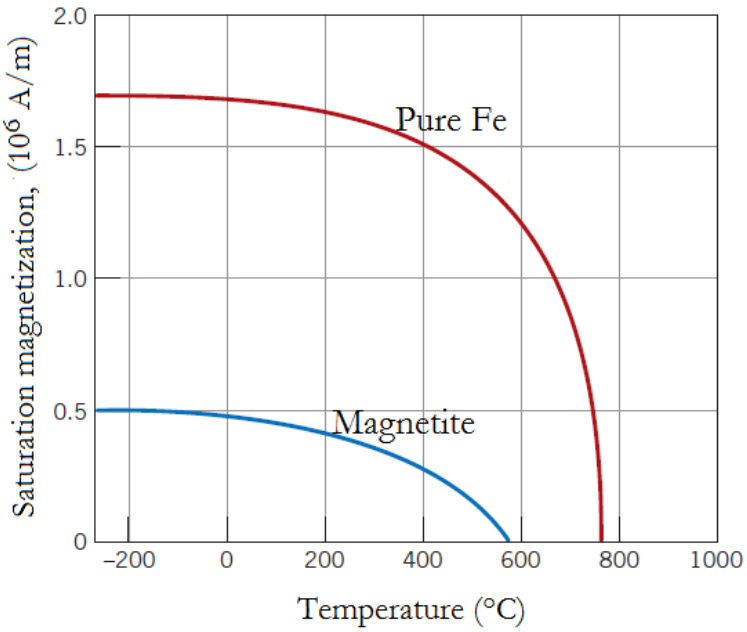

Figure 8. Saturation magnetization as a function of temperature for iron and magnetite; adopted from [33]

2.2.2 Domains

The collective behavior of magnetic moments in atoms of ferromagnetic materials results in domain formation. Domains are the microscopic small-volume regions, in which vector of magnetization has the same value, and direction. Linear dimension of spontaneously magnetized areas is 10^{-5} – 10^{-3} m. The presence of domains occurs in ferromagnetic materials only at temperatures below T_C. The domains are separated by domains boundaries or so called Bloch walls, across which the direction of magnetization gradually changes. The total magnetization M is the vector sum of the magnetization of all domains. The contribution of each domain is weighted by its volume fraction [33 – 35].

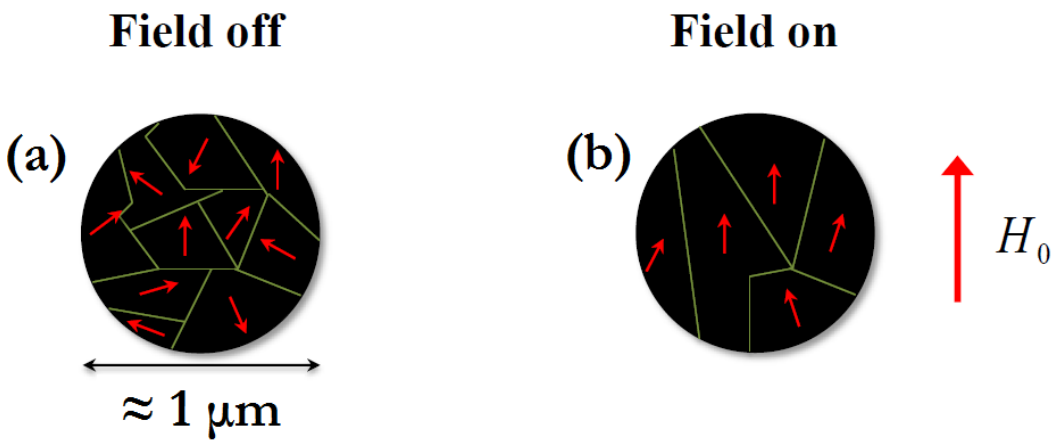

Figure 9. Orientation of magnetic moments in domains in the absence (a) and in the presence (b) of external magnetic field; adopted from [1]

2.2.3 Hysteresis curve

B-H relation can be illustrated by a hysteresis loop. Figure 28 illustrates the magnetization process of a ferromagnetic sample. If it is used initially unmagnetized sample (the sample is heated above T_C and cooled in the absence of magnetic field) and the magnetic field strength increase, it can obtain the initial magnetization curve. The curve begins at the origin and as *H* increases, the *B* (respectively *M*) begins to increase slowly then more rapidly and finally become independent on *H*. As an *H* is applied, the domains change shape and size by the variation of domain boundaries. At the point "S" the sample reaches the magnetic saturation, which means that domains are entirely rotated in the direction of *H* and the macroscopic specimen becomes a single domain.

If we decrease *H* to zero value, the curve does not go back its original path, and at zero *H* field, inside the ferromagnetic sample will remain the field with magnetic flux density B_r which is called the remanence.

To reduce the *B* field in the specimen to zero, an H_c field must be applied in an opposite direction. H_c is called coercitivity or coercive force. When the increasing of *H* with reverse direction continues, the saturation magnetization can be reached in the opposite sense. A second reversal of the external magnetic field completes the symmetrical hysteresis loop [33, 34]. The area defined by the hysteresis loop is proportional to the energy that must be expended to magnetize the material. The material is heated by this energy, which creates hysteresis losses.

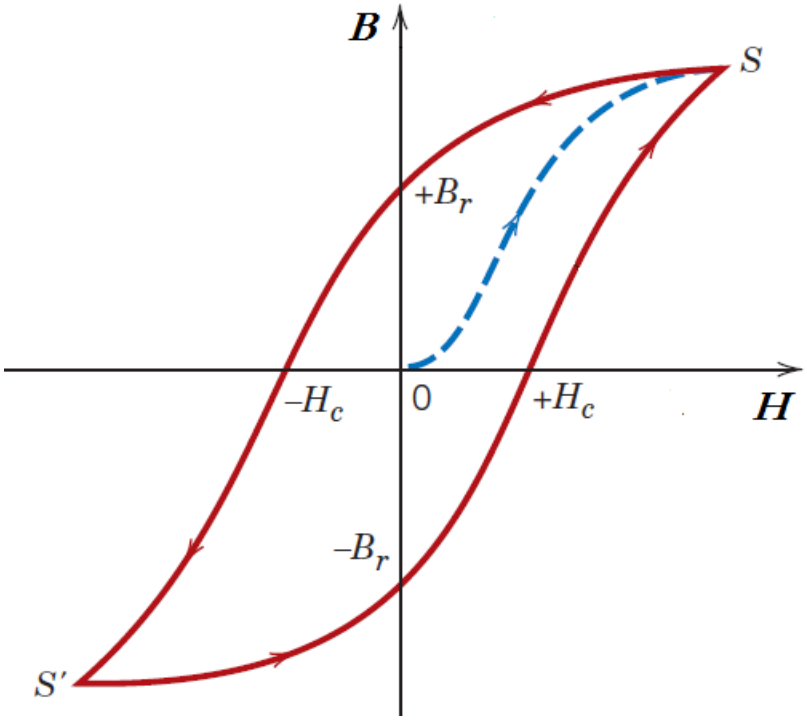

Figure 10. Magnetic flux density versus the magnetic field strength for a ferromagnetic material. Hysteresis loop is represented by the solid red curve; the dashed blue curve indicates the initial magnetization; adopted from [33]

2.2.4 Suitable magnetic properties of particles in MR suspensions

Now it should be easy to derive which magnetic properties are appropriate for particles used in MR suspensions. The most often used particle types in MR suspensions are described in the Section 1.1. Generally, it is suitable for these materials having a high saturation magnetization value, which is important for large yield stress (Section 3.4). Particles in MR suspensions should appropriately react to external magnetic field, thus it should be easy to magnetize them and demagnetizing process should exhibit low magnetic hysteresis; field-induced structures of particles with high remanent magnetization would not break completely after removal of external magnetic field. Therefore, the return to original state would be problematic. For good response on external magnetic field also high magnetic susceptibility and magnetic permeability are important.

Materials with these parameters are classified as soft magnetic materials and upon described properties make materials such as CI superior to hard magnetic materials [12]. Soft magnetic materials exhibit narrow hysteresis loop which represents a low magnetic energy loss of the material. Hard magnetic materials have high magnetic hysteresis therefore they are unsuitable for magnetorheology purposes with the aim to obtain fast reversible control of rheological characteristics. CI particles are micron-sized and therefore, they behave as magnetic multidomains [1]. The magnetic properties of CI can be described by the Frohlich-Kennely equation:

$$M = \frac{\mu_i H}{1 + \frac{\mu_i}{M_S} H} \tag{6}$$

where μ_i is the initial permeability at $H \to 0$, and M_S is the saturation magnetization.

This section was dedicated to magnetic properties of ferromagnetic MR particles. Although magnetic properties of the particles can greatly affect the behavior of incurred MR suspensions, from a practical point of view it is more important to determine behavior of particles in conjunction with a carrier liquid. Therefore, the following section deals with rheological behavior of MR systems.

3 RHEOLOGICAL PROPERTIES OF MR SUSPENSIONS

Rheology is defined as the science dealing with the deformation and flow of the matter. Crucial rheological parameter characterizing the internal friction of the fluid is the viscosity. Shear viscosity can be expressed as a ratio of shear stress and shear rate.

There are many different materials which exhibit several types of flow behavior. The simplest is Newtonian behavior and the fluids which exhibit this kind of behavior are called Newtonian fluids. Such behavior is described by Newton´s model (Equation 7):

$$\tau = \eta\dot{\gamma} \tag{7}$$

where τ [Pa] is the shear stress, η [Pa·s] is the dynamic viscosity and $\dot{\gamma}$ [s^{-1}] is the shear rate . In the case of MR suspensions, rheological properties can be measured either in the presence of external magnetic field (on-state) or without the effect of external magnetic field (off-state). The rheology of MR fluids will be discussed in the Section (3.2), but let us firstly describe the general rheological behavior of suspensions, as the MR fluids are suspensions.

3.1 Viscosity of the suspensions

Suspensions are the mixtures of dispersed solid particles in carrier liquid. Viscosity is the material characteristic which is considerably dependent on temperature and partly on pressure. In suspensions, viscosity is also dependent on the volume fraction of the dispersed phase [36].

Increase in volume fraction of solids (Φ) [-] causes a considerable increase in viscosity. This phenomenon was described by Einstein and is expressed by the equation:

$$\eta = \eta_C \cdot (1 - 2{,}5\Phi) \tag{8}$$

η is the viscosity of the suspension and η_C is the viscosity of carrier liquid.

Later was found that the Equation (8) can be applied only for quite low volume fractions. At higher volume fractions (a few percent) the Equation (8) predicts lower viscosities. Therefore, Krieger and Dougherty proposed another Equation (9) which better describes the full relationship between volume fraction and viscosity [36].

$$\eta = \eta_C(1 - \frac{\Phi}{\Phi_m})^{-[\eta]\Phi_m} \quad (9)$$

Symbol Φ_m in Krieger-Dougherty equation is the maximum possible volume fraction for given particles. Maximum volume fraction has a value of 65 % for randomly close-packed particles. The parameter *[η]* is called intrinsic viscosity, which is defined as:

$$[\eta] = \lim_{\Phi \to 0} \frac{\eta/\eta_C - 1}{\Phi} \quad (10)$$

The intrinsic viscosity is 2.5 for spherical particles. For non-spherical particles *[η]* is always higher. Behavior of the suspension is also affected to what extend are particles in the carrier liquid flocculated or dispersed [36].

3.2 Steady shear flow

Currently there is a great interest in the understanding of the flow behavior of MR suspensions [1]. In the absence of external magnetic field MR suspensions exhibit nearly Newtonian behavior (Equation 7). When the external magnetic field is applied, the properties of MR suspensions change due to creation of internal structures and belong to non-Newtonian fluids. These fluids exhibit viscosity dependence on the shear rate. Unlike Newtonian fluids, behavior of these fluids is not described with simple Newton´s model. MR suspensions due to their behavior require different rheological models [37].

3.2.1 Constitutive rheological models and analytical techniques

Rheological models describe the constitutive behavior – a relationship between shear stress τ and shear rate $\dot{\gamma}$. With a few rheological parameters of the models it is easier to determine flow behavior of especially more complex non-Newtonian fluids (MR suspensions) under various flow conditions (various shear rates, presence of external magnetic field etc.) [36]. Many theoretical and empirical models have been proposed to describe flow curves of various materials, for instance Cross model, Carreau model, Yasuda *et al*. model, Ellis model, Sisko model, etc. [38]. Following models have been chosen with respect to subject of this Master thesis.

Bingham model (1922) was the first two-parameter (2P) model used for the description of rheological behavior of the fluids, which exhibit a yield stress. After overcoming a yield stress, this model assumes a linear relationship between shear stress and shear rate.

$$\tau = \tau_0 + \mu_P \dot{\gamma} \tag{11}$$

where τ_0 [Pa] is the (field dependent) yield stress, and symbol μ_P [Pa·s] denotes to plastic viscosity which is independent on the shear rate [38].

Power-law model (1926) is the equation commonly used for modeling of rheological behavior of pseudoplastic materials, and is expressed as:

$$\tau = K\dot{\gamma}^n \tag{12}$$

In the Power-law the viscosity term from the Newtonian model is replaced with a constant K [Pa·s^n], termed as the consistency index. The factor n [-] is called the flow behavior index. Symbol n is the power index which represents the deviation from Newtonian behavior [38, 39].

Herschel-Bulkley model (1926) is the combination of the Power-law with the Bingham model, which defines fluid by three parameters. This model is described by the following equation:

$$\tau = \tau_0 + K\dot{\gamma}^n \tag{13}$$

Fluids which exhibit a yield stress and their viscosities or the shear stresses are strain rate dependent cannot be adequately described by Bingham model therefore the Herschel-Bulkley model can be employed. In Herschel-Bulkley model the term $\mu_P \dot{\gamma}$ from Bingham model is replaced with the Power law expression.

Casson model (1959) is an empirical model, originally proposed to describe rheological behavior of printing inks [39]. This model has more gradual transition from Newtonian to the yield region and provides very good fit for materials, such as blood and food products.

$$\sqrt{\tau} = \sqrt{\tau_0} + \sqrt{\mu_P \dot{\gamma}} \tag{14}$$

MR suspensions exhibit Bingham plastic behavior in the presence of external magnetic field, but in low shear regime Casson predictions do better fit with the experimental data instead of the Bingham model. Casson model also provides good fit for MR suspensions with the concentrations up to 50 vol% of the particles [1].

Robertson-Stiff model (1976) – also called ***Vocadlo model*** was developed to describe rheological behavior of drilling fluids and cement slurries. The constitutive equation of this model is:

$$\tau = \mu(\dot{\gamma} + C)^n \tag{15}$$

where τ, μ, $\dot{\gamma}$, C and n represent the shear stress, consistency factor, shear rate, initial shear rate and power exponent. Robertson-Stiff model can reduced to Bingham model when $n = 1$, to the Power-law model when $C = 0$, and to Newtonian model when $n = 1$ and $C = 0$ [40].

Petr Filip *et al.* have shown that three-parameter (3P) Vocadlo model better corresponds to reality than the 3P Herschel-Bulkley model for process of annular pumping. On the Figure 3 is demonstrated, that the flow curve does not exhibit an infinite slope at zero shear rate as in the case of the Herschel-Bulkley model. Vocadlo model attains a finite value of the slope which is closer to reality [41].

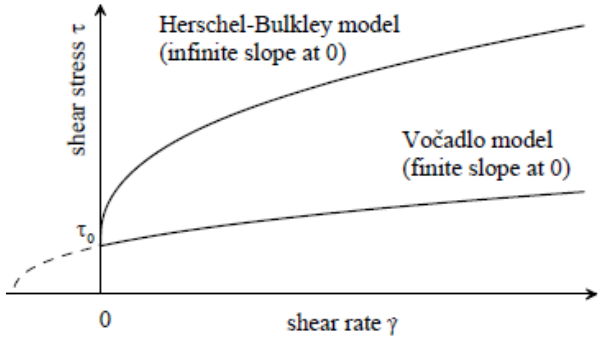

Figure 3. Vocadlo vs. Herschel-Bulkley model predictions of the yield stress [41]

For some models (Bingham, Herschel-Bulkley, Casson) is the zero shear rate if the following condition is fulfilled (Equation 16).

$$|\tau| \leq \tau_0 \tag{16}$$

Thus, these models give non-zero results after external operating yield stress overcomes a certain yield stress.

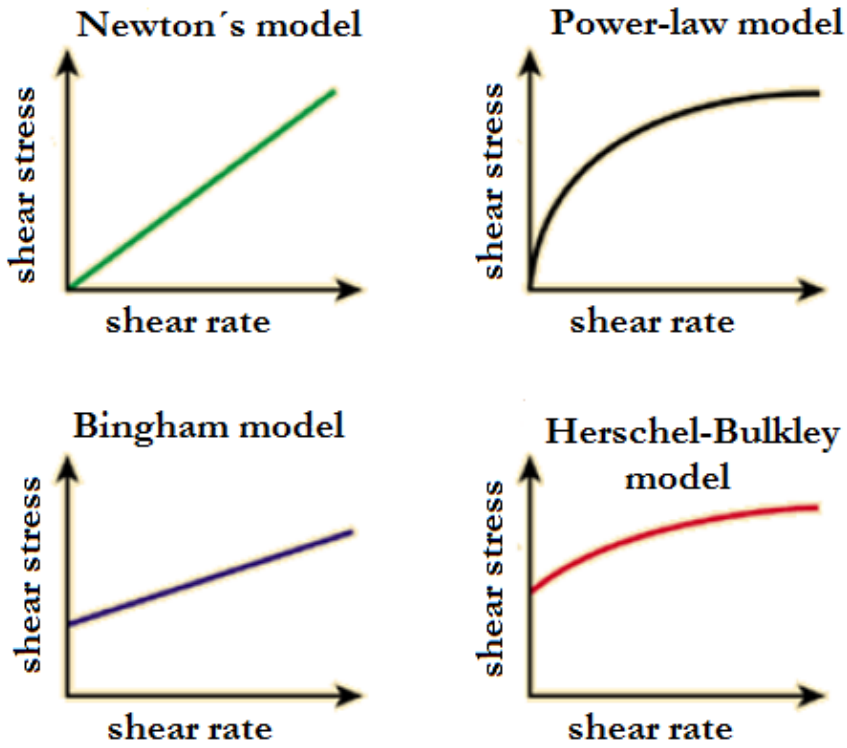

Figure 11. The mathematical predictions of rheological behavior according to different models

3.3 Rheometry of MR suspensions

Currently a lot of devices utilize MR suspensions, therefore the accurate measuring methods are required to provide reliable results in conditions close to the behavior in practical devices, for instance high shear rate, high energy dissipation. The reliability of rheology results can be judged by using different measurement geometries or different types of rheometers [42]. Nowadays, there are modern rheometers which are able to very precisely measure the viscosity of MR systems. In history very simple devices were used for this purpose – in 1991 Lemaire and Bossis used a plate-plate geometry inserted into a coil.

3.3.1 Rheometers

Rheological properties of MR suspensions are usually measured with the help of conventional rheometers which have been modified by a special MR device which is able to generate magnetic field. The parallel-plate (PP) or cone-plate (CP) geometries are broadly used to study this phenomenon. In the CP geometry, the shear rate is constant inside the suspension but variable structures of dispersed particles can be formed due to variable thickness of the gap. In the PP geometry the induced structures of dispersed particles are identical since the gap is constant, but on the other hand the shear rate is not constant in this geometry [2]. The shear rate in PP geometry is given by the equation:

$$\dot{\gamma} = \frac{\omega r}{h} \tag{17}$$

where $\dot{\gamma}$ [s^{-1}] is the shear rate, ω [s^{-1}] is the angular frequency, r [m] is the radius of the geometry, and h [m] is the height of the position between the plates for which shear rate is calculated. In this study the priority was given to PP geometry, due to conformity of induced column-like structures, which affects the yield stress.

3.4 Yield stress

Non-Newtonian fluids including MR suspensions (on-state) may exhibit a yield stress, which is the minimum stress to initiate flow. Below the yield stress the material is solid-like and has an infinite viscosity. Above the yield stress the material deforms as a fluid and the viscosity is a function of shear rate according to different constitutive relation [43, 44].
Although highly accurate rheometers are available, the fluid yield stress is historically difficult to measure in any rheometer. Currently there is contradiction among researchers whether a true yield stress exists or not. Measurement of the yield stress from a flow curve can give faulty results for a number of reasons. First, the yield stress must be determined by extrapolation of the flow curve to zero shear rate. Low shear rates are finite and limited by a rheometer, which making parameter estimation (especially yield stress) difficult. Second, measurements performed at low shear rates may be inaccurate (true for MR suspensions) because of the slip at the walls [1, 44].

3.4.1 Types of the yield stress

There are three kinds of yield stresses that can be defined through shearing flow experiments – the static yield stress, the dynamic yield stress and elastic-limit yield stress [1].

a) Static yield stress is defined as the minimum stress required in order make the fluid flow. It is typically associated to the slip of the aggregates on the plates, not with the structure collapse or brake under the shear.
b) Dynamic yield stress corresponds to the stress required to continuously break the aggregates during the shear in external magnetic field.
c) Finally, elastic-limit yield stress is defined as the maximum shear stress which can be applied and the structure will recover when the stress is removed.

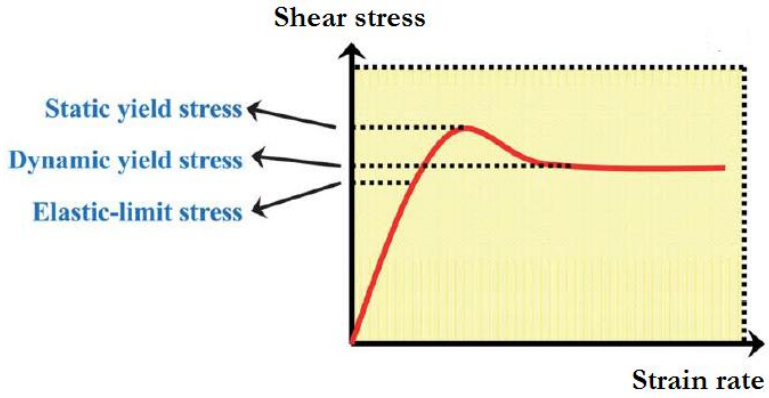

Figure 12. Yield stresses under shear flow test, adopted from [1]

High yield stress is a desirable property in MR suspensions, because the performance of a MR suspension is typically judged by the magnitude of its field-induced yield stress. The yield stress can be increased by the amplification of the external magnetic field or by increasing particle concentration. If particle fraction increases, the off-state viscosity of MR suspension increases according to Krieger-Dougherty equation (Equation 9), which is undesirable. It is equally important to maintain a low off-state viscosity in conjunction with maximum possible yield stress. This connection between the viscosity increment under the field and the viscosity value in the absence of the field is called relative MR effect (or turn-up ration) [1].

3.5 MR effect

Nearly reversible [3] and very fast (in the fraction of milliseconds) transition of MR suspension from a liquid-like to a solid-like state in external magnetic field is called MR effect. The principle of this effect is basically field induced magnetization of the suspended particles. In the absence of magnetic field the MR suspensions have a relatively low viscosity. When a magnetic field is applied the particles create anisotropic aggregates along the field lines. Under such conditions material exhibits high yield stress. This behavior is characterized by shear rate-dependent apparent viscosity [1].

As was mentioned above, variables measured without the presence of external magnetic field for a given shear rate are called off-state (shear stress or viscosity). The shear stress increase $\Delta\tau(H)$ [42] due to applied field is given by the equation:

$$\Delta\tau\,(H) \equiv\ \tau(H) -\ \tau(0) =\ [\eta(H) - \eta(0)] \cdot \dot{\gamma} \tag{18}$$

The external magnetic field causes also viscosity increase. The relative viscosity $\eta_r(H)$ defines the degree of the viscosity increase compared to the field off-state:

$$\eta_r(H) \equiv \frac{\eta(H)}{\eta(0)} = \frac{\tau(H)}{\tau(0)} \tag{19}$$

In Equations (18) and (19), $\tau(0)$ and $\eta(0)$ denote shear stress and viscosity measured for a given shear rate in off-state. Symbols $\tau(H)$ and $\eta(H)$ denote shear stress and viscosity measured for a given shear rate at imposed magnetic field strength H. Again, note that the MR effect and the viscosity ratio are defined for a given shear rate ($\dot{\gamma} = const.$).

In some literature sources dealing with MR suspensions [45] we can find that the MR effect is completely reversible. However, study [3] shows that in some instances, the "residual" structures can be formed which leads to incomplete reversibility of the fluid properties, or restoration of the original state when the external magnetic field is removed. The information about irreversible features in MR suspensions can be important especially in MR devices operating with cyclic control.

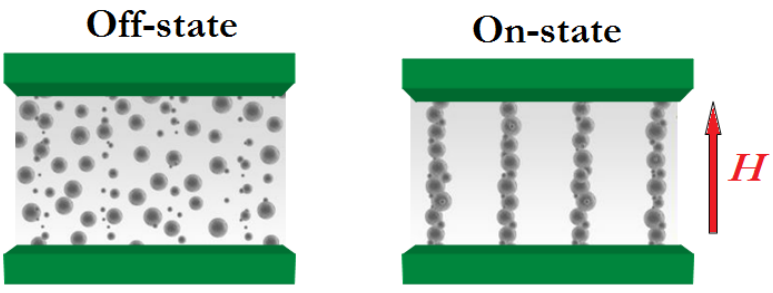

Figure 13. Schematic figure of MR effect

3.6 Dynamic flow behavior

Dynamic techniques are used for characterization of viscoelastic materials [36]. Viscoelastic material is a material which behaves simultaneously as a flexible (elastic) solid and as a viscous liquid under the presence of external mechanical stress. Such material always responds to the mechanical stress with a delay [46]. MR suspensions exhibit Bingham plastic behavior with yield stress therefore they can be described as viscoelastic materials in the range of a small strain of oscillatory flow [16].

Dynamic measurements can provide the information about the energy storage on the material which is related to structure of the MR suspensions and also the information about the energy associated to the dissipation under the flow [47].

Knowledge of these parameters is important especially from a practical point of view since MR devices often operate in oscillatory mode. There are four areas of the dynamic rheological behavior – linear viscoleastic (LVE), nonlinear viscoelastic (NLVE), viscoplastic (VP) and Newtonian (N) [1]. This master thesis is focused on oscillatory flow measurements in linear viscoelastic area, but we consider important to mention all forms of the possible behavior.

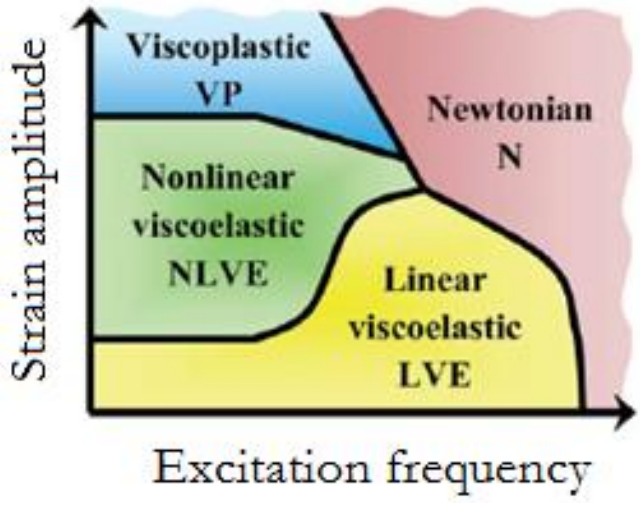

Figure 14. Diagram of different dynamic behavior of MR suspensions, adopted from [1]

LVE measurements of the MR suspensions can be carried out on rotational rheometers with the use of small amplitude oscillatory tests. The one part of the measuring geometry, the strain respectively, oscillates according to a sine function and the viscoelastic moduli $G´$ and $G´´$ are evaluated. The relation between $G´$ and $G´´$ can be expressed by a complex shear modulus:

$$G^* = G´ + iG´´ \tag{20}$$

where $G´$ [Pa] is the phase modulus, $G´´$ [Pa] is the loss modulus, and i [-] is the imaginary unit.

$G´$ denotes the real component which is a measure of the elastic response. $G´$ is related to energy storage inside the material and it is in phase with the external shear stress. Elastic solids have some storage modulus and a zero loss modulus. Analogously to that, viscous liquids have some loss modulus and zero storage modulus.

On the contrary, G'' denotes the imaginary component which is responsible for viscous fraction of the material behavior. $G´´$ is associated to the dissipation of the energy inside the material and is in phase with the shear rate. In the linear viscoelasticity region (LVR) the both components of the complex modulus are independent of the applied excitation frequency. In LVE measurement the deformation of structures in the system does not occur. Quantity which expresses the ratio between the viscous and elastic behavior of the examined material is called a loss angle δ (damping factor), which is defined by the relationship [1, 46]:

$$\tan\delta = \frac{G´´}{G´} \tag{21}$$

In MR suspensions the storage modulus $G´$ associated with field-induced structures is typically at least an order of magnitude larger than the loss modulus $G´´$, in the presence of magnetic field. There are derived equations which allow estimate the value of the storage modulus for MR suspensions. For intermediate magnetic field the $G´$ is predicted by [1]:

$$G´ = 3\Phi\mu_0 M_S H \tag{22}$$

At large fields when the saturation magnetization is reached, the Equation 22 transforms to following:

$$G´ = 0.3\Phi\mu_0 M_S^2 \tag{23}$$

Symbols used in Equations (22) and (23) are explained in previous sections of this thesis.

4 FACTORS INFLUENCING MR EFFECT

Although the principle of MR effect is discussed in the previous section (Section 3.5), this phenomenon is extremely important characteristic of MR suspensions therefore, the following section deals with factors which influence the MR effect. Moreover, this section is included in relation to this Master thesis as this thesis deals with particle modification and the particle properties are one of the major factors affecting this phenomenon.

4.1 Properties of dispersed phase

4.1.1 The effect of the size of particles

The most of the studies reported in the literature were performed with spherical microparticles in a non-magnetic medium. Larger particles tend to increase the MR response but also rapidly settle. On the other hand smaller particles are more stable against the sedimentation, but the MR response is insufficient. When the size of the particles approaches 10 nm, Brownian motion limits magnetic-field induced structuration.

In the presence of an external magnetic field, particles contained in MR suspensions create column-like structures which are able to support shear stresses, presenting large field dependent viscoelastic modulus and a yield stress. A lot of researchers deal with improving the MR response by addition of thickeners and stabilizers in order to provide more kinetically stable structures in their on-state MR suspensions. The main idea of magnetic additives is that physical networks can be formed among particles, which increase magnetic permeability [48].

4.1.2 The effect of the shape of particles

The influence of various particle shapes on MR performance was studied; for instance the spheres [4 – 9, 49], rods [50], wires [51], and fiber-like [13, 21] magnetic particles. The influence of plate-like particles on MR response in the literature is missing.

In general, MR suspensions prepared with non-spherical particles exhibit stronger structuration, which leads to higher storage modulus and higher yield stress. But in large particle concentrations and for large applied field the effect of larger structuration is less

noticeable. Non-spherical particles magnetize more easily, therefore are more effective in lower concentrations [48]. However, it should be noticed that particles more irregular in shape are more abrasive. Furthermore, highly irregular large particles lead to higher fluid off-state viscosity compared to spherical particles at the same volume fraction [31].

4.1.3 The effect of the porosity of the particles

In 2011 Vereda *et al.* showed that behavior of MR suspensions can be affected by particle porosity and roughness. Their study revealed that voids within particles lead to smaller density than that of the bulk material. Therefore, the same mass concentration of porous particles occupies a larger volume fraction which leads to different rheological behavior. Moreover, they derived simple mathematical models, which can quantitatively predict the differences in MR behavior of suspensions containing porous CI particles compared to conventional ones of a similar size [52].

4.1.4 The effect of particle coating

The effect of particle coating on MR effect is not well described in literature. The reason is that there are many possible coatings which can be grafted *via* many different processes and with many different thicknesses. Therefore, it is not easy to derive a relation which would precisely describe this phenomenon. However, the polymer coating may affect the off-state viscosity, which definitely causes a change in MR effect and in overall MR behavior, respectively. Hu *et al.* [53] reported that too high molecular weight of polymer coating can cause undesirable large increase in off-state viscosity.

4.2 Magnetic field

The magnetic field strength is the other factor, which affects the MR effect. The larger magnetic field strength strongly organizes particles which results in higher yield stress. This dependence is not linear and can be divided into three regions. The value of the yield stress can be predicted according to volume fraction of the particles Φ, magnetic field strength H, and saturation magnetization M_S. In conventional MR fluids the yield stress increases quadratically with the field strength, which describes the following equation [1]:

$$\tau_0 \approx \Phi \mu_0 H^2 \tag{24}$$

In larger fields, the yield stress can be calculated according to equation:

$$\tau_0 \approx \Phi \mu_0 M_S^{1/2} H^{3/2} \tag{25}$$

In very large fields, when the saturation magnetization is obtained, the yield stress reaches a maximum value, the yield stress is given by:

$$\tau_0 \approx \Phi \mu_0 M_S^2 \tag{26}$$

From the Equation 26 implies, that large saturation magnetization of the particles is the key to the ultimate strength of an MR suspension. The best available particles are alloys of iron and cobalt known as Permendur (M_S = 2.40 Tesla). However, such alloys are very expensive therefore, CI particles (M_S = 2.14 Tesla) appears to be the best option [54].

4.3 Temperature

The commercial devices using MR suspensions often operate at elevated temperatures, which can be a consequence of surrounding environmental conditions or the effect of viscous heating. Recently (2007), MR suspensions were used in devices for oil and gas exploration, where in subterranean operations the temperatures can be relatively high (up to 150 °C) because of the geothermal gradient. Ocalan *et al.* [55] reported that increasing temperature results in the MR stress reduction. Reduction in stress can be solved by application of higher magnetic field strength. However, there is a limitation in high-flux regime, when saturation magnetization is reached. Research and calculations how to estimate the stress drop with increasing temperature are described in literature [55].

In less concentrated suspensions the opposite effect was observed. The viscosity and toughness of the structures generated in the MR suspension by application of external magnetic field increase with increasing temperature [6, 25]. The results demonstrating this temperature dependence were proved by Mrlik *et al.* [25] with the use of CI particles coated with PPy ribbons in suspension containing 40 wt% of the particles. The detailed explanation of the temperature effect on the MR behavior is shown in the study by Machovsky *et al.* [6].

5 STABILITY OF MR SUSPENSIONS

The stability of the MR suspensions is complex problematic and affects the operational life of devices utilizing MR systems. Proper MR suspension should be resistant against external factors such as time, acid environment, air, temperature etc. In following sections are described individual factors and possibilities how to prevent potential drawbacks.

5.1 Sedimentation stability and redispersibility

The sedimentation stability is very important characteristic of MR suspensions. The possible settled particles may result in device failure. It is not possible to fully overcome this problem, because the dispersed particles are dense compared to the carrier liquid. For instance the density of dispersed particles such as iron is large (~ 7.80 g/cm^3) compared to density of common carrier liquid – silicone oil (~ 0.97 g/cm^3). In typical MR suspension dispersed particles settle out over a relatively short period of time (i.e. a few minutes to a few hours) [27]. Sedimentation stability is closely related to redispersion problems.

Once the particles are settled, the residual magnetic forces among them make redispersion difficulties. Such state of the suspension exhibits much lower MR effect of the system.

The possible solution for overcoming this problem can be the use of core-shell structured particles as a dispersed phase [4 – 9, 49]. Also the use of MR suspensions composed of magnetizable fibers exhibit improved stability against sedimentation, compared to suspensions of spherical magnetizable particles at the same concentration [1]. In relation to enhanced sedimentation stability, dimorphic MR suspensions can be prepared with a great success as shown by Sedlacik *et al*. [13]. In the study [13] the mixture of spherical and rod-like particles was used and besides better sedimentation stability, also increased MR activity was observed due to solid friction among fibers. In the other recent study [56] halloysite (clay mineral nanofiller) was successfully used, in order to improve sedimentation stability.

Also mixtures of magnetizable particles of the same material but of two different diameters so called bidisperse suspensions can be used to enhance MR behavior. Bidisperse suspensions show larger field-induced yield stresses and smaller off-state viscosities than monodisperse systems of small spheres or large spheres for the same total particle volume

fraction. This enhancement is due to small diameter spheres tend to break up aggregates of the larger particles which also contributes to enhanced redispersibility [1].

Recently Klingerberg *et al.* [57] described new approach how to enhance the stability of the MR suspension. The principle of this method is adding nonmagnetizable particles into MR suspension. Part of iron particles is replaced by cheap nonmagnetizable particles which is also great economical advantage. The addition of such particles (as fumed silica) alters the suspension microstructure, which is likely related to the observed rheological changes [57]. Such MR suspensions have lower densities, which should possibly lead to improved sedimentation stability, but the literature dealing with this kind of problematic have not been written yet.

5.2 Chemical stability

Very important characteristic of MR suspensions especially for practical applications is their chemical stability and anticorrosion properties. Chemical stability may be defined as a tendency of a material to resist change or decomposition due to internal reaction, or due to the action of air, acids, light etc. For instance, in the study [2] was studied durability of a MR damper. This study revealed that the carrier liquid thickens progressively and as a result the off-state (zero field) viscosity multiply by a factor 3 after 6×10^5 cycles. The increase in off-state viscosity results in lower efficiency of MR suspension. The thickening has been identified as a consequence of oxidation and changes in chemical composition of the carrier liquid. The operating condition in a damper was high shear rate in the range 10^4 – 10^5 s^{-1}. A similar problem reported Ulicny *et al.* in an MR fan clutch, where chemical changes of the particles caused undesirable decrease in torque capacity [58].

Nowadays the MR suspensions which exhibit good chemical stability are available. The MR suspension developed by Lord Corporation does not show substantial thickening even after 2 million cycles in the same conditions. For this purpose cobalt-iron alloys were used [2].

5.3 Thermo-oxidative stability

The next common drawback of MR suspensions is weak thermo-oxidative stability. A good thermo-oxidative stability of the particles used in MR suspensions is considerably important for practical utilization in devices. Due to poor temperature stability, metal oxides can be formed on the surface of the particles, which is undesirable. Non-magnetic metal oxides reduce magnetic properties which in case of MR suspensions lead to lower efficiency of the suspension and deterioration of MR effect [18, 26].

The oxidation can be prevented by adding suitable antioxidant additives into base suspensions, or preventing the access of the oxygen to the operating system of a MR device. The choice of antioxidant additives is a complicated issue. All additives must be chosen to not affect the other compounds of MR suspension. Furthermore, so-called depletion of antioxidant can occur, which is situation when the antioxidant can no longer fulfill its function [18].

The methods how to enhance chemical stability and thermo-oxidative stability of the particles are often similar. These methods include metal coatings, coupling agents, alloying of iron, organic (pain-like) coatings [26]. Some of these methods are discussed in US patent 5,578,238 [11]. The protective coatings of the MR particles can be composed of materials including:

- nonmagnetic metals – titanium, zirconium, hafnium, vanadium, niobium, tantalum, chromium, molybdenum, tungsten, copper, silver, gold, lead, cobalt-based alloys and nickel-based alloys
- ceramics – carbides, nitrides, borides, silicides, various cermets and many others
- thermoplastic polymeric materials – acrylics, polyphenylene sulfides, polyquinoxilines, polyetherimides and polybenzimidazoles
- thermosettic polymers – polyesters, polyimides, phenolics, epoxides, urethanes, rubbers and silicone

6 APPLICATIONS OF MR SUSPENSIONS

The automotive is one of the main areas of MR suspensions usage. The engineers are still trying to build safer, cheaper and better performing vehicles. For example the traditional mechanical systems are being replaced by electromechanical systems that are able to manage the same tasks faster, more reliably and more accurately.

6.1 Brakes

Conventional hydraulic brakes are being replaced by MR brakes with performance advantages. Hydraulic brakes have a lot of limitations, including delayed response (200-300 ms) due to pressure build up in hydraulic lines, heavy weight of components, low breaking performance in high speed and high temperatures and others [59]. MR brake consists of multiple rotating discs immersed in a MR suspension and an enclosed electromagnet. When a current is applied to the electromagnet, the MR suspension solidifies. Yield stress of the MR suspension varies as a function of applied magnetic field. This controllable yield stress produces shear friction on the rotating disks, generating the breaking torque. MR brakes are controlled electronically and as a result they have faster response and shorter breaking time.

Despite of all advantages of MR brakes there are still some problems with these devices. The main problem of MR brakes is their inability to generate sufficient breaking torque to stop a vehicle. The other problem of MR brakes is extremely severe heating which restricts their application in high-power situations. It is possible that this problem could be solved by different and more effective design of MR brake [59, 60].

The most recent type of MR brake (2013) has a water cooling system which assists in heat dissipation and results indicate that this MR brake is capable of producing a highly controllable brake torque [60].

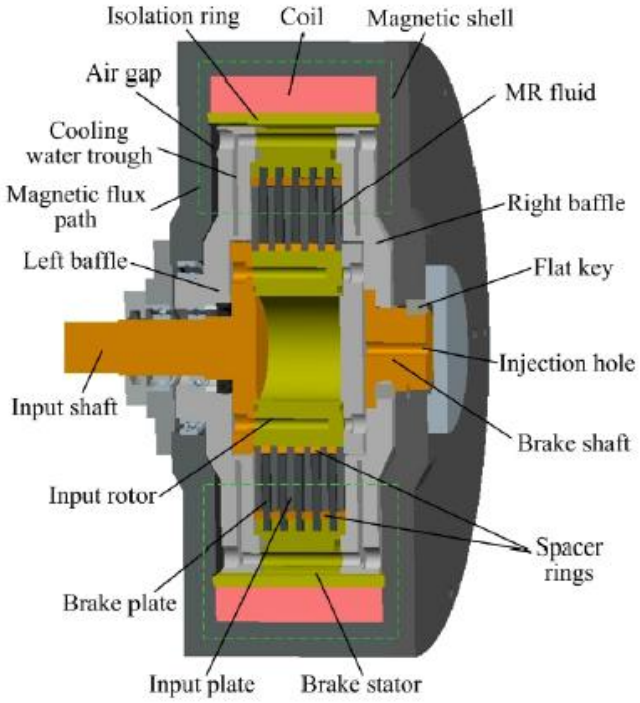

Figure 15. Schematic figure of high-torque MR brake [60]

6.2 MR dampers

MR dampers can be used in various applications – absorbers of seismic vibrations, foundation columns of the bridges, but the most widespread use of MR dampers is in automotive. Producers of the cars, manufacturers of the dampers respectively, are looking for new technologies in order to increase the driving comfort and improve handling.

MR damper used in [61] has twin-tube structure, which can operate in flow and shear modes. MR damper consist from piston in the centre and two chambers (left and right). These chambers are fully filled with an MR suspension. When the piston moves from left to right, the MR suspension will flow through the gap between inner cylinder and piston. Magnetic field generated by the coil has perpendicular direction to the movement of the piston. Magnetic field causes increase in apparent viscosity of the MR suspension which reduces the movement of the piston. Damping force depends on the force of magnetic field respectively on electric current which flows through the coil. The current for this type of damper is limited no more than 1.5 A, and the time of delay of MR damper is in about tens of milliseconds.

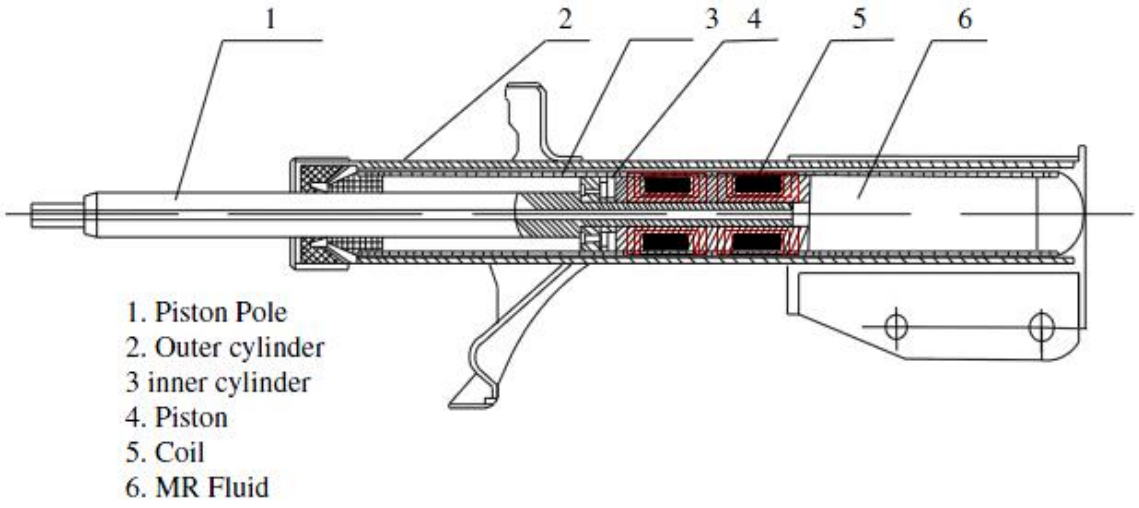

Figure 16. Schematic figure of MR damper [61]

The study of MR dampers is still in progress. In 2014, authors of the study [62] developed the FEM (finite element method) model built on the ANSYS platform to portray the behavior of the MR dampers. The graphical results were in good conformity with the experimental results obtained from a prototype of the MR damper. The results of their study can help the designers to create more efficient and reliable MR dampers.

MR materials are promising candidates for use in high-rise buildings or cable-stayed long-span bridges which are able to automatically and intelligently react to external dynamic loadings such as vibration shocks, strong winds and earthquakes. The constructions of such buildings must be very complex, because failures or collapses would mean tragic human and economic loses. The MR technologies integrated in building structures can mitigate the impact of these devastating natural effects [63].

The Donting bridge in China was the world´s first application of MR dampers on cable-stayed bridges. The bridge was completed in 1999, but its cables were sensitive to rain- and wind-induced conditions, therefore MR damping systems were installed and successfully finished in 2002 [64]. Currently, the studies are focused on algorithm development and optimization dealing with appropriate reaction on vibrations [63].

Figure 17. The Donting Lake Bridge equipped with MR dampers in China [64]

6.3 Clutches

The concept of MR torque transition was initially proposed by Rabinow [14]. The recent developments in MR technology also result in intense research of MR clutches. These devices were studied by General Motors with the objective of reducing the fuel consumption due to the lower off-state viscosity and smoother torque transitions of MR suspensions. The MR suspension is located between the lamellas and the coil is around the perimeter of the clutch. The viscosity of MR suspension and thereby a size of transmitted torque is controlled by the current applied in the coil. Main problem of these devices is insufficient performance. With the intention of torque increase double-plate MR clutch was designed [65].

6.4 Other applications

MR suspensions are also used in medical devices, for instance robotic leg [66], smart rehabilitation devices [67], and body fitness equipment [68].

6.4.1 Application of modified magnetic particles

Magnetic particles such as CI are not only used in MR suspensions, they are also promising materials in medicine and biotechnology for delivering drugs to specific locations within the body, hyperthermia or magnetic separation. Conventional drug use results in non-specific distribution to tissues, and only a small fraction of the dose reaches the intended site. Therefore, large amounts of drugs must be administrated, and the residual dose burdens the organs which are not involved in the pathological process.

In this approach, the drug is first bound on the magnetic particles and then the magnetic system is injected into a regional artery feeding the targeting site, while the external magnetic field is imposed onto this area. The drug will not redistribute, high local concentrations of the drug are created and the rest of patient´s body is unaffected. For magnetic targeting drugs the surface of magnetic particles is very often functionalized with various chemical groups so that they are able to bind active molecules. However, this technique is very complex and requires the properties such as biocompatibility, stability of particles as well as their surface coatings [69].

II. ANALYSIS

7 MATERIALS

CI powder used throughout this work is a commercial product of BASF Corporation, SL grade (Ludwigshafen, Germany). Chemical composition of CI given by manufacturer is min. 99.5 % of pure iron, and max. 0.05 % of carbon as an impurity.

Monomer, glycidyl methacrylate (GMA) (purity = 97%; contains 100 ppm monomethyl ether hydroquinone as inhibitor) was used for ATRP polymerization. Other chemicals involved in ATRP were Ethyl α-bromo isobutyrate (purity = 98%), α-Bromo isobutyryl bromide (purity = 98%), (3-Aminopropyl) triethoxysilane (purity ≥ 98%), Triethylamine (purity ≥ 99%), *N,N,N´,N´´,N´´*- Pentamethyl-diethylenetriamine (purity ≥ 99%), Copper (II) bromide (purity ≥ 99%), Anisole (ReagentPlus®, purity = 99%), Aluminum oxide (neural, Brockmann I), all were produced by Sigma Aldrich Chemie GmbH (St Louis, USA) and were used as received.

Silicone oil used for preparation of MR suspensions was Lukosiol M200 (Chemical Works Kolín, Czech Republic).

Solvents and purification agents, namely Tetrahydrofuran p.a. (purity ≥ 99.8%), Acetone p.a. (purity ≥ 99.5%), Ethanol absolute anhydrous p.a. (purity ≥ 99.88%), Toluene p.a. (purity ≥ 99%) were obtained from Penta Labs (Praque, Czech Republic).

All the chemicals were used without further purification.

8 MODIFICATION OF THE PARTICLES WITH POLYMER

The primary aim of this study was to prepare modified CI particles with enhanced stability for magnetorheology purposes. Particle coating is one of the approaches how to improve the stability of fluids containing particles [53]. For surface modification of CI particles was selected poly(glycidyl methacrylate) (PGMA) and polymer chains were covalently grafted onto the surface of CI particles *via* surface-initiated ATRP. Polymer surface treatment of CI particles provides long operating life and prevents damage of devices which utilize MR suspensions. Moreover the surface treatment of particles prevents aggregation among the particles, reduces abrasion, settling, redispersibility, chemical stability, and durability of MR suspensions [7, 25, 58, 70].

But in addition, its monomer glycidyl methacrylate (GMA) has recently gained special interest in very specific applications such as drug and biomolecule binding, due to the presence of easily transformable oxirane group. This functional group retains the reactive nature, and it can undergo further reactions in order to receive additional useful properties (e.g. ability to respond to heat, change in pH, etc.) [71]. It is important to note that PGMA is biocompatible, so PGMA-treated particles can be further used in medicine. The epoxy group may be used for binding drugs which might be controllably delivered to desired areas within the body.

The modification of particles with PGMA was conducted in several intermediate steps as described below.

8.1 Surface activation

The first step in the modification of CI particles with polymer is the surface activation of the particles. Their surface should be substantially free of contamination products. Therefore, the treatment of the CI particles with 0.5 M HCl was utilized and non-magnetic iron oxides and possible contaminants were removed. In MR suspensions, dispersed particles with contamination-free surface exhibit significantly enhanced MR effect [11]. Therefore, 100 g of raw CI particles was transferred into a beaker with 250 mL of 0.5M HCl aqueous solution, and generated suspension was mechanically stirred for about 10 minutes. The intensity of mixing was chosen at 400 rotations per minute (rpm). Then the

CI particles were captured by magnet at the bottom of the beaker and solution was thoroughly washed with distilled water, ethanol and finally with acetone.

After washing, the suspension was poured into a Petri dish and placed for 3 hours into a drying oven heated at 60 °C. Then, the residual acetone was removed by the evacuation at a pressure of 200 mbar for 1 hour. Dry particles were poured together into a sealable container. The yield of this process in laboratory conditions is > 95%. Some of the particles were not captured by magnet during the washing process and the suspension was not quantitatively transferred from the beaker into a Petri dish, which caused losses.

8.2 Functionalization of activated CI particles

The next step in the modification is functionalization of the activated CI particle surface. Due to previous reacting step (Section 8.1) the surface of particles has more active sites, therefore it is able to bind larger amount of coupling agent, in our case (3-Aminopropyl)triethoxysilane (APTES).

Activated iron particles (90 g) were weighted into 500mL three-necked flask. These particles were dispersed in 300 mL non-polar solvent, toluene. Then 10 mL of silane agent (3-Aminopropyl)triethoxysilane was added into the suspension. Into three-necked flask was placed a mechanical stirrer and thermometer. The entire assembly was placed into a heating mantle and stirred for 6 hours at 110 °C. Intensity of agitation was 250 rpm.

After the reaction, suspension was thoroughly washed with toluene, ethanol and acetone. Then the suspension was similarly as in the first step poured into a Petri dish and placed into an oven heated at 60 °C to evaporate the residual acetone.

With this reaction was reached that the coupling agent APTES was covalently attached on the surface of CI particles. Through functional groups ($–NH_2$) of APTES was possible to perform the other reaction (Figure 18). In other words the specific ATRP initiator α-Bromoisobutyryl bromide (synonym: 2-Bromo-2-methylpropionyl bromide, BIBB) was grafted in following reacting step. The –Br groups reacted with $–NH_2$ and formed –NH–CO– linkage (Figure 19) and simultaneous cleavage of HBr.

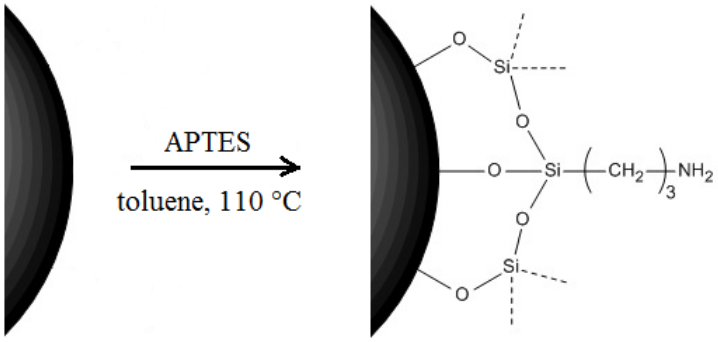

Figure 18. CI particle activated (left) and functionalized with silane agent (right)

8.3 Immobilization of the initiator

Binding of the initiator takes place in the environment of tetrahydrofuran (THF) which preferentially reacts with water. In this reaction the water is very undesirable. Therefore, into 100 mL of THF was thrown a piece of sodium, which reacts with water present in the THF and gives NaOH so the water was removed.

Into Schlenk flask (SF) was added 40 g of CI particles modified with APTES silane agent (CI/APTES) and the space of the flask was evacuated for 30 minutes. After that, the argon atmosphere and 16 mL of triethyleneamine (Et_3N) was put into the flask through a needle. Then 8 mL of BIBB was added into the solution. This reaction is usually performed in the absence of the moisture to obtain as high yield as possible. After that, the initiator-treated CI particles (CI/BIBB) exhibited formed molecular structure of BIBB on their surface.

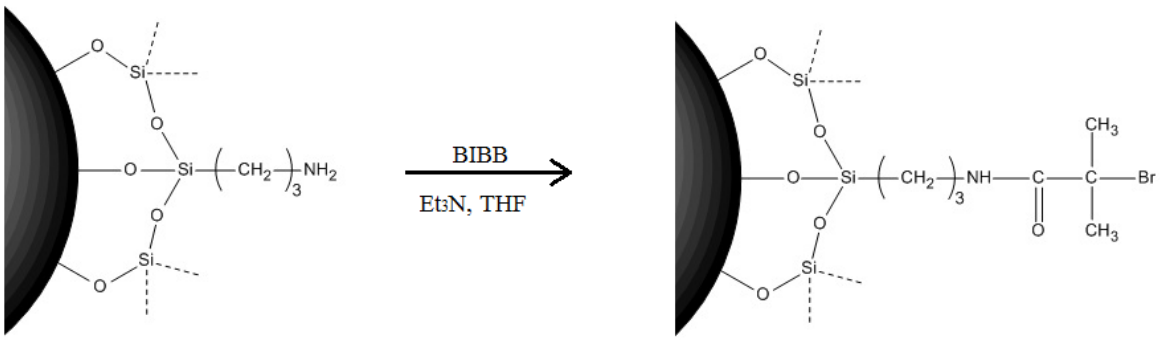

Figure 19. Immobilization of initiator

8.4 ATRP polymerization

ATRP is widely used to synthesize polymers with controlled morphologies, functionality, and composition. For this polymerization technique is necessary organic halide initiator and metal halides, e.g. cuprous halide, as a catalyst and ligand to improve the solubility metal salt in the organic reaction system [70]. ATRP can be performed with wide range of monomers at mild conditions or elevated temperature. ATRP appears to be an effective tool in covalently grafting various polymers onto the inorganic surface. The polymers synthesized by this technique exhibit controlled chain-length and narrow polydispersity index.

8.4.1 Reference polymerization

Before the ATRP polymerization, the reference polymerization was performed to determine kinetics of polymerization with no particles in the system. The overall rate of polymerization is influenced by several internal factors, such as initiator, catalyst, ligand, type of transferring halogen, and external variables such as temperature and time [53].

The polymerization was carried out in SF which was evacuated and then filled with argon. All required components for polymerization were gradually injected into prepared SF. CuBr was used as a catalyst and *N,N,N ',N'',N''*-pentamethyldiethylenetriamine (PMDETA) was used as a ligand, and the anisole served as suitable environment for ATRP process. The reason of usage ethyl α-bromoisobuthyrate will be discussed in Section 11.1.

The molar ratio of components was:

[GMA]:[ethyl α-bromoisobuthyrate]:[CuBr]:[PMDETA]:[anisole] = [100]:[1]:[1]:[1]:[100]

SF was frozen in liquid nitrogen after injecting all of the reactants into the system (except for CuBr). The space of the flask was evacuated in the frozen state in order to eliminate pertinent air. If the evacuation was carried out at normal temperature, the air but also others volatile components (monomer) would be evacuated, which is undesirable. The content of the flask was again transferred to a liquid state after the evacuation. It was possible to observe the air bubbles outgoing from the volume of the mixture. Therefore, the SF was frozen again and the evacuation was performed again. This freeze-pump-thaw cycles were repeated several times until the amount of leaking air bubbles was minimized.

Successful ATRP requires fast initiation so that all propagating species begin to grow at the same time, which results in a narrow molecular weight distribution [53]. Therefore, the argon atmosphere was maintained in the SF and weighted CuBr was added as quickly as possible. The reacting system was placed into pre-heated silicone oil (M50) bath at temperature 50 °C. The volume of the flask was well stirred, after 16 hours the reaction was stopped by opening the flask.

8.4.2 Polymerization in the presence of silane-treated CI particles

This reaction was performed in order to investigate the polymerization kinetics in the presence of the CI particles. CI particles did not contained BIBB structure on their surface, therefore the polymerization could not proceed from the surface, but presence of CI particles affected the kinetics of the reaction. The procedure was the same as in the previous case (Section 8.4.1), but this time CI particles were put into system besides the other components.

It is advisable to use a mechanical mixer and work in an inert atmosphere, otherwise work can be done in the vacuum using a magnetic stirrer when magnetic particles are not involved in the system. The sample was taken after 16 hours.

It was found that the polymerization is much faster in the presence of the particles under the same process conditions compared to polymerization without particles. The result of the polymerization after 16 hours was elastomer-like matter, which meant that the polymer chains started to crosslink. For this reason, the molar ratio of reactants was modified to:

[GMA]:[ethyl α-bromoisobuthyrate]:[CuBr]:[PMDETA]:[anisole] = [200]:[1]:[1]:[1]:[200]

It is important to correctly estimate the kinetics of the polymerization, thus the time of polymerization necessary for growth of suitable polymer chains. The molecular weight of grafted polymer chains has a great influence on properties of incurred MR particles. Molecular weight of coating polymer can affect the viscosity and settling rate of MR fluid. If it is too low, the polymer will not prevent CI particles from settling. On contrary, too high molecular weight of coating polymer can cause undesirable large increase in off-state viscosity [53]. Therefore, CI particles coated with PGMA of two different molecular weights were prepared. The length of polymer chains and molecular weight respectively was increased with an increase of molar ratio between GMA and initiator.

8.4.3 Graft ATRP polymerization I (lower molecular weight polymer chains)

CI particles with linked initiator were used in this polymerization described in Section 8.3. Working procedure was similar to the previous one (Section 8.4.2). After the last re-freezing cycle SF was placed into a glove box where its content was stirred with a mechanical stirrer at 175 rpm intensity. After two hours, the stirring was stopped. Then the particles could sediment and a sample was taken for the characterization of the polymer by gel permeation chromatography (GPC) and nuclear magnetic resonance (NMR).

Notice that in the reaction was involved Ethyl α-bromo isobutyrate. Thus, the polymer chains were growing from the CI/BIBB particles as well as from this compound. Therefore, the NMR and GPC measurements could be performed.

8.4.4 Graft ATRP polymerization II (higher molecular weight polymer chains)

The aim of this polymerization was to prepare CI particles, which have grafted longer polymer chains on their surface (shell). As mentioned before, molecular weight of polymer was increased with an increase of molar ratio between GMA and initiator. Therefore, the molar ratio of the reactants was selected:

[GMA]:[ethyl α-bromoisobuthyrate]:[CuBr]:[PMDETA]:[anisole] = [300]:[1]:[1]:[1]:[300]

Preparation of these particles was carried out the same like in the case (Section 8.4.3).

Prepared core-shell structured particles were washed with THF (several times) and acetone and then dried several hours at 60 °C. After drying, the particles were characterized by several analytical methods and further suspensions of such particles were prepared and investigated. The schematic figure (Figure 20) shows the PGMA polymer chain grafted on CI particle *via* ATRP.

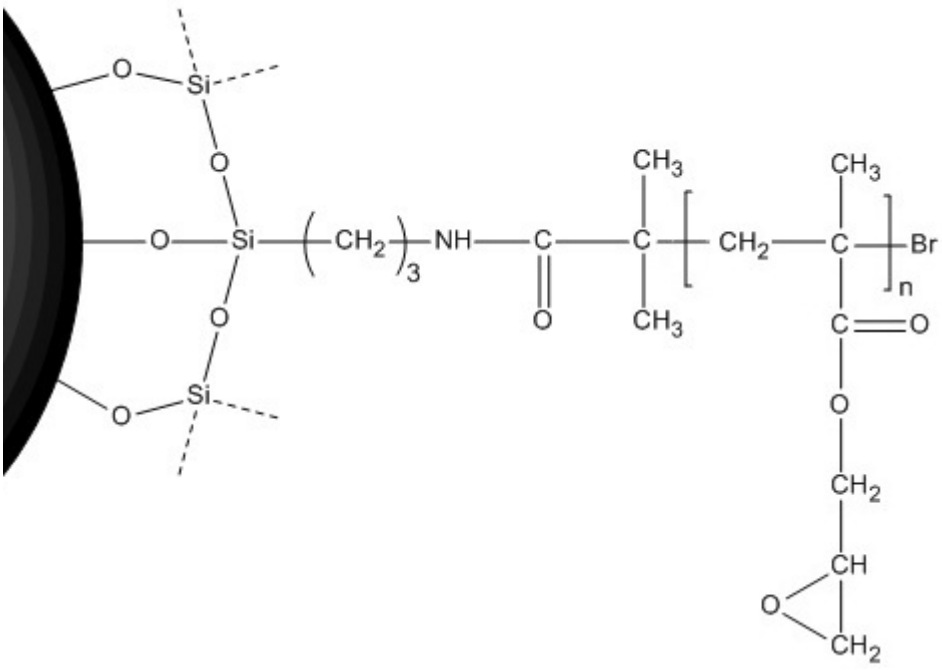

Figure 20. Schema of the structure of prepared CI/PGMA particle

9 CHARACTERIZATION OF THE PARTICLES

9.1 Nuclear magnetic resonance (NMR)

NMR spectroscopy was used in order to determine ATRP polymerization processes (Sections 8.4.3, 8.4.4) also molecular weights of prepared polymer chains were analyzed. NMR measurements were performed on a 400 MHz VNMRS Varian NMR spectrometer (Varian Inc. since 1999 part of Agilent, USA) equipped with a 5 mm 1H–19F/15N–31P PFG AutoX DB NB probe at 25 °C using deuterated chloroform ($CDCl_3$) as a solvent.

Both samples were taken after 2 hours from the beginning of each polymerization. The sample (green polymer solution) was taken by the injection and then was passed through aluminum oxide (neutral), absorbent cotton and microfilter in order to remove the copper-containing chemicals. The colorless filtrate was additionally supplemented by $CDCl_3$ and evaluated using NMR.

9.2 Gel permeation chromatography (GPC)

GPC also referred as Size Exclusion Chromatography (SEC) is an analytical method in which the components of a mixture are separated on the basis of their size. In GPC, the sample is applied into a column filled with porous beads. The smaller molecules can enter the pores, in which they spend more time, therefore large molecules elute from the column first [72].

GPC PL-GPC220 (Agilent, USA) was used to determine the relative molecular weight of the polymer samples as well as the distribution of molecular weights, during the polymerization. THF was used as an eluent (mobile phase) at a flow rate of 1.0 mL/min. The polystyrene was used as a standard to calibrate the GPC, and anisole was used as an internal standard to correct any fluctuations in THF flow rate.

The sample of polymer was taken two hours after beginning of the polymerization then was mixed with the solvent contained in the GPC column, namely THF. The polymer solution was passed through aluminum oxide (neutral), absorbent cotton and microfilter. Aluminum oxide reacts with copper ions and separates them from the prepared sample. However, this purification method associated with the need of high concentration of catalyst was overcome. In modern ATRP techniques the removal of the copper is not a

problem due to development of higher activity catalysts, which reduced the amount of copper down to ppm levels [10]. The purified polymer solution was applied into a GPC column. The temperature of the column was maintained at 30 °C.

9.3 Scanning electron microscopy (SEM)

Physical properties of prepared particles including size, shape, and surface morphology were studied with the use of scanning electron microscopy (SEM). For this purpose device (Tescan Vega II LMU, Czech Republic) was employed using 5 – 10 kV accelerating voltage.

SEM microscope used during this study has two different detectors. The primary electron beam interacts with the specimen and the electrons undergo two types of collisions. Elastic collisions in which the energy of the incident electrons is uncharged give rise to the backscattered electron signal (BSE). Inelastic collisions give rise to the secondary electron (SE) signal [73]. In this study all images were taken with the use of SE detector, due to its higher depth of field. The SE detector is also superior for displaying surface detail and particle morphology but does not generally show chemical heterogeneity.

9.4 Energy dispersive spectroscopy (EDS)

The SEM microscope (Tescan Vega II LMU, Czech Republic) is equipped with an energy-dispersive spectroscope which provides the information on the chemistry, surface elemental analysis respectively of individual prepared particles.

Interaction of primary beam with atoms in the sample causes inner electron shell transitions, which result in the emission of X-rays. Two types of X-rays are generated. The continuous X-rays generate a broad background over the entire X-ray spectrum. Characteristic X-rays generate narrow discrete peaks whose energies are characteristic for specific elements in the sample. The fraction of X-rays is analyzed by an EDS analyzer. A standard sampling depth is 1 – 2 μm. EDS detection is limited for elements Na to U in bulk materials. Therefore, the EDS was utilized as an effective tool for elemental analysis of particle surface [73].

9.5 FT-IR spectrometry

The surface chemical structure of pure (CI) and composite particles (CI/PGMA) was investigated using FT-IR (Fourier transform infrared) spectroscope (Nicolet 6700, USA) equipped with iD5 ATR accessory. The technique was employed in order to prove the successful coating process performed on the CI particles.

This analytical method is based on the absorption of infrared (IR) radiation passing through the test sample of the material. An attenuated total reflection (ATR) accessory measures the changes that occur in a totally internally reflected IR beam when beam comes into contact with a sample. The depth of penetration into a sample is dependent on the refractive index of the ATR crystal therefore we note that diamond crystal was used for this purpose. The measurement was performed with the radiation from mid-infrared (mid-IR) region, which covers wavenumbers in the range 4000 – 400 cm^{-1}. The radiation covers energies which are too low to cause electron transitions in the molecules. However, vibrational transitions occur from the absorption of mid-IR radiation [74]. These transitions correspond with distinct wavenumbers that depend on molecular structure of the compound. Therefore, the result of the mid-IR spectral analysis provides the information on the chemical bonds and the molecular structure of the test sample.

9.6 Magnetic properties

Measurements of the magnetic behavior of the iron powder and also both types of prepared core-shell particles were made using Vibrating-Sample Magnetometer (VSM); (Lakeshore, USA). VSM belongs to most widespread magnetometers. In VSM the vibrating sample is placed in an external magnetic field. The sample induces a voltage which is detected by the detection coils. The value of voltage is directly proportional to the magnetic moment *m*, respectively, the magnetization *M* of the sample. This technique is very suitable for detecting the saturation magnetization [75].

Approximately 200 – 300 mg of sample was subjected to magnetic field. Strength of magnetic field was ±10 kOe. The measured data include the hysteresis curves, which show the magnetization as a function of the magnetic field strength. But the primary interest was M_S which is important for MR devices. The saturation magnetization determines the maximum yield stress obtainable for MR fluid prepared from such a powder.

9.7 Chemical stability

Anti-acid-corrosion properties of raw uncoated CI particles and both variants of CI/PGMA composite particles were investigated. The 1 g of appropriate particles was placed into a beaker and 20 mL of 0.05M HCl was poured into the system. The generated suspension was mechanically stirred and the sensor of digital pH-meter (Greisinger electronic, GPRT 1400, AN, Germany) was inserted into resulting suspension. Before the measurement the pH-meter was calibrated with two standard buffer solutions. After each measurement the probe of pH-meter was rinsed with distilled water to remove any traces of measured solution. Than the remaining water was removed with a scientific wipe because the remaining water could dilute following measured sample. All measurements were performed at room temperature. The pH value was plotted as a function of time.

9.8 Thermo-oxidative stability

Thermo-oxidative stability is very important characteristic of the MR particles which importance was discussed in theoretical part of this thesis. Therefore this property of prepared particles was also measured and compared to bare CI particles. The thermo-oxidation resistance of raw CI particles and both variants of coated particles was examined using thermogravimetric analysis (TGA); (TA Instruments Q500, USA) under an air atmosphere at a heating rate of 10 K/min. TGA is an analytical technique used to determine material thermal stability and its fraction of volatile components. TGA device works as precise analytical scales and monitors the weight change that occurs when a specimen is heated. The weight changes are the result of the evaporation, thermal decomposition or chemical reaction. They can be also a consequence of gas absorption (oxygen, moisture, and others). During all TGA measurement weight gain of samples was observed, which indicated the ongoing chemical reactions. The weight gain was further plotted as a function of temperature.

10 CHARACTERIZATION OF THE SUSPENSIONS

10.1 Preparation of the suspensions for magnetorheology measurements

Three variants of MR suspensions with the same particle concentrations (60 wt%) in silicone oil were prepared. The first suspension contained 60 wt% of bare CI particles in silicone oil, the second suspension contained 60 wt% of CI particles coated with PGMA with lower molecular weight (prepared according to procedure in Section 8.4.3), while the last suspension contained 60 wt% of CI particles coated with PGMA with higher molecular weight (prepared according to procedure in Section 8.4.4).

The calculated amount of CI particles was inserted into a vial and the appropriate amount of silicon oil was added by the injection. The preparation was carried out very precisely with the use of analytical scales (KERN ABJ 120-4N, Germany). The tested MR suspensions were prepared by thoroughly mixing the CI particles in the silicon oil, with the intention to create well-dispersed system for the measurement. All MR suspensions were prepared using silicone oil. The measurements were carried out with bare CI particles in the suspensions and also with both coated CI particles analogues.

10.2 Rheological properties in steady shear flow

The rheological properties of MR suspensions in steady shear flow in various magnetic flux densities were experimentally studied. To obtain the flow curves (shear stress vs. shear rate), measurements were carried out on Physica MCR502 (Anton Paar GmbH, Austria) parallel plate rheometer equipped with a magnetic cell (Physica MRD 170+H-PTD200). Parallel plate (PP20/MRD/TI) geometry with a diameter of 20 mm was selected for this study to obtain flow properties of MR suspensions in the absence as well as in the presence of various magnetic flux densities. The PP geometry was used despite the fact that the shear rate is not constant in this geometry, unlike the CP geometry. The reason is that field-induced structure in MR fluids strongly depends on the geometry, and the average aggregate length is one of the major features determining the rheological response, so in PP geometry the gap thickness is constant in all the sample volume which is desirable [47]. A gap of 0.5 mm was maintained between the plates and a 0.2mL sample of MR fluid was placed between them.

At this point it is important to mention, that Chen *et al.* [76] have shown that rheological measurements are also influenced by important factor – the plate gap distance. Basically, the shear stress increases with increasing gap distance. Theoretically, the number of particle chains in the gap with the same volume fraction remained constant, but with the increase of the gap distance, the length and the tilt angle of the particle chains increase. As a result, a larger shear stress is achieved. Therefore, the plate gap distance was maintained on the same value during this study.

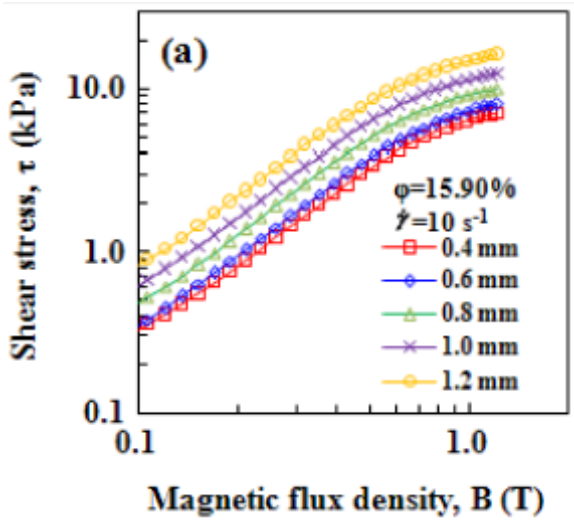

Figure 21. The effect of the plate gap distance [76]

A magnetic flux density perpendicular to the plates from 0 to 363 mT was used for measurements and the temperature of all samples was maintained at 25 °C with a closed-cycle cooling system (Julabo FS18 and Julabo F12, Germany). To avoid sedimentation, the tests were started as soon as the thoroughly mixed fluid was injected into the measuring system. Two different operate modes of MR suspensions were selected – steady shear flow and oscillatory shear mode.

For the mathematical analysis the function “Solver” as a part of Microsoft Excel was used. This function can be considered as a good tool for non-linear data fitting.

10.3 Rheological properties in oscillatory flow

The preparation of the suspensions for oscillatory tests was carried out with the same manner as for steady shear flow measurement. Also process conditions for the small-strain oscillatory shear tests were retained same.

The small-strain oscillatory tests were carried out through strain sweeps and frequency sweeps. The linear viscoelasticity (LVE) region was found through G' and G'' measurement as a function of strain γ. The used strain range was (10^{-5} – 10^{1}) % at a fixed frequency 1 Hz under all magnetic flux densities.

After finding border of LVE region, the frequency sweeps were measured in the range of frequencies (0.1 – 10 Hz) at a constant amplitude strain (obtained from LVE investigation). A representative sample was prepared before each measurement (Section 10.1). Then, an appropriate amount of suspension was injected into measuring geometry and prior to each measurement field-induced structures were agitated by continuous shearing (shear rate 50 s^{-1}) for one minute. Then, the new magnetic field was imposed.

10.4 Sedimentation stability

Sedimentation measurement was performed with Tensiometer Krüss K100 (MK2/SF/C, GmbH, Hamburg, Germany) which allows study the sedimentation velocity of the suspensions, surface tension, among other material properties. The funnel-shaped measuring probe is hung up on scales and immersed in the test suspension. The measuring probe captures the settling particles and evaluates their weight as a function of time, which allows determination of the sedimentation velocity.

For this purpose the suspensions containing 10 wt% of the CI particles (or coated CI particles respectively) in silicone oil (M200) were prepared. Each suspension was placed into a clean beaker then properly mixed and then was put into ultrasound device (UP400S Ultrasonic processor, Hielscher Ultrasound Technology, Germany) for 2 minutes. The measurement was carried out at the room temperature. The taken sample correctly represented the MR dispersion. The measuring time was set until plateau in mass increment was observed (in our case 2 hours).

11 RESULTS AND DISCUSSION

11.1 NMR – results

During polymerization two different compounds from which polymer chains were able to grow were in the reacting system. First compound was Ethyl α-bromo isobutyrate which molecules were unbound in the system. Second compound was α-Bromo isobutyryl bromide which was covalently bounded on the surface of CI particles. Once the polymer chains are grafted on the substrate (in our case CI), the NMR (and also GPC) measurements are not possible. Therefore, NMR and GPC measurements were performed with the use of unbound polymer chains in the system.

Thus, molecular weight of unbound polymer chains and the amount of unreacted monomer were analytically measured, and the molecular weight of bounded polymer chains was indirectly determined.

Two different variants of CI/PGMA particles differing in molecular weight of grafted PGMA polymer chains were prepared. Both polymerizations were stopped after two hours. NMR analysis was used to monitor the ATRP process. NMR measurement revealed higher amount of monomer units linked to Ethyl α-bromo isobutyrate compared to CI/BIBB particles in both polymerizations.

Reaction performed according to procedure described in Section 8.4.3 was stopped after reaching 87.0% conversion while the unbound polymer chains exhibited molecular weight 24 708 g/mol. Conversion value expresses the percentage of monomer units built into polymer chains (unbounded and bounded polymer chains together). For reaction performed according to procedure described in Section 8.4.4 conversion value 88.5% was reached and unbound polymer chains exhibited with 37 701 g/mol molecular weight.

Notice that both polymerizations took place separately with different molar ratios of reactants, therefore the small difference in conversion means a large difference in molecular weights.

11.2 GPC – results

Figure 22 shows the GPC curves for the PGMA polymer chains with lower (a) and higher (b) molecular weight grafted on the surface of CI particles. Both GPC curves of polymers exhibit monomodal character in the sense of one main peak. The width of both curves is similar, that is the sign of similar molecular weight distribution.

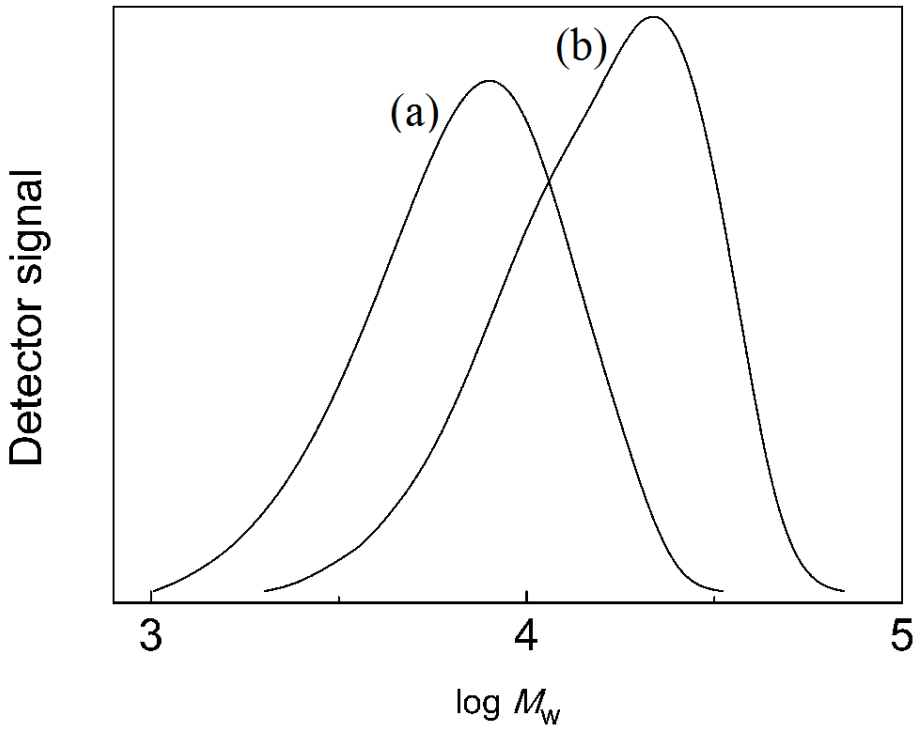

Figure 22. GPC chromatograms of PGMA polymer chains with (a) lower and (b) higher molecular weight

GPC analysis revealed that PGMA polymer chains of first variant prepared core-shell structures exhibited number average molecular weight ($\bar{M}_n$) 6600 g/mol with 1.31 PDI. The conversion of monomers built into polymer chains bounded on the initiator-treated CI/BIBB particles was determined as 23 %. The $\bar{M}_n$ of the second variant polymer chains grafted on CI particles was 12500 g/mol with 1.29 PDI. Result of conversion obtained from GPC measurement was in the second case 29 %. The relatively low values of PDI´s mean that ATRP system was well controlled.

11.3 SEM – results

The particles were not metal-coated for the SEM analysis, because they are composed from electrically conductive material. However, particles containing the polymer shell were a little charging by electron beam and the brightening was observed in the micrographs. SEM micrograph of commercial CI particles grade SL is displayed on the Figure 23, whereas micrographs of coated particles are presented in the Figures 24, 25.

SEM analysis revealed that bare CI particles as well as CI/PGMA particles have spherical shape and average particle size around 1 – 5 microns. Moreover, SEM analysis also found the presence of the rod-like particles in the sample which is probably an incomplete product of CI synthesis (Figure 23). Changes in morphologies between bare CI particles and CI/PGMA particles were also observed. The surface of bare CI particles is quite smooth, whereas surface of coated CI particles is rougher, which indicates the presence of grafted PGMA polymer chains.

On micrographs of PGMA-coated particles (Figures 24, 25) can be seen the black spots or the holes in the surface of the particles, which leads us to presume, that some defects within the polymer coating also appear.

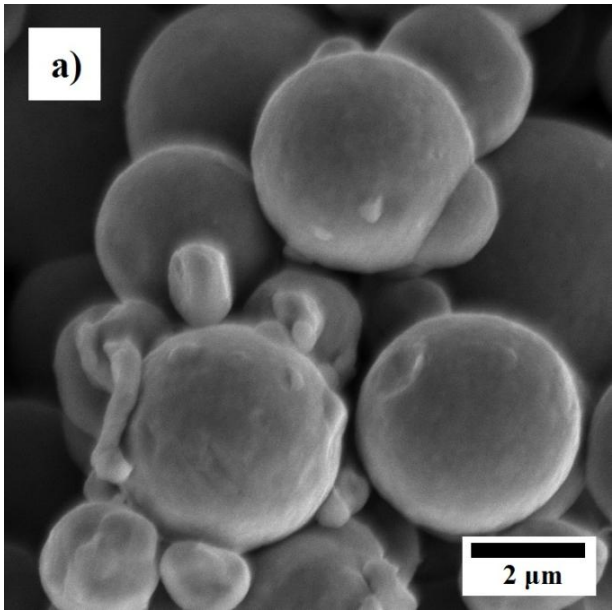

Figure 23. SEM image of bare CI particles

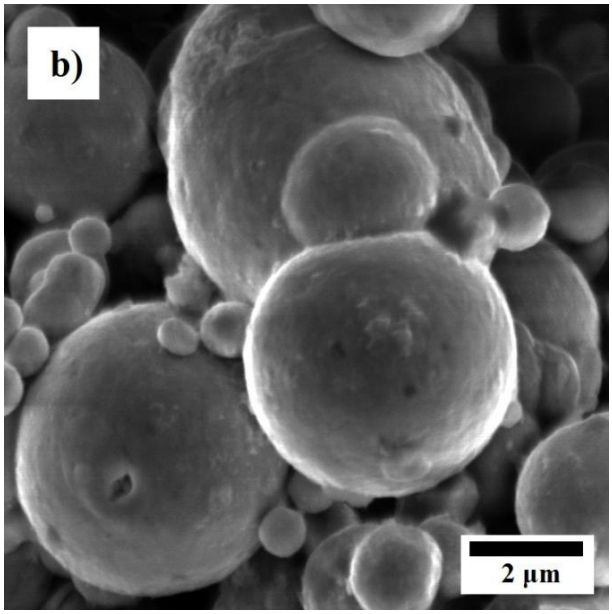

Figure 24. SEM image of CI particles coated with PGMA with lower molecular weight

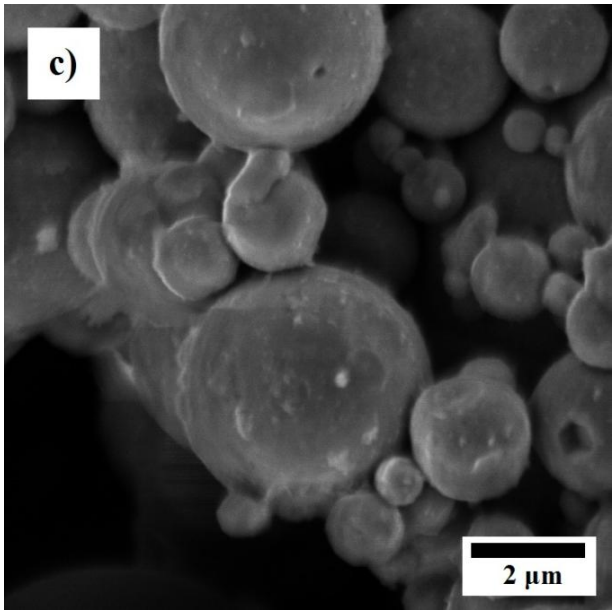

Figure 25. SEM image of CI particles coated with PGMA with higher molecular weight

However, the SEM analysis provides the information about the particle shape and morphology, with SEM only a small fraction of particles can be measured, thus an accurate measurement of particle size distribution (PSD) is not possible in this case.

11.4 EDS – results

Figure 26 shows a representative EDS spectrum of raw CI powder. As expected, the examined sample is almost pure Fe with some C contained as an impurity. However, the content of C impurity was little higher then producer states.

The EDS spectrum of PGMA-coated CI particles with lower molecular weight is illustrated in the Figure 27. The most represented element is the Fe. The second frequent element is C, which is partly from CI impurity and partly from the individual components (coupling agent, residue of initiator, PGMA chain) which constitute the whole polymer chains. These components also contain O which is also part of the spectrum. EDS analysis also revealed the Si atoms which comes from the coupling agent (3-Aminopropyl)triethoxysilane.

Atoms of N originating from coupling agent and atoms of Br originated from initiator were not revealed, probably because they are in very low concentrations in the sample. In general, EDS analysis proved the presence of expected elements, which indicates a successful coating process.

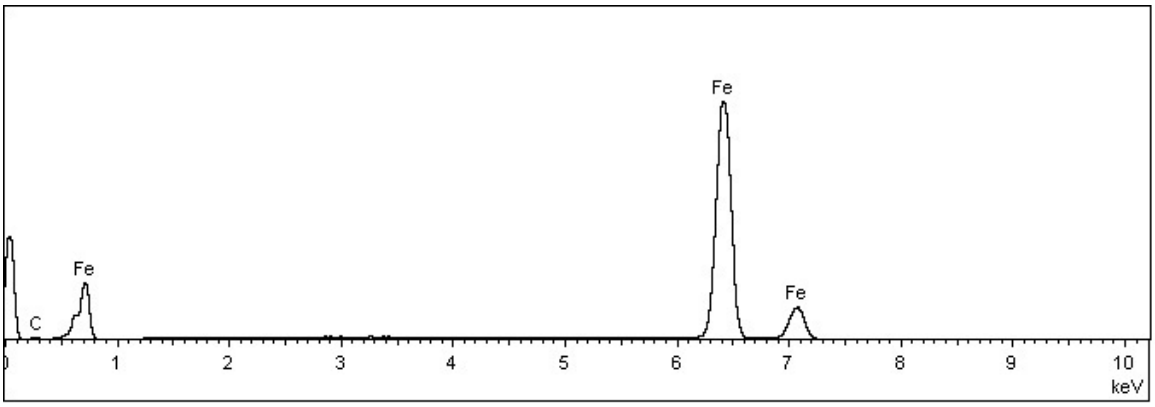

Figure 26. EDS spectrum of bare CI particles

Table 2. Result of EDS analysis for bare CI particles

Element	Weight%	Atomic%
Fe	95.48	81.97
C	4.52	18.03

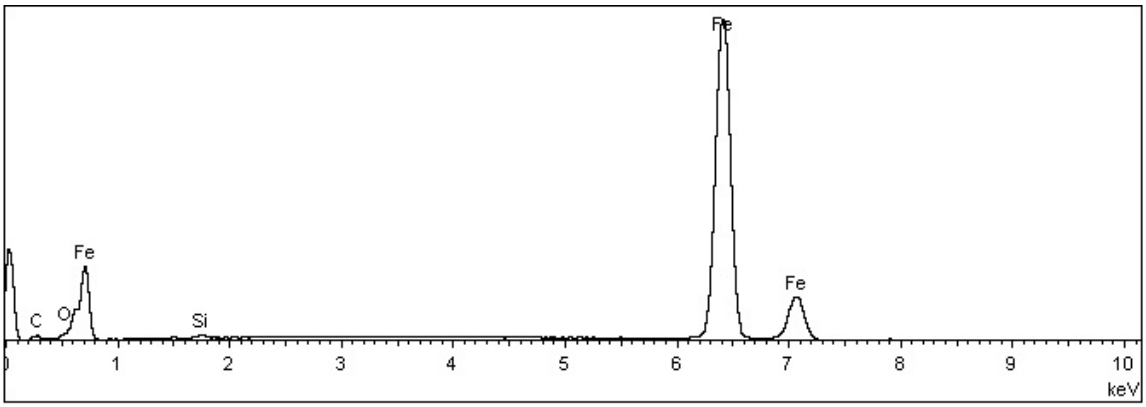

Figure 27. EDS spectrum of CI particles coated with PGMA (with lower molecular weight)

Table 3. Result of EDS analysis for CI particles coated with PGMA (with lower molecular weight)

Element	**Weight%**	**Atomic%**
Fe	89.14	65.71
C	8.12	27.84
O	2.21	5.69
Si	0.52	0.77

11.5 FT-IR – results

FT-IR spectral curves of bare CI particles and PGMA-coated CI particle were compared. Figure 28 illustrates the differences in wavenumbers of individual spectra. In the spectrum of the CI/PGMA composite particles, the appearance of characteristic peak around 1714 cm^{-1} reflects the stretching vibration of –C=O carbonyl group. Vibrations at 1305 cm^{-1} indicate C–O–C bond of methacrylate. Sharp peaks at 904 cm^{-1} and 815 cm^{-1} are oxirane ring contraction vibration and unsymmetrical expansion [77]. FT-IR spectroscopy as the other method based on different principle compared to EDS proved the successful coating process of CI particles with PGMA.

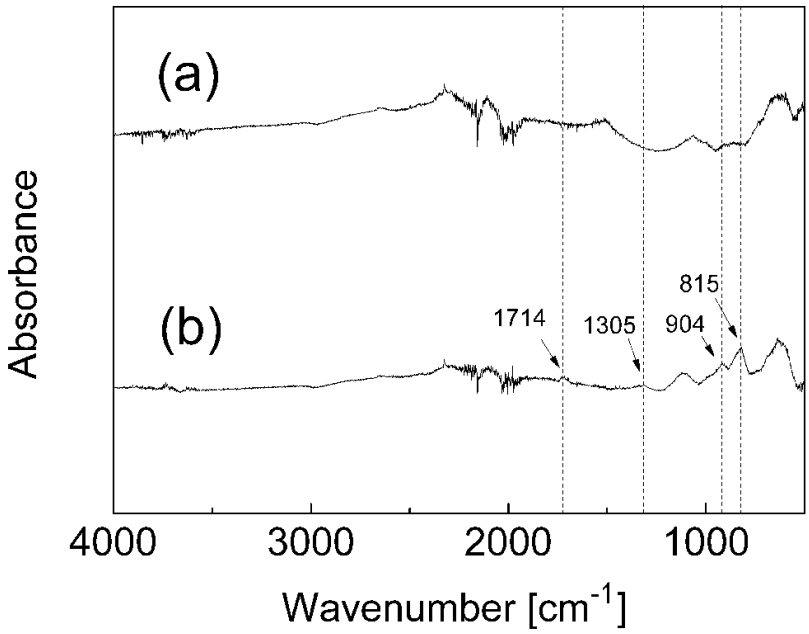

Figure 28. FT-IR spectra of (a) bare CI particles, (b) PGMA-coated CI particles

11.6 Magnetic properties – results

CI/PGMA structures and structures with any polymer on the CI surface tend to have smaller mass magnetization which is undesirable for MR devices, therefore magnetic measurements were performed to determine the magnetization decrease. The hysteresis loops of bare CI particles and both variants of PGMA-coated CI particles are presented in the Figure 29.

Magnetic behavior of CI/PGMA is basically similar to the pure CI particles, but shows lower magnetization due to non-magnetic coating. The measured saturation magnetization of utilized bare CI particles was 178.79 emu/g. For coated particles the saturation magnetizations were 171.77 emu/g respectively, 169.32 emu/g, which is only 3.9%, respectively, 5.3% decrease compared to bare CI particles. Decrease in saturation magnetization was expected due to non-magnetic polymer shell, but notice that the decrease is very little, nearly negligible. So the impact on the MR effect should not be severe. In 2014 Kim *et al.* [8] fabricated CI/PGMA particles by cross-linking PGMA with ethylene glycol dimethacrylate and they carried out the similar experiment. Unfortunately, their saturation magnetization decreased from 175 emu/g to 85 emu/g.

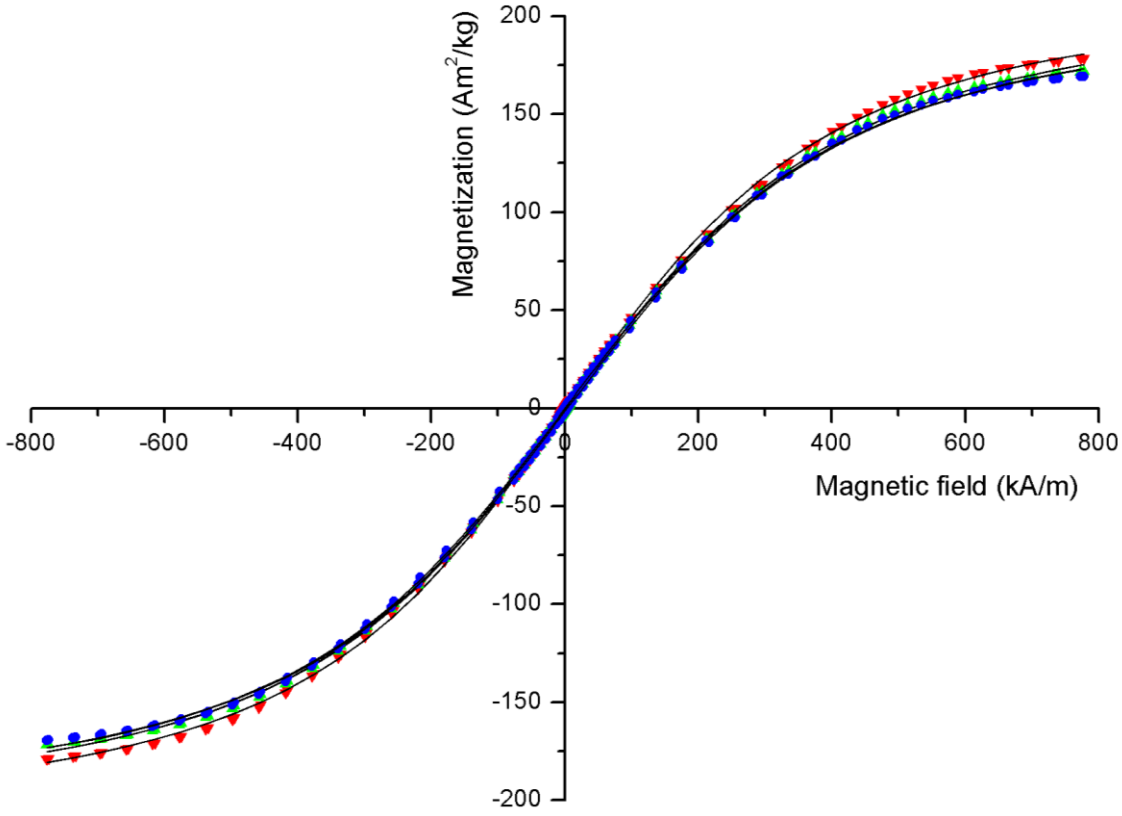

Figure 29. Hysteresis curve of (▼) bare CI particles, (▲) low molecular weight PGMA coated CI particles, (●) high molecular weight PGMA coated CI particles, and (–) Langevin model predictions

The hysteresis loops for pure CI and for both PGMA-coated CI particles were analyzed by applying the Langevin equation:

$$M(H) = M_S \left[\frac{1}{\tanh\left(\frac{m\mu_0 H}{kT}\right)} - \frac{1}{\left(\frac{m\mu_0 H}{kT}\right)} \right] \quad (27)$$

where M_S is the saturation magnetization [A·m^2/g], m is the magnetic moment [A·m^2], μ_0 is the permeability of vacuum ($4\pi \times 10^{-7}$ H·m^{-1}), H is the magnetic field [A/m], k is the Boltzmann constant (1.38×10^{-23} J·K^{-1}) and T is the thermodynamic temperature [K].

The saturation magnetizations calculated according to Langevin equation were 226.3 emu/g for bare CI particles, and for coated variants were 221.0 emu/g, respectively 218.6 emu/g. The values obtained by the application of Langevin equation are higher than those which resulting data from experimental measurement. This might be due to incomplete saturation magnetization during the saturation magnetization measurement [13]. The summary of resulting values from measurement of magnetic properties is shown in the Table 4.

Table 4. Results from VSM measurement

	measured M_S [emu/g]	**measured coercivity [Oe]**	**M_S prediction according to Langevin model [emu/g]**
CI pure	178.79	11.984	226.3
CI/PGMA_lower_$\bar{M}_n$	171.77	11.466	221.0
CI/PGMA_higher_$\bar{M}_n$	169.32	11.807	218.6

The other monitored parameter was the coercivity of the CI particles and both coated analogues. The coercivity is the intensity of magnetic field that can cancel out the remanent magnetization [18]. The lower it is the better dynamic of demagnetization of the particles. VSM measurements show that the polymer coating almost did not affect the coercivity which is also positive result (Table 4).

Retained high values of saturation magnetizations and unaltered coercivity values make these prepared CI/PGMA particles very promising candidates for their effective utilization in MR suspensions used for practical applications.

Note that values of magnetic properties such as magnetization and coercivity are usually reported in emu/g and Oe. Conversion factors to SI units are included in Table 1.

11.7 Chemical stability – results

Figure 30 shows the pH value as a function of time for all measured suspensions subjected to acid environment. As shown pH value initially decreased, which may be due to two factors. First, pH meter operates with delays. Second, the pH value depends on a consistency of the environment around the probe. Also pH value was measured during initial sedimentation of the particles, which could affect the final pH. Shortly after the initiation of the experiment the pH value of dispersion containing uncoated CI particles stared to increase. The aqueous solution of HCl reacted with atoms of CI particles according to equation:

$$Fe + 2HCl + 6H_2O \rightarrow [Fe(H_2O)_6]Cl_2 + H_2 \qquad (28)$$

and forms hexaaquairon(II) chloride complexes and hydrogen molecules.

For bare CI particles, an intense bubble generation (H_2) was observed during the reaction. Approximately after 50 minutes the bubble generation decreased and the pH value started to increase with a greater slope. However, the overall increase of pH value may be described as almost linear.

CI/PGMA composite particles were subjected to the same environment consisting of 0.05M HCl. As was expected, the PGMA shell covers the CI core and the reaction almost did not proceed. The bubble generation was minimal. This was probably due to the fact that some protons diffused through polymer shell and reacted with iron. Generally, the pH remained at the similar value throughout all experiment. The similar situation occurred with the use of CI particles coated with PGMA with higher molecular weight. The increase of pH value was also negligible as shown on the Figure 30.

CI particles with PGMA shell have compact surface, which enhanced chemical stability of raw CI particles, therefore such composite structures exhibit anti-acid-corrosion properties which increase the implementation of these particles into practice. For the purpose of chemical stability enhancement, it is fully sufficient to use only a thin polymer shell grafted onto surface of CI particles as was also confirmed by other authors [49]. A further improvement of chemical stability did not occur with increasing thickness of polymer layer (as illustrated on the Figure 30). On the Figure 31 is shown a tremendous difference between tested MR particles approximately 20 hours after the experiment.

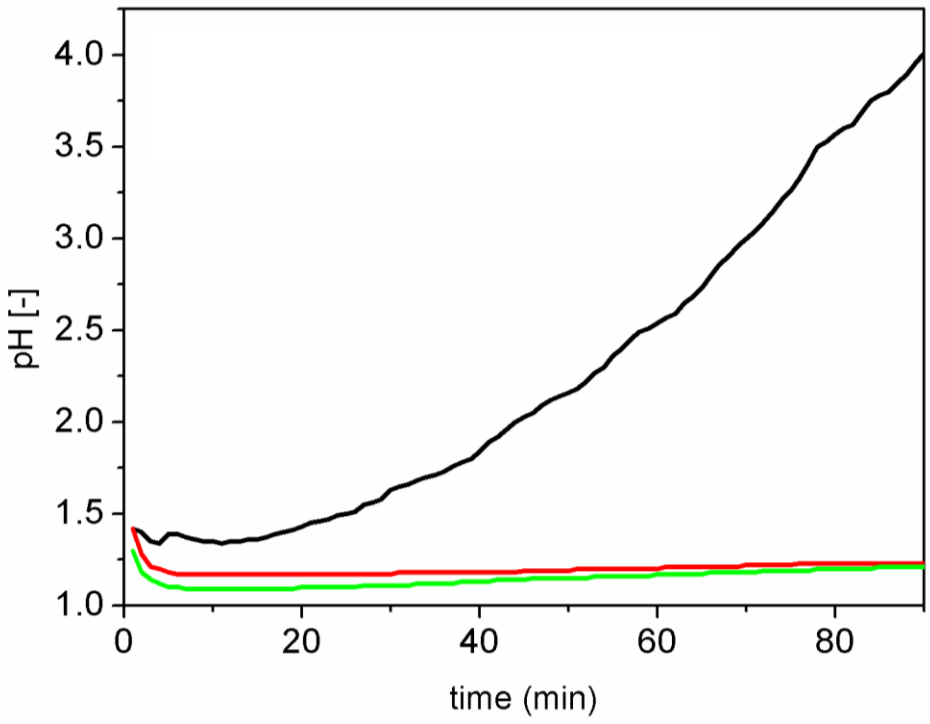

Figure 30. Resistance of uncoated CI (–) particles and CI/PGMA particles with lower molecular weight (–) and CI/PGMA particles with higher molecular weight (–) against acids (0.05M HCl)

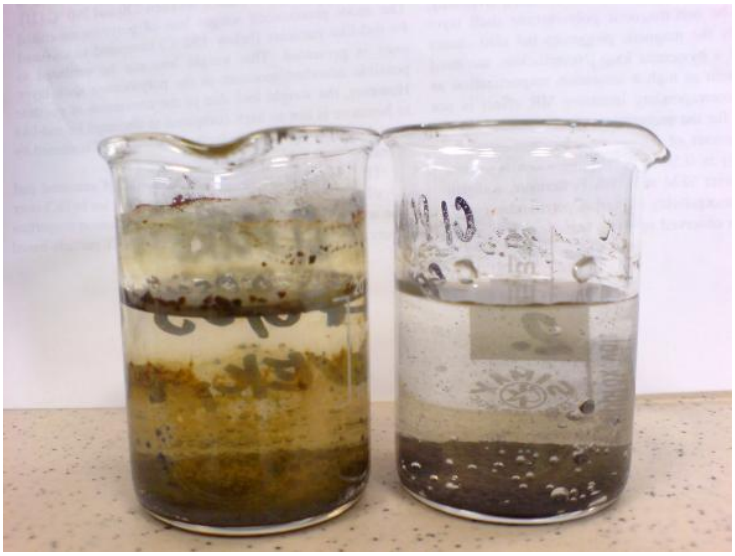

Figure 31. Comparison of samples after chemical stability measurement between uncoated CI particles (left beaker) and CI/PGMA (lower molecular weight) core-shell structures (right beaker) after 20 hours

11.8 Thermo-oxidative stability – results

The weight gain was plotted as a function of temperature as shown on the Figure 32. It is shown that such weight gain is a result of iron oxides formation. Iron powder takes up 40 wt% oxygen and forms oxides as follows FeO, Fe_3O_4 and finally Fe_2O_3 [78]. The graph shows that the reaction requires an exceptionally wide temperature range to achieve full conversion.

As was expected, the PGMA polymer coating on the surface of CI particles leads to considerable thermo-oxidative enhancement. The weight of bare CI particles started to grow in lower temperatures compared to core-shell structured CI particles. The first weight changes of bare CI particles were observed at temperatures around 200 °C. Both variants of PGMA coated CI particles were thermally stabile up to 300 °C. The significant increase in weight of uncoated CI particles occurs at temperatures around 400 °C. The similar sharp weight gain due to severe oxidation can be observed in coated CI particles, but it is shifted to temperatures around 500 °C.

TGA analysis revealed and confirmed that the difference in polymer shell thickness is very small, therefore the difference in thermograms of polymer coated particles is nearly negligible. The Figure 32 also presents that the polymer coated CI particles thermally decomposed and the inner iron core simultaneously oxidized by heating. If the polymer decomposed first, the weight decrease would be displayed on the thermogram, so probably the reactions took place concurrently. A small weight decrease occurred around 650 °C in both variants of coated particles. This could be due to some absorbed gases on the particle surface. However, grafted polymer coating provides a protective over layer on the CI particles, which shifted the oxidation process to higher temperatures.

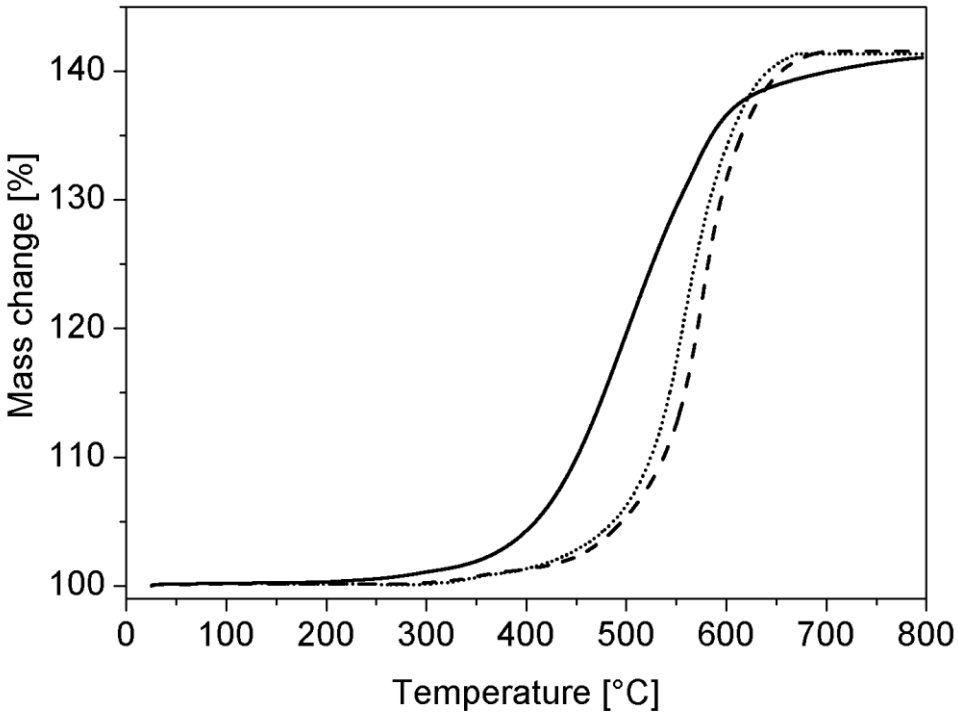

Figure 32. TGA analysis of bare CI particles (–), CI/PGMA particles with lower molecular weight (····) and CI/PGMA particles with higher molecular weight (- - -) in the air atmosphere

11.9 Rheological properties in steady shear flow – results

The Figures (33 – 50) illustrate steady shear behavior of prepared suspensions at different magnetic flux densities. The range of shear rates from 1 s^{-1} to 300 s^{-1} was applied, and shear stresses were obtained. The experimental rheological data were fit with two rheological models – Bingham model and Robertson-Stiff model in order to judge the ability of both models to describe flow curves of MR suspensions. The performance of MR suspensions can be judged according to their yield stresses, therefore dynamic yield stresses were determined with the use of models (Section 11.9.2). It is also important to mention that utilized rheological models (Equation 11), (Equation 15) are not actual data, but predictions of rheological behavior according to constitutive relations presented above.

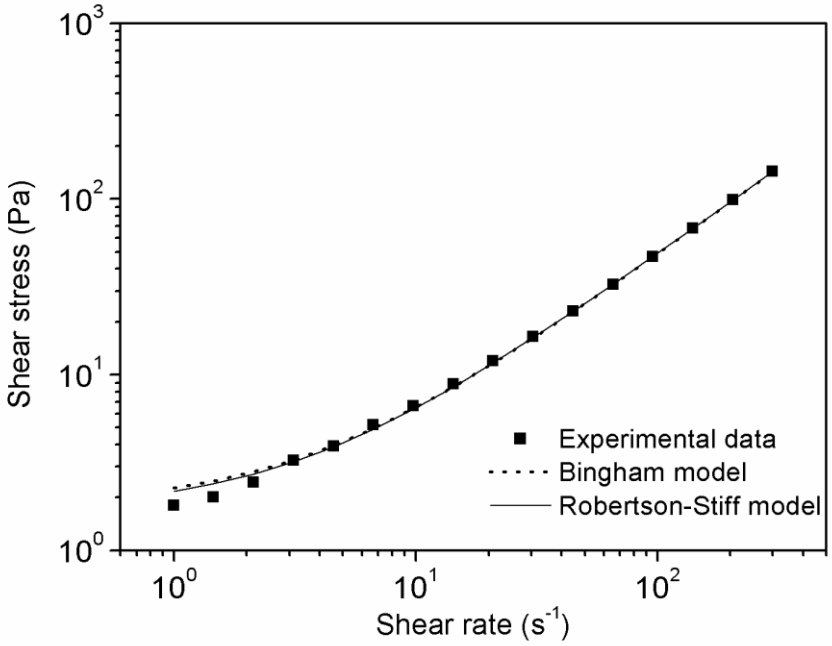

Figure 33. Dependence of the shear stress on the shear rate for suspension of 60 wt% of bare CI particles at magnetic flux density 0 mT

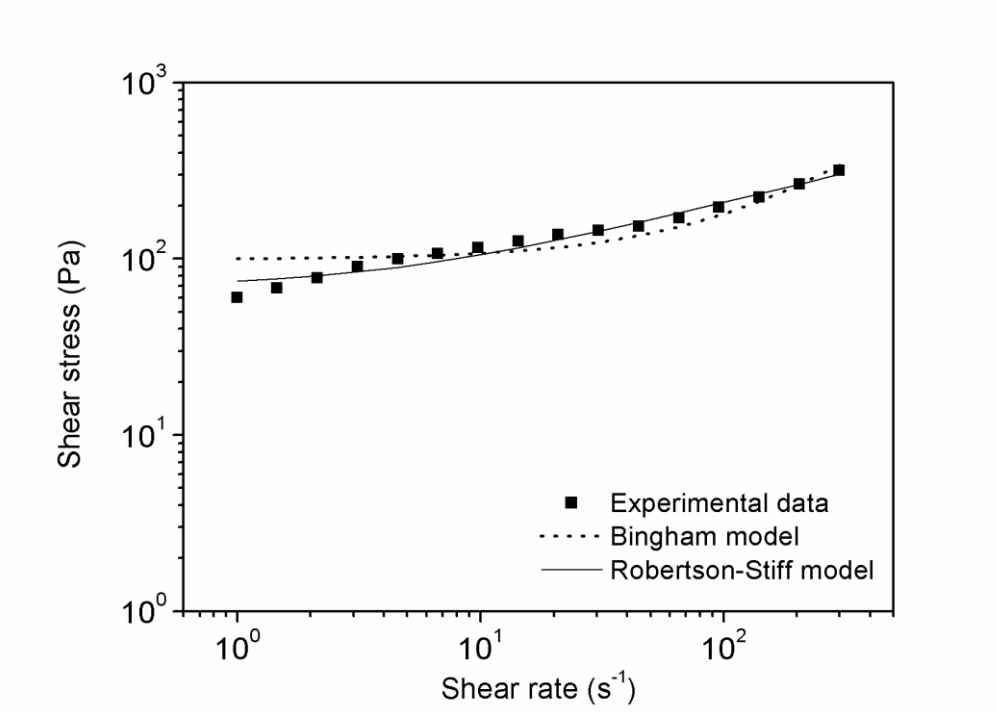

Figure 34. Dependence of the shear stress on the shear rate for suspension of 60 wt% of bare CI particles at magnetic flux density 67 mT

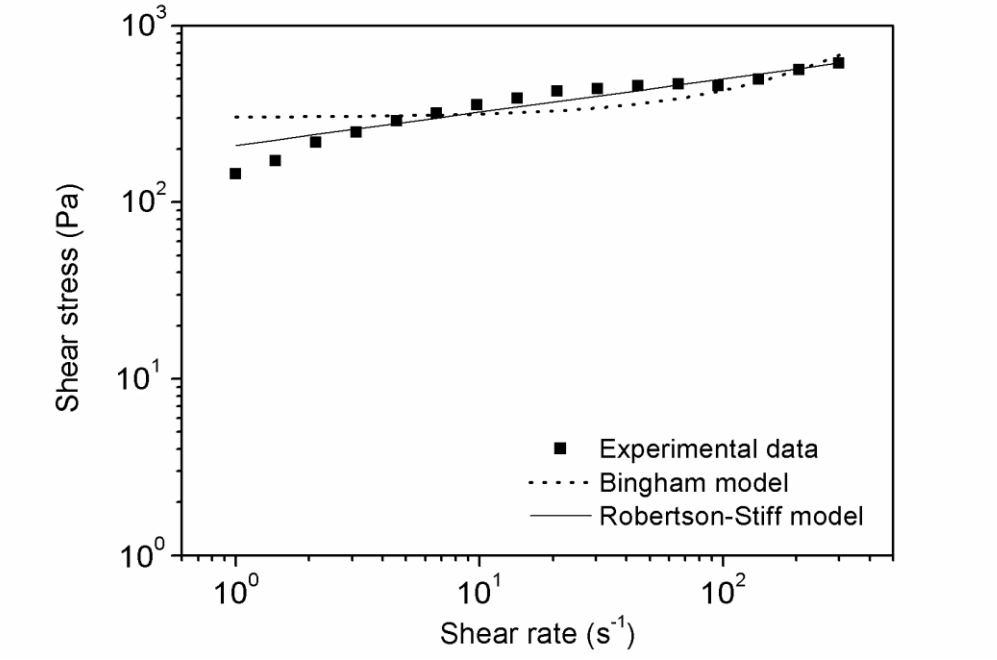

Figure 35. Dependence of the shear stress on the shear rate for suspension of 60 wt% of bare CI particles at magnetic flux density 144 mT

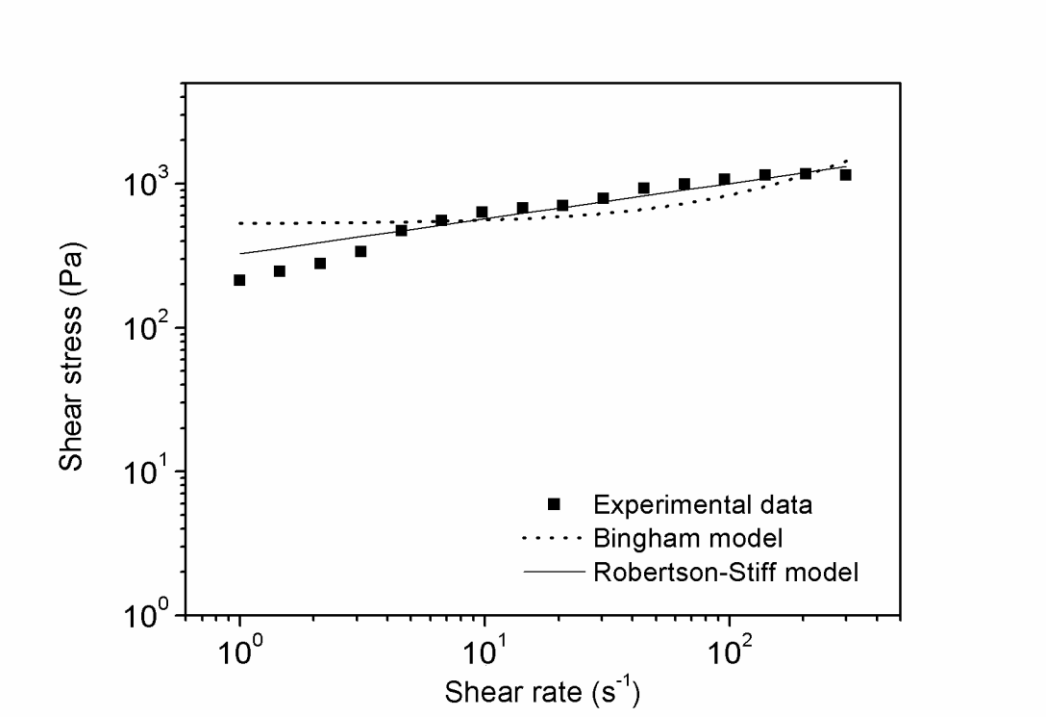

Figure 36. Dependence of the shear stress on the shear rate for suspension of 60 wt% of bare CI particles at magnetic flux density 218 mT

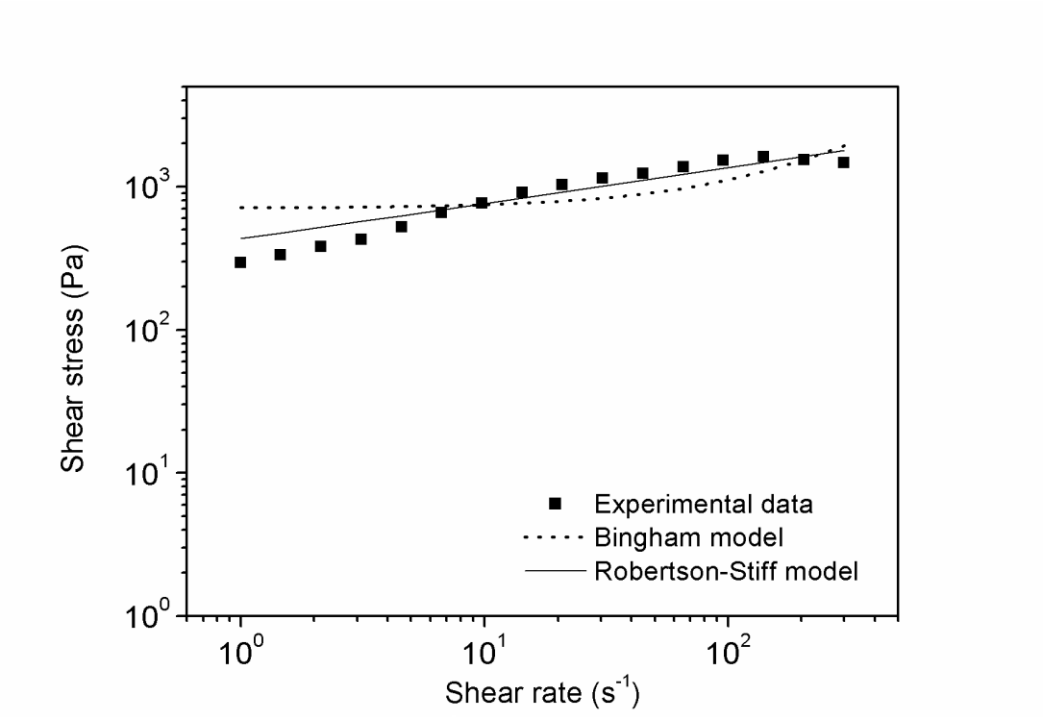

Figure 37. Dependence of the shear stress on the shear rate for suspension of 60 wt% of bare CI particles at magnetic flux density 292 mT

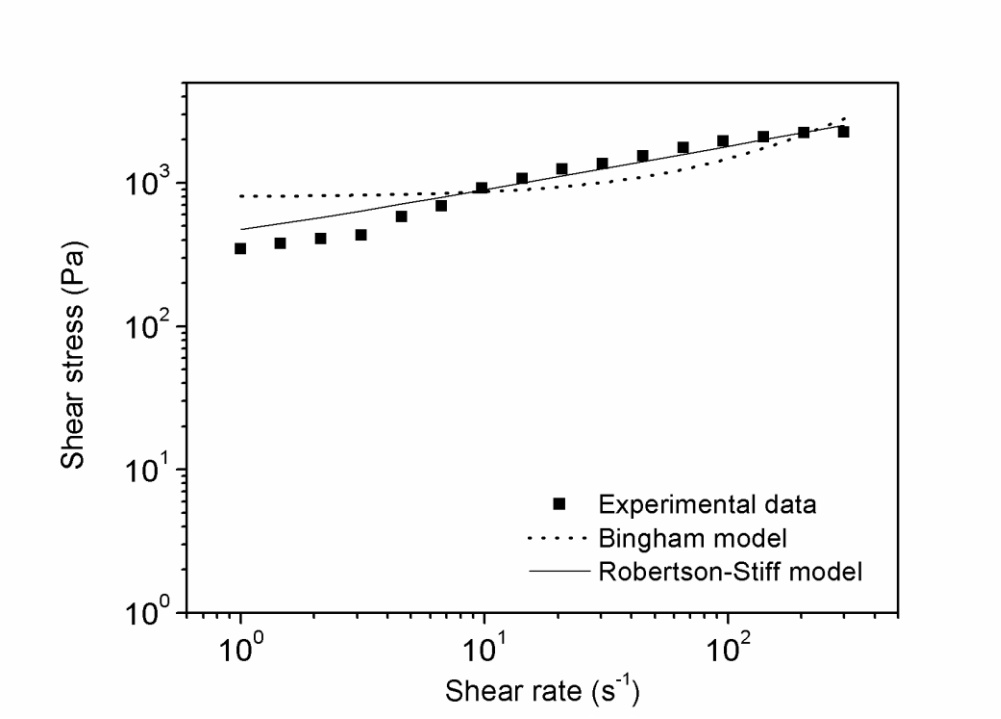

Figure 38. Dependence of the shear stress on the shear rate for suspension of 60 wt% of bare CI particles at magnetic flux density 363 mT

The results have shown that in the absence of external magnetic field all studied suspensions exhibited nearly Newtonian behavior, in the sense of linear dependence between shear stress and shear rate. After the application of external magnetic field, the chain-like structures were created and the suspensions exhibited a yield stress. Increase in the shear stress of MR fluid in the presence of external magnetic field is typical feature of MR materials. The application of external magnetic field makes the MR suspensions behave like viscoelastic materials, therefore equations describing non-Newtonian materials were used for their characterization.

As mentioned above, mathematical modeling was performed with the use of Bingham model (Equation 11) and Robertson-Stiff model (Equation 15). Both models predict very similar rheological behavior of all suspensions compared to experimental data in the absence of external magnetic field.

In the on-state, Robertson-Stiff model provided good fit with experimental data while Bingham model always gave the worse one. It is nothing unexpected, as Robertson-Stiff model is 3P, while Bingham model is just two-parameter (2P). Bingham model predicted

very large yield stresses due to its mathematical aspect. It appears that Robertson-Stiff model is a suitable constitutive model for MR suspensions.

All tested MR suspensions exhibited largest yield stress at the highest used magnetic flux densities (363 mT). That means that the toughness of field-induced internal structures increases with increasing magnetic flux density. This trend would proceed until the saturation magnetization would be reached. The higher magnetic flux density strongly organized the column-like structures, which resulted in higher values of the yield stress.

Widely known and studied is also the effect of particle concentration on the MR effect which is related to yield stress. In the Section 4.2 are described mathematical predictions of yield stress at different magnetic field strengths which show that yield stress of MR suspension is directly proportional to its volume fraction of the particles.

11.9.1 The effect of polymer coating

The suspensions containing PGMA-coated CI particles exhibit slightly lower values of the yield stress, due to non-magnetic polymer shell on the particles. This decline corresponds with the values of saturation magnetization obtained from VSM measurement. High values of saturation magnetizations of the particles are important for high performance of the MR suspensions.

The trends of the shear stress on the shear rate dependences are similar for both suspensions containing coated particles. PGMA-coated CI particles with higher molecular weights have a thicker polymer shell therefore their saturation magnetization is minor as well as their yield stress. Therefore, their flow curves are slightly shifted to lower values compared to suspensions of CI particles with thinner polymer shell (lower molecular weight polymer shell).

Research has shown that the suspensions containing PGMA-treated CI particles prepared *via* ATRP are still able to develop considerable and sufficient yield stresses. Results are illustrated in following Figures (39 – 50).

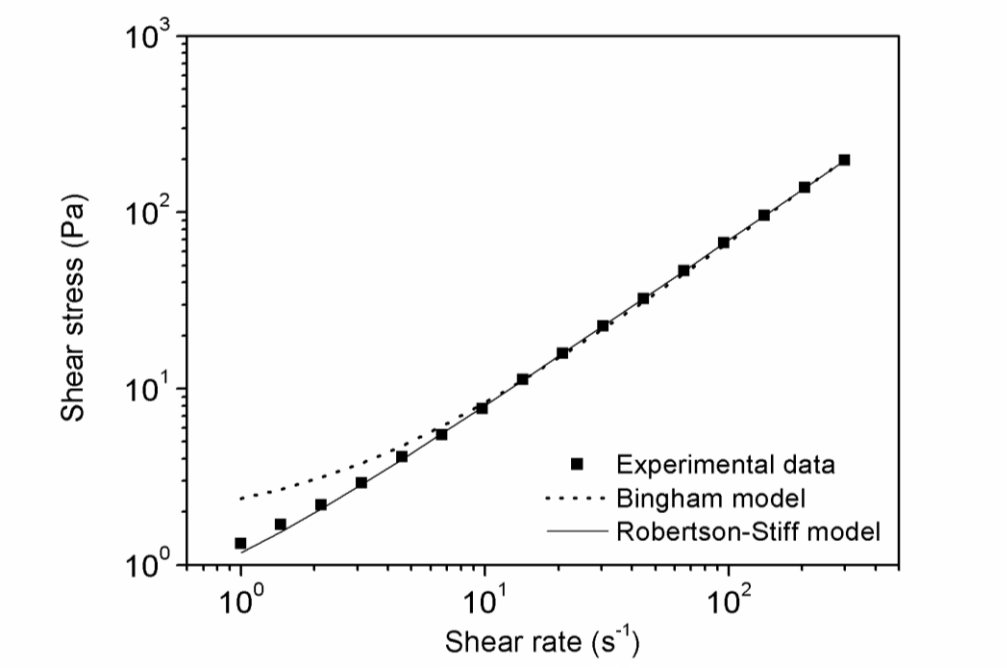

Figure 39. Dependence of the shear stress on the shear rate for suspension of 60 wt% of CI particles coated with lower molecular weight PGMA at magnetic flux density 0 mT

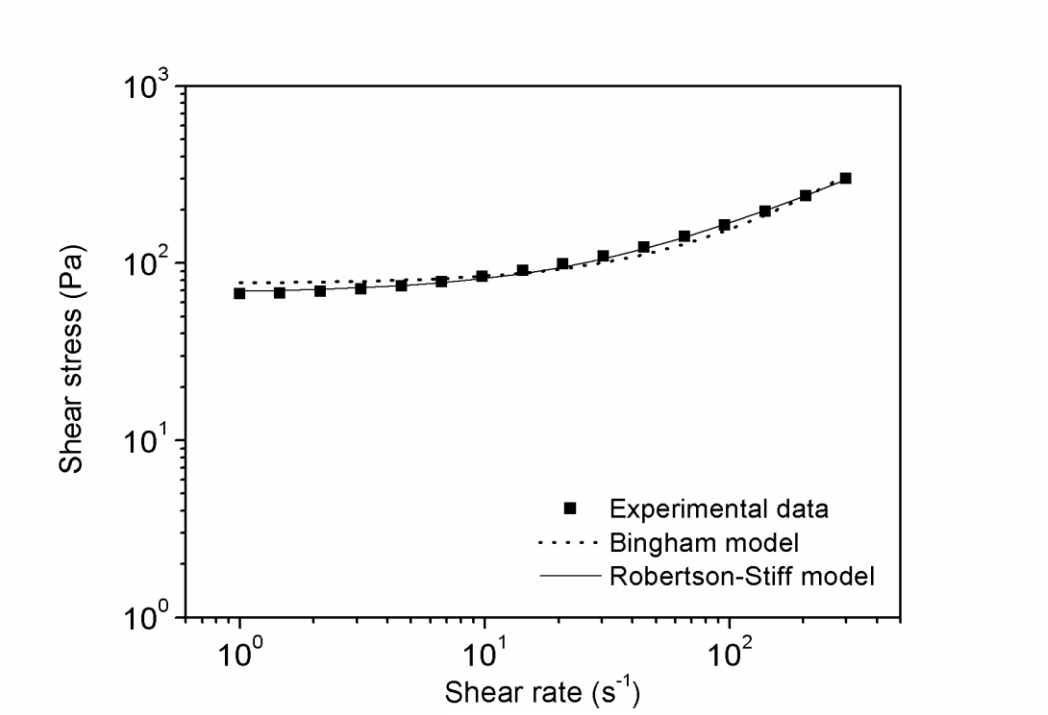

Figure 40. Dependence of the shear stress on the shear rate for suspension of 60 wt% of CI particles coated with lower molecular weight PGMA at magnetic flux density 67 mT

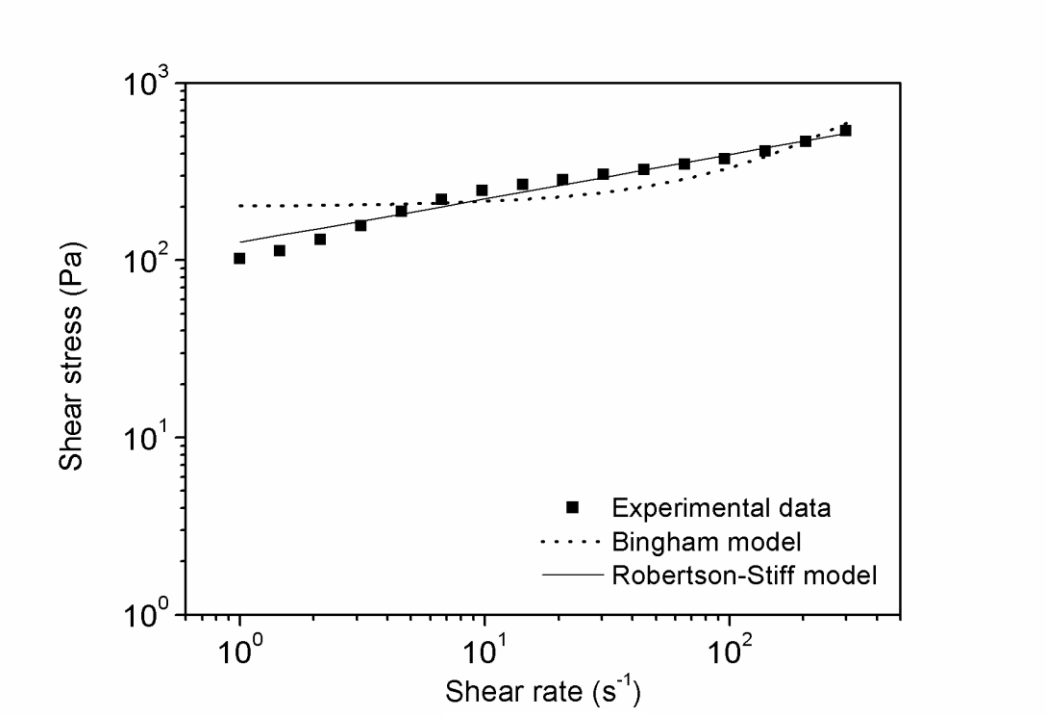

Figure 41. Dependence of the shear stress on the shear rate for suspension of 60 wt% of CI particles coated with lower molecular weight PGMA at magnetic flux density 144 mT

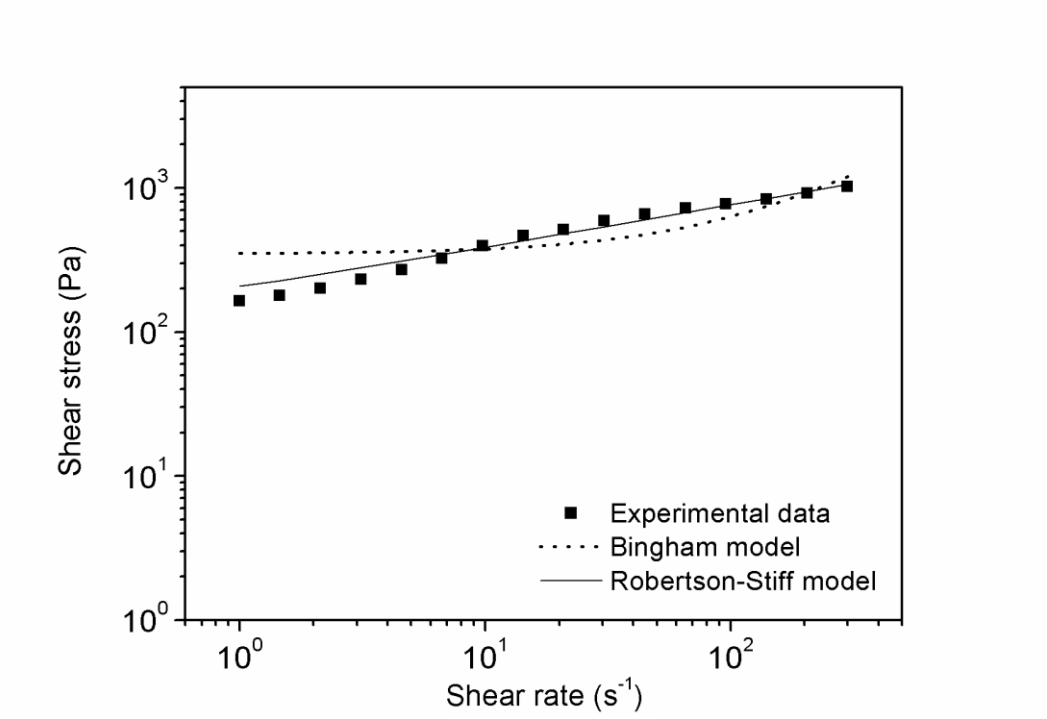

Figure 42. Dependence of the shear stress on the shear rate for suspension of 60 wt% of CI particles coated with lower molecular weight PGMA at magnetic flux density 218 mT

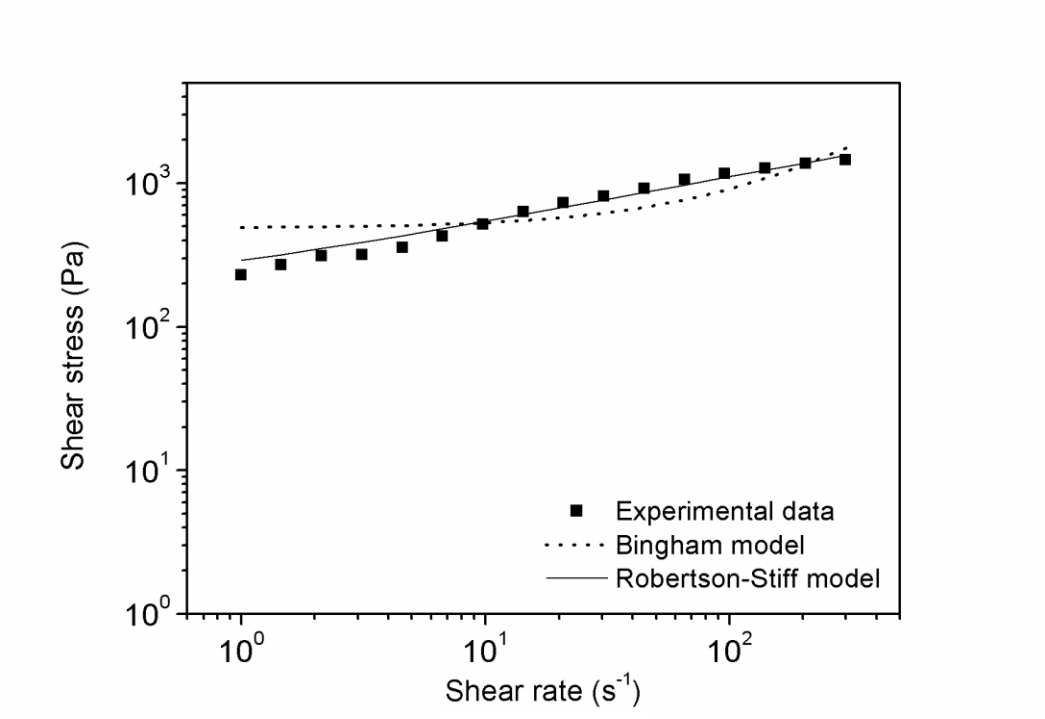

Figure 43. Dependence of the shear stress on the shear rate for suspension of 60 wt% of CI particles coated with lower molecular weight PGMA at magnetic flux density 292 mT

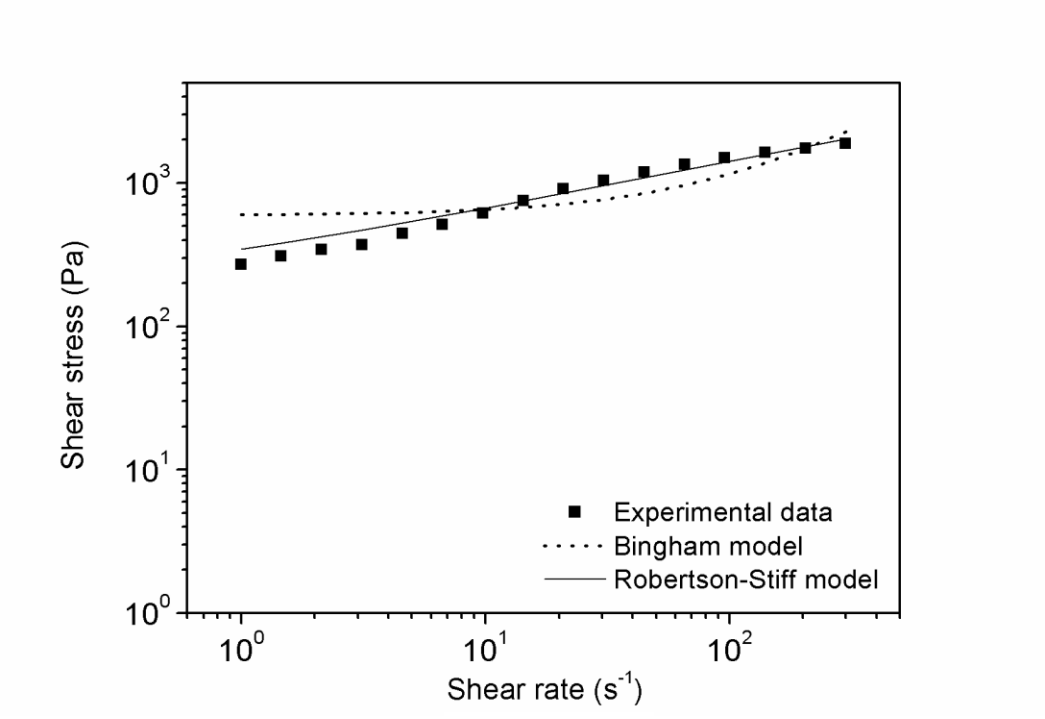

Figure 44. Dependence of the shear stress on the shear rate for suspension of 60 wt% of CI particles coated with lower molecular weight PGMA at magnetic flux density 363 mT

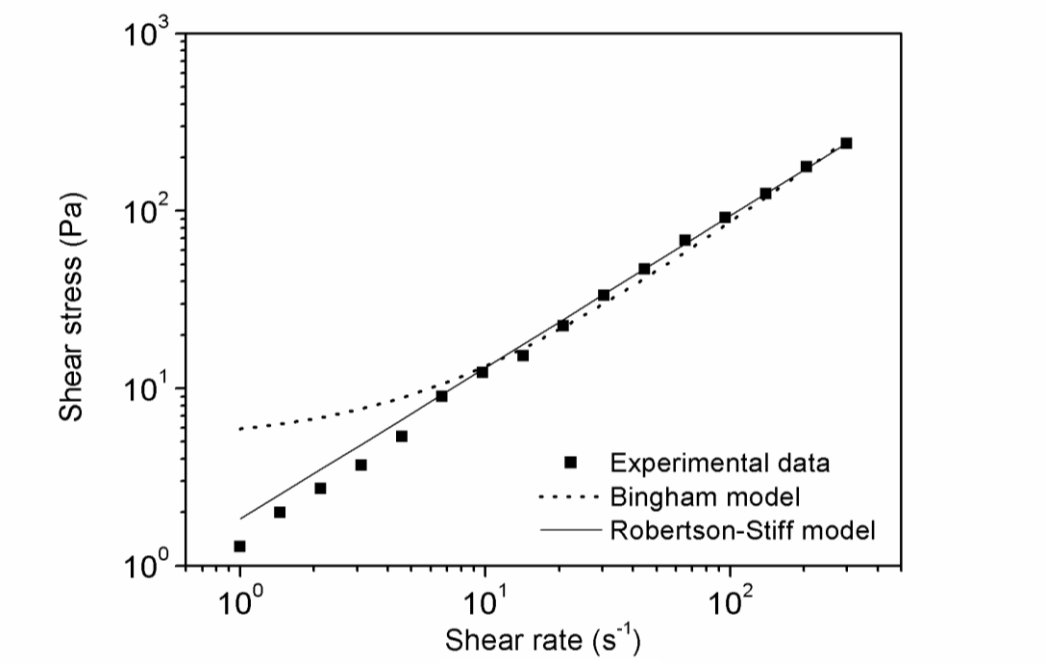

Figure 45. Dependence of the shear stress on the shear rate for suspension of 60 wt% of CI particles coated with higher molecular weight PGMA at magnetic flux density 0 mT

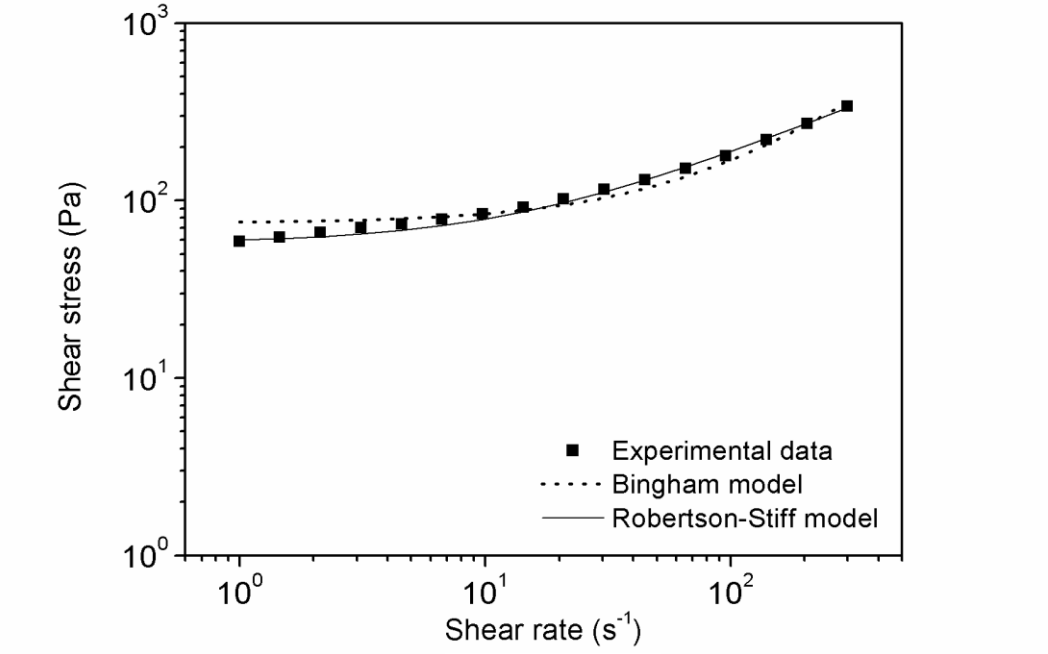

Figure 46. Dependence of the shear stress on the shear rate for suspension of 60 wt% of CI particles coated with higher molecular weight PGMA at magnetic flux density 67 mT

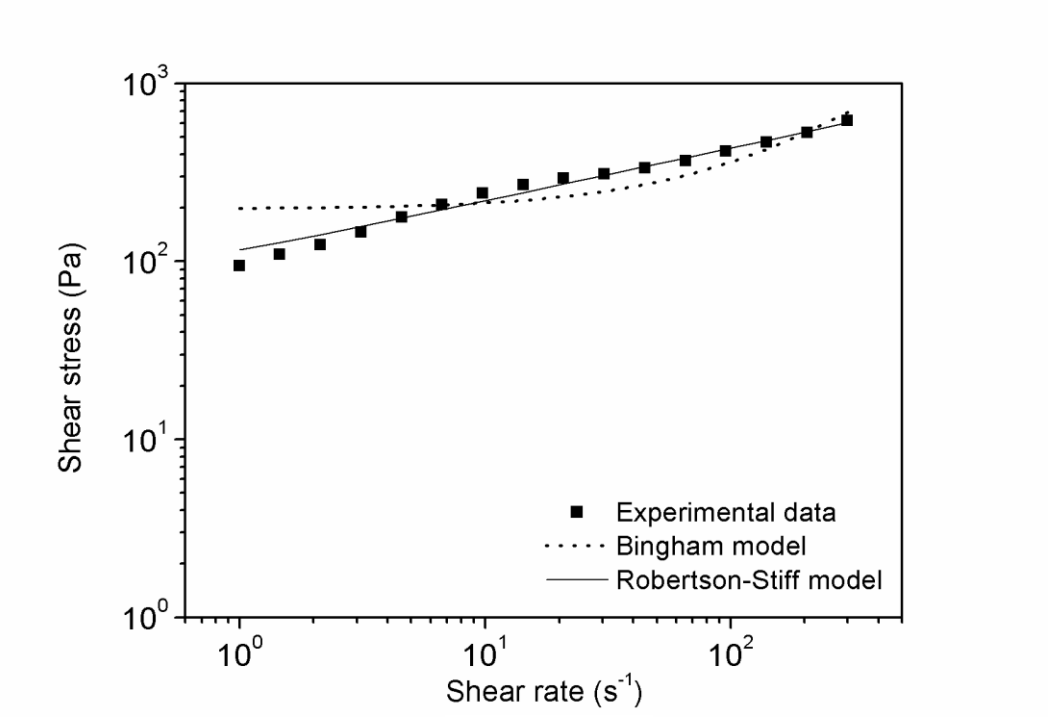

Figure 47. Dependence of the shear stress on the shear rate for suspension of 60 wt% of CI particles coated with higher molecular weight PGMA at magnetic flux density 144 mT

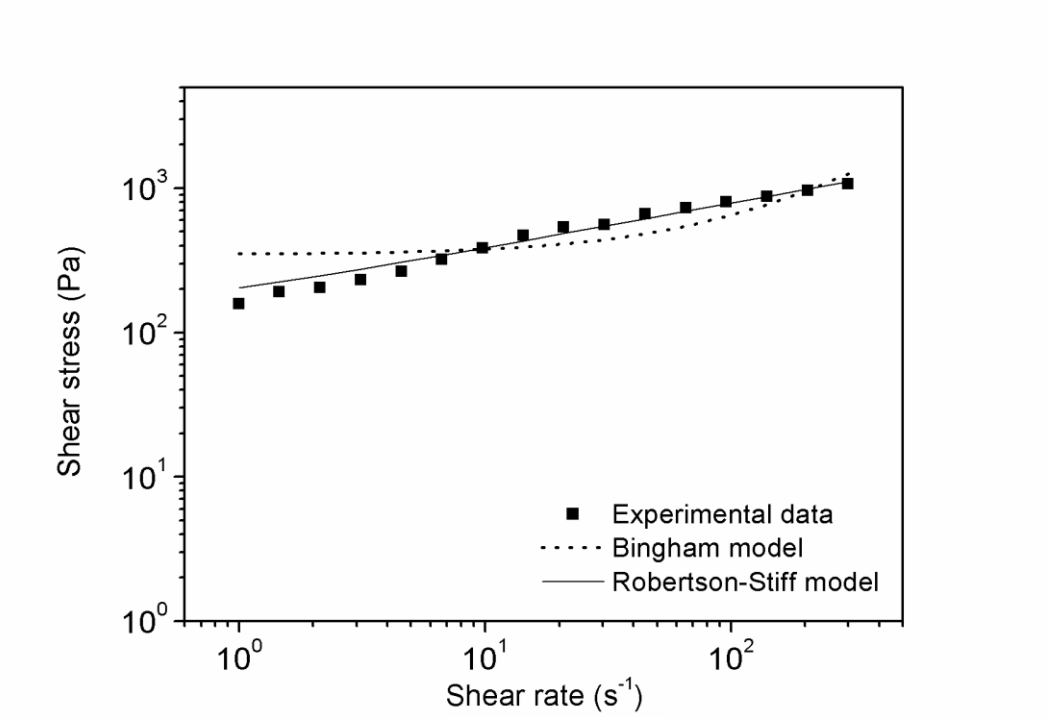

Figure 48. Dependence of the shear stress on the shear rate for suspension of 60 wt% of CI particles coated with higher molecular weight PGMA at magnetic flux density 218 mT

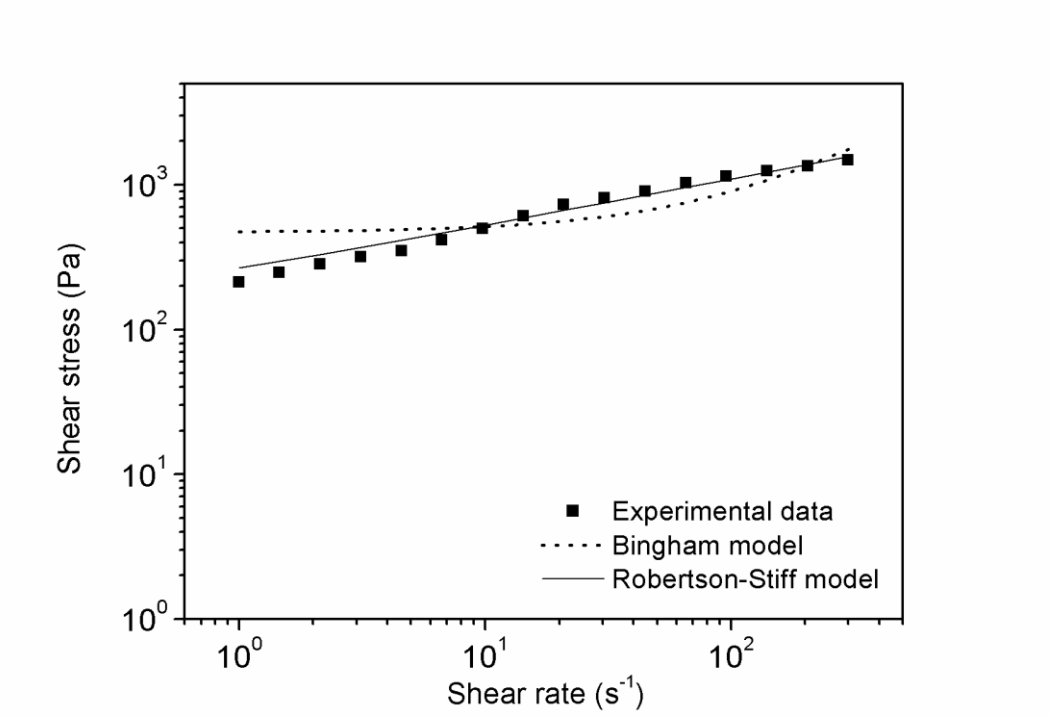

Figure 49. Dependence of the shear stress on the shear rate for suspension of 60 wt% of CI particles coated with higher molecular weight PGMA at magnetic flux density 292 mT

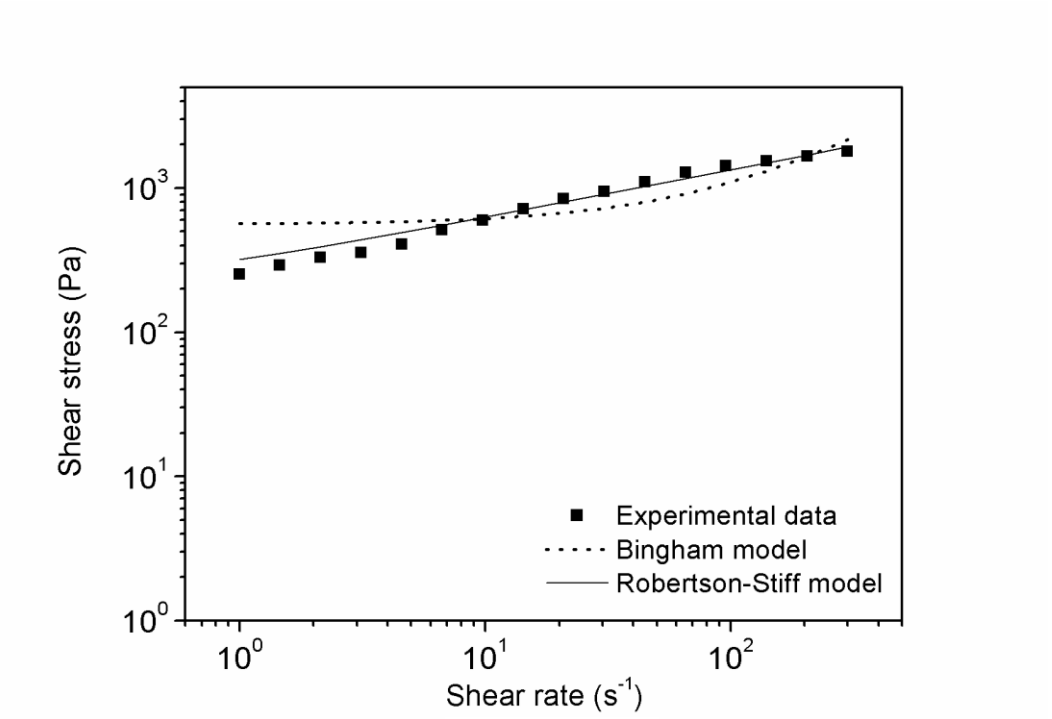

Figure 50. Dependence of the shear stress on the shear rate for suspension of 60 wt% of CI particles coated with higher molecular weight PGMA at magnetic flux density 363 mT

11.9.2 Yield stress evaluation

Dynamic yield stress gives a quantitative idea of the point where all internal structures in suspensions are broken [19] and the values of dynamic yield stress were obtained by fitting the flow curves with Robertson-Stiff model. In the Figure 51 the yield stress is plotted as a function of applied magnetic flux density.

Yield stress of all prepared MR suspensions increases with increasing magnetic flux density, which was also observed in the studies [5, 6, 79]. Data of the yield stress were fit with power-law equation $\tau_y \approx B^a$ in order to investigate the mechanism of the internal structures development.

The formation of internal structures is due to dipole mechanism at low magnetic flux densities and the yield stress varies with B^2. At intermediate magnetic flux densities the yield stress is proportional to $B^{3/2}$. MR suspensions at this state exhibit local saturation magnetization which is responsible for further internal structures development. This mechanism started to be noticeable at a critical magnetic flux density (B_C) which was around 220 mT. Observed dependence was in conformity with mathematical predictions; the slope of the dependence was 2.15 and beyond the B_C the value of the slope changed to 1.31.

This phenomenon was not observed for MR suspensions containing particles coated with PGMA, probably because mathematical models which describe the yield stress dependence on applied magnetic flux density were derived for conventional MR suspensions [1] (containing bare CI particles without any polymer shell). The polymer coating decreased the value of yield stress compared to MR suspension with the same concentration of bare CI particles. On contrary, there are not significant differences between curves obtained for MR suspensions containing variants of PGMA-coated CI particles. However, suspension containing particles coated with PGMA with higher molecular weight exhibited slightly lower values of yield stress for appropriate magnetic flux densities.

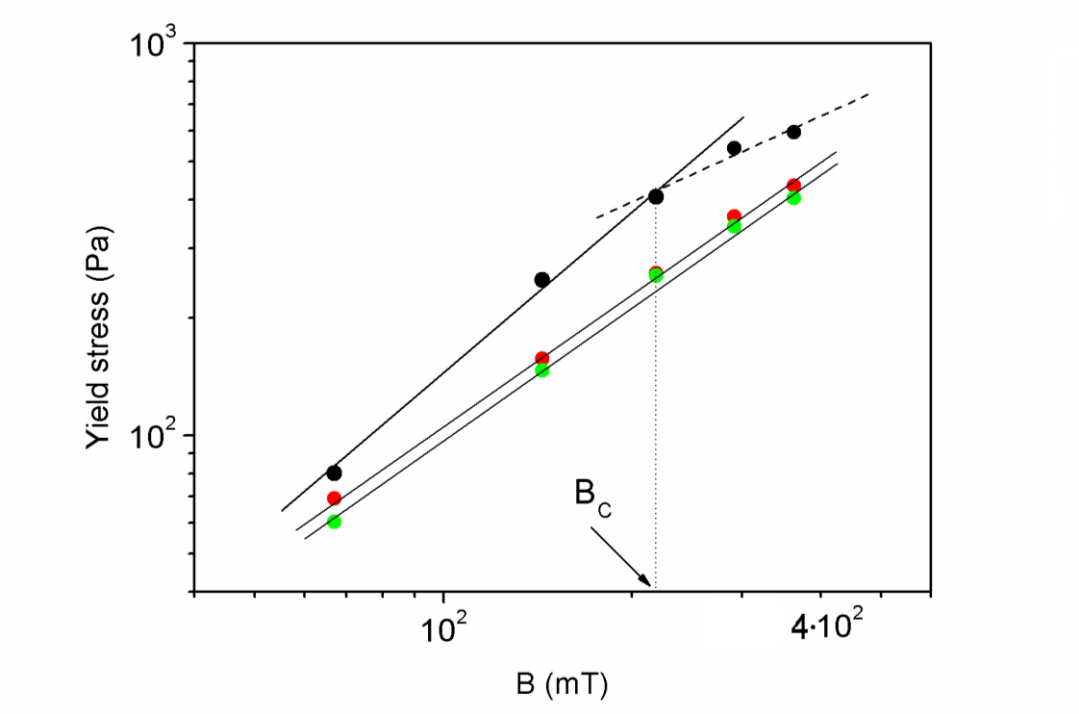

Figure 51. Yield stress (Robertson-Stiff model) as a function of magnetic flux density for MR suspensions containing 60 wt% fraction of bare CI particles (●), CI particles coated with PGMA with lower molecular weight (●) and with higher molecular weight (●)

11.9.3 Viscosity measurement in steady shear flow

Besides yield stress increase of MR suspensions, also considerable increase of shear viscosity (with increasing magnetic flux density) was observed and measured. Shear viscosity increased by several orders of magnitude (e.g. Figure 52). In other words the toughness of internal structures increased with increasing magnetic flux density.

Furthermore, the dependence of the viscosity on the strain rate was observed in all chosen magnetic flux densities. The Figures 52 – 54 show results of viscosity measurements.

For all prepared MR suspensions the viscosity is nearly independent on the strain rate in the absence of external magnetic field, only a small decrease in viscosity in higher strain rates was observed. This behavior can be described as nearly Newtonian or slightly pseudoplastic. The most Newtonian character exhibits the suspension containing PGMA-coated CI particles with higher molecular weight (Figure 54).

Really interesting is the fact, that the off-state viscosity of the suspensions containing both variants of PGMA-coated CI particles even decreased in low shear rates compared to suspension of bare CI particles. This may lead to even higher efficiency of MR fluid compared to suspensions of bare CI particles. Only in higher shear rates the off-state viscosity of the suspension containing bare CI particles was lower compared to both suspensions of coated particles.

The change in rheology behavior of the coated CI particles can be attributed to surface modification which provides better interactions of dispersed particles with silicone oil.

After the application of external magnetic field the viscosity dramatically increased. The viscosity increase was a function of magnetic flux density. With higher magnetic flux density, the higher viscosity was obtained. The consequence of increasing viscosity of the suspension was formation of internal structures consisting from dispersed particles oriented in the direction of the applied field. The highest viscosities in all suspensions were reached in very low shear rates. Viscosity of all suspensions on-state was gradually decreasing with increasing shear rate. The behavior of all suspensions on-state can be ascribed as pseudoplastic behavior.

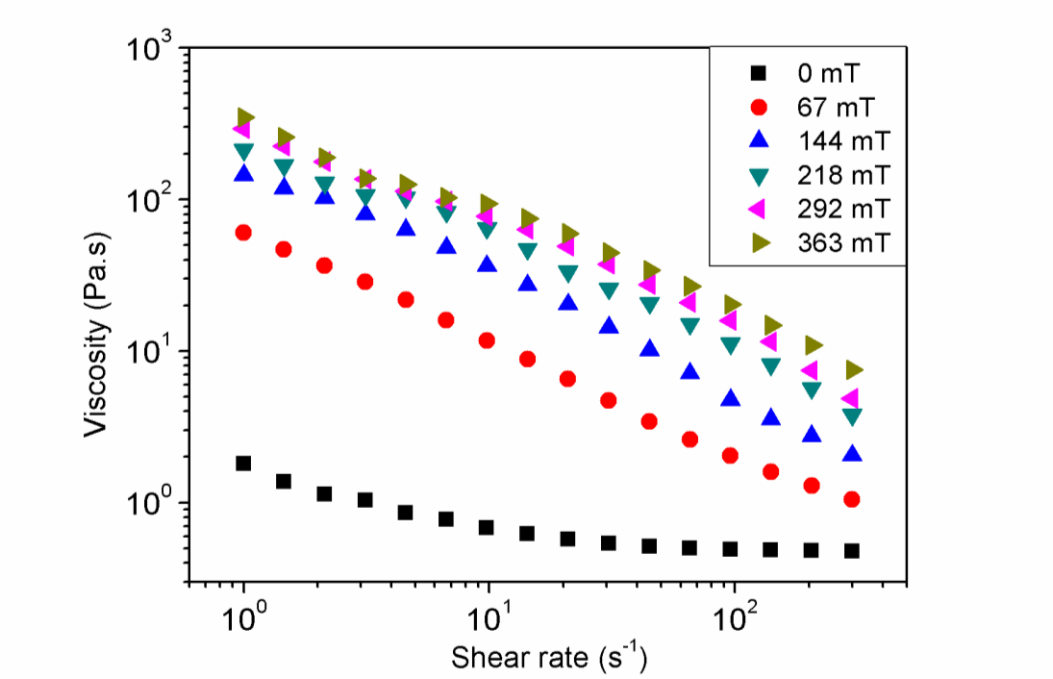

Figure 52. Flow curves of the suspension containing 60 wt% of bare CI particles at different magnetic flux densities

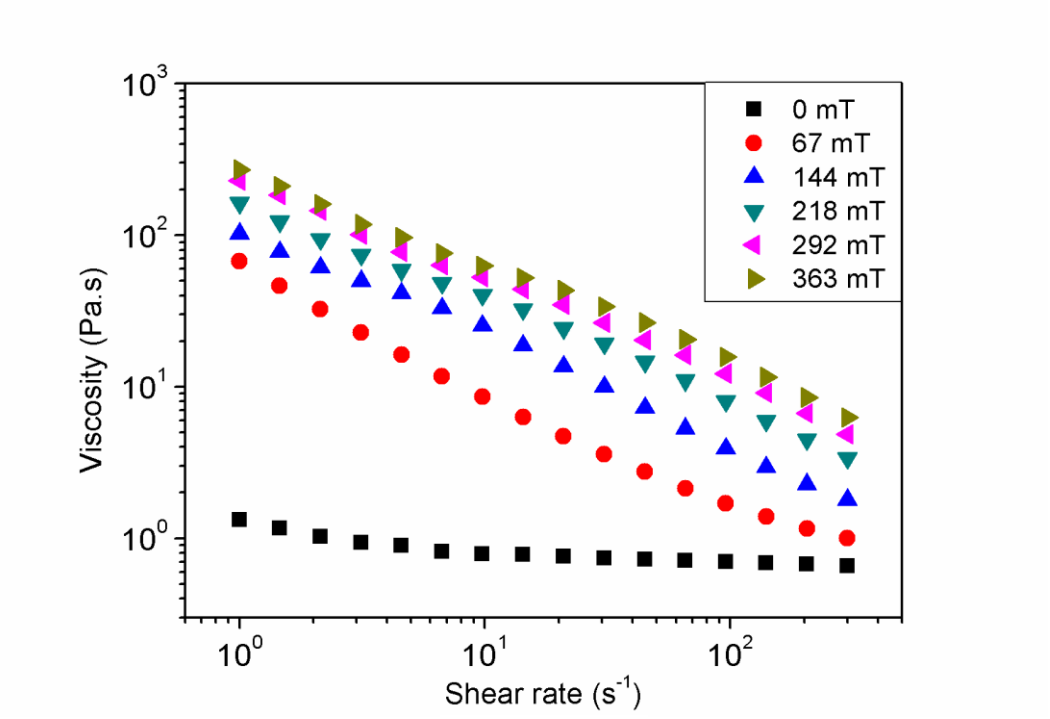

Figure 53. Flow curves of the suspension containing 60 wt% of CI particles coated with lower molecular weight PGMA at different magnetic flux densities

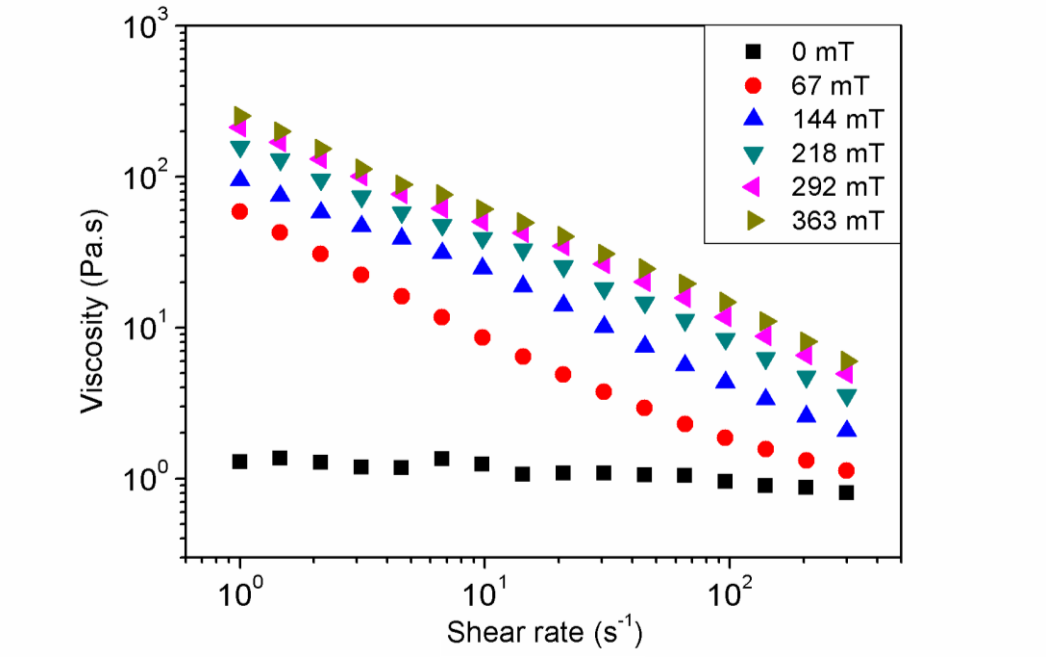

Figure 54. Flow curves of the suspension containing 60 wt% of CI particles coated with higher molecular weight PGMA at different magnetic flux densities

11.10 Rheological properties in oscillatory mode – results

The oscillatory tests at sufficiently low deformations do not destroy the structure [80] therefore they were established as a suitable tool to understand the behavior of the MR internal structures. For given conditions, the deformation limit where irreversible destruction of the structure occurs must be determined in amplitude sweep test.

Dynamic strain measurements were performed in order to determine LVR. Figures 55, 56, 57 show the dependence of G' and G'' on the strain amplitude (γ) for oscillatory shear flow for all prepared suspensions. The values of G' and G'' have a physical meaning only in small strain amplitude, where the internal structures are not broken, because they are calculated assuming that MR suspension exhibits ideal viscoelasticity [47].

The position of LVR changes depending on the strength of an applied magnetic field [13], but the change was somewhat minor in our case (Figures 55 – 57). G' and G'' started to decrease at certain value of the strain amplitude. The nonlinearities became apparent at about 0.05 % for 60 wt% MR suspension of bare CI and 0.04 % for 60 wt% MR suspensions of both variant of PGMA-coated particles.

For easy reference in the Figures 55 – 57 G' and G'' are illustrated only for certain magnetic flux densities, namely 0 mT, 67 mT and 363 mT.

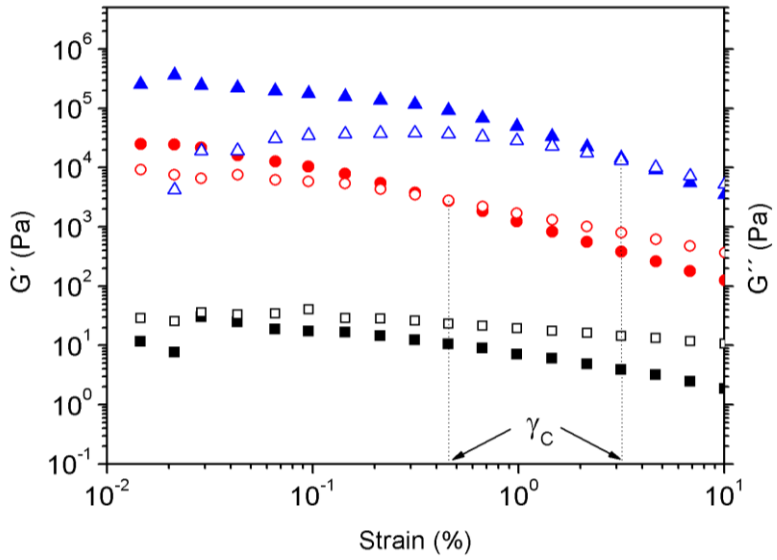

Figure 55. Amplitude sweep results for 60wt % MR suspension of bare CI particles at different magnetic fields. Variation of G´ (■, ●, ▲ filled symbols) and G´´ (□, ○, Δ open symbols) at different magnetic flux densities (0 mT, 67 mT, 363 mT)

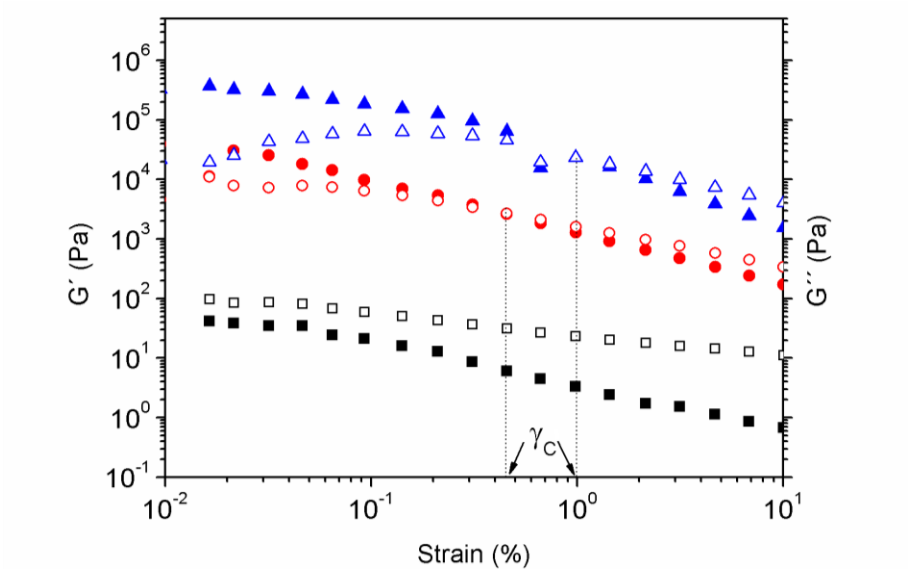

Figure 56. Amplitude sweep results for 60wt % MR suspension of CI/PGMA particles (with lower molecular weight) at different magnetic fields. Variation of G´ (■, ●, ▲ filled symbols) and G´´ (□,○, Δ open symbols) at different magnetic flux densities (0 mT, 67 mT, 363 mT)

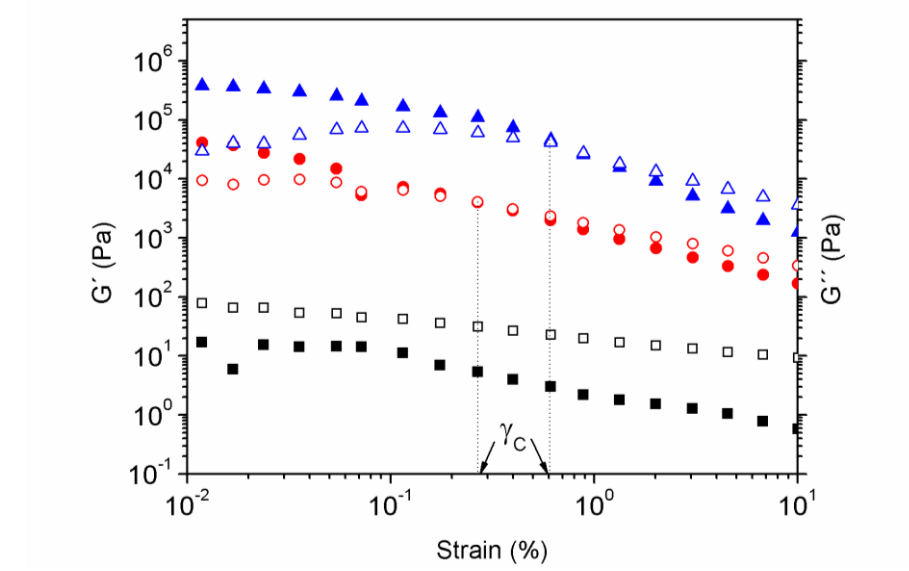

Figure 57. Amplitude sweep results for 60wt % MR suspension of CI/PGMA particles (with higher molecular weight) at different magnetic fields. Variation of G´ (■, ●, ▲ filled symbols) and G´´ (□,○, Δ open symbols) at different magnetic flux densities (0 mT, 67 mT, 363 mT)

MR suspensions in the off-state regime exhibit G'' larger than G' within whole strain range. This is due to fact, that MR suspensions show a liquid-like behavior. After the application of magnetic field, the chain-like structures were created and the MR suspension exhibited solid-like behavior, yield stress appeared and the storage modulus G' became higher than the loss modulus G''. The value of strain where loss modulus and elastic modulus are equal is called critical strain γ_C. This physical parameter describes the state of the structure, because it represents the transition between the viscoelastic-solid at low strain and the viscoelastic-liquid at high strain. Moreover, this parameter is responsible for competition between magnetic forces and hydrodynamic forces [80]. For these concrete examples it was observed that higher magnetic flux density leads to higher value of critical strain, which stems from the dependences illustrated on the Figures 55 – 57. However, it is meaningful thus field at higher magnetic flux density is able to retain solid structure to higher strains.

Determined amplitude strains of LVR positions were maintained within the whole range of frequencies (0.1 Hz – 10 Hz) and the viscoelastic moduli were obtained (Figures 58 – 63) for all prepared MR suspensions.

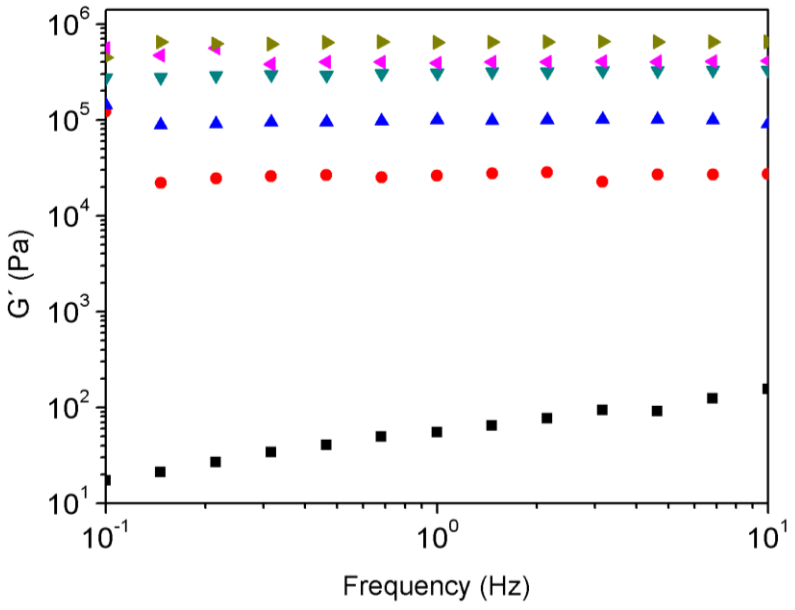

Figure 58. Frequency sweep results for 60wt % MR suspension of bare CI particles at different magnetic fields. Variation of G´ at different magnetic flux densities (0 mT ■, 67 mT ●, 144 mT ▲, 218 mT ▼, 292 mT ◀, 363 mT ▶)

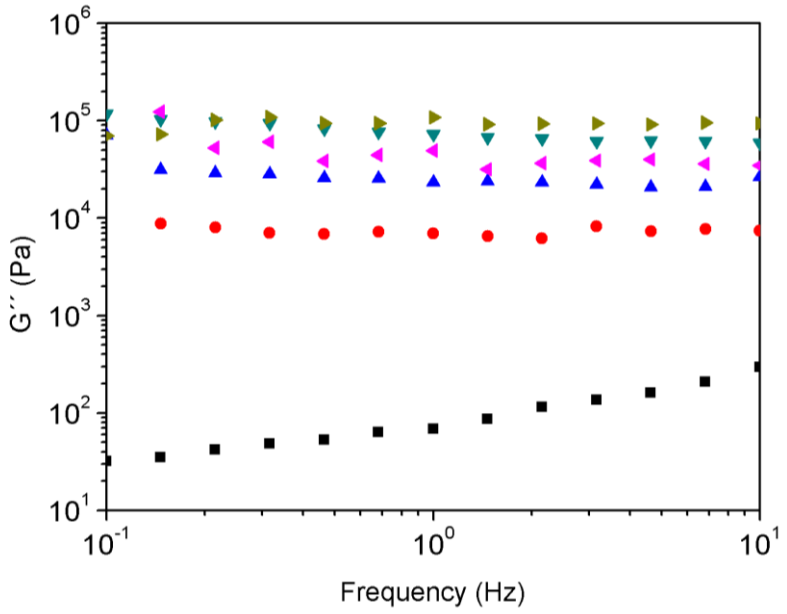

Figure 59. Frequency sweep results for 60wt % MR suspension of bare CI particles at different magnetic fields. Variation of G´´ at different magnetic flux densities (0 mT ■, 67 mT ●, 144 mT ▲, 218 mT ▼, 292 mT ◀, 363 mT ▶)

Figures 58, 59 show *G´* and *G´´* as a function of strain frequency for MR suspension containing 60 wt% of bare CI particles. The storage shear modulus exhibits slow but gradual increase over a wide range of frequencies when MR is off-state. When on-state, the *G´* and *G´´* were almost independent on the excitation frequencies. The magnetic flux density caused the increases of *G´* as well as *G´´* for all prepared suspensions (Figure 58 – 63). If we compare suspension off-state to on-state at 363 mT, the storage modulus will increase almost by a factor of 10^6, whereas the loss modulus will increase almost by a factor of 10^5. This phenomenon is similar for all prepared suspensions as shown on following figures.

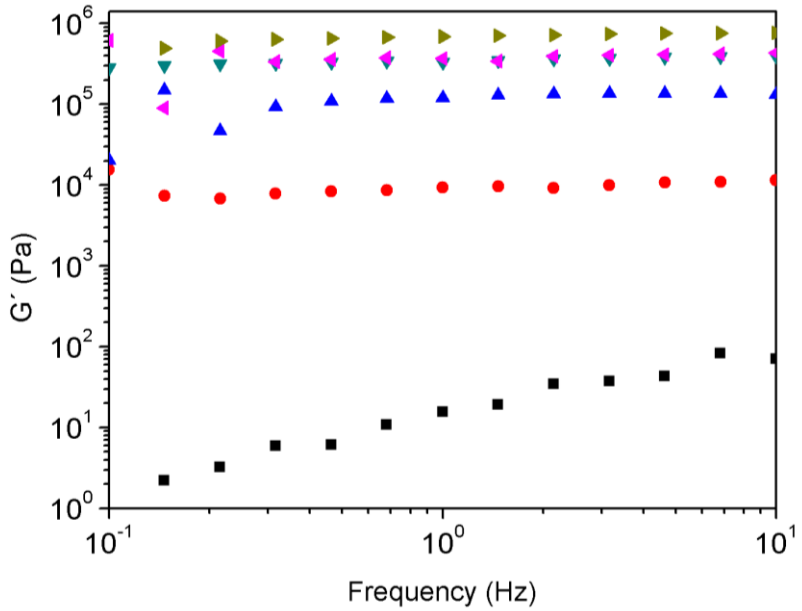

Figure 60. Frequency sweep results for 60wt % MR suspension of CI/PGMA particles (with lower molecular weight) at different magnetic fields. Variation of G´ at different magnetic flux densities (0 mT ■, 67 mT ●, 144 mT ▲, 218 mT ▼, 292 mT ◀, 363 mT ▶)

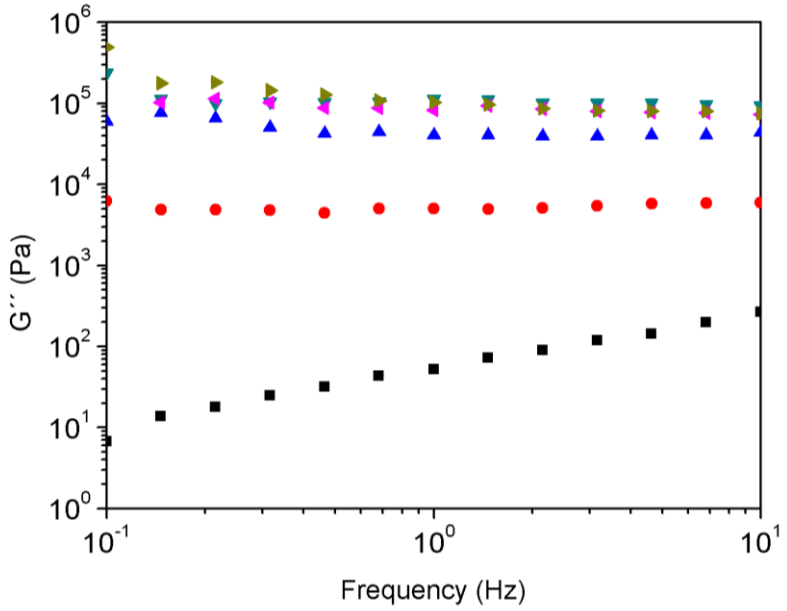

Figure 61. Frequency sweep results for 60wt % MR suspension of CI/PGMA particles (with lower molecular weight) at different magnetic fields. Variation of G´´ at different magnetic flux densities (0 mT ■, 67 mT ●, 144 mT ▲, 218 mT ▼, 292 mT ◀, 363 mT ▶)

Notice, that some values of viscoelastic moduli especially in low frequencies are out of chart or do not fit well to measured trend of results. There are many possible reasons for this negative phenomenon. First, rheological measurements in very low frequencies are out of the range of utilized measuring device. But rather there is a general problem in rheometry of suspensions [81].

Possible reason may be the non-homogeneity of measured sample also sedimentation of the particles can be a problem. Therefore, the suspensions were well stirred before each measurement and the measurements were performed as soon as the sample was placed into the geometry. In rotational rheometers may also occur the centrifugation of the particles in the direction of centrifugal velocity vector. However, in on-state measurements of MR suspensions this problem should not occur due to arrangement of particles to column-like structures.

Also repulsion interactions between wall of measuring geometry and the particles resulting in the formation of the interlayer of pure liquid, so that the dispersed particles do not contribute to transfer of shear stress and the measurement result is distorted [81]. This difficulty, known as the slip on the wall can be removed by changing the material of the measuring element and its demagnetization or modifying the surface treatment (degreasing, roughening). Therefore, the measuring geometry was before each measurement thoroughly purified.

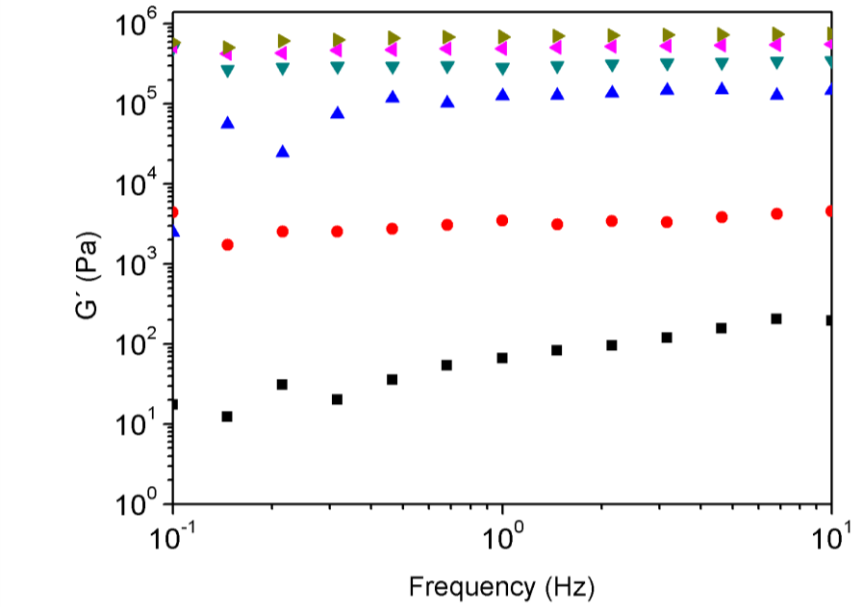

Figure 62. Frequency sweep results for 60wt % MR suspension of CI/PGMA particles (with higher molecular weight) at different magnetic fields. Variation of G´ at different magnetic flux densities (0 mT ■, 67 mT ●, 144 mT ▲, 218 mT ▼, 292 mT ◀, 363 mT ▶)

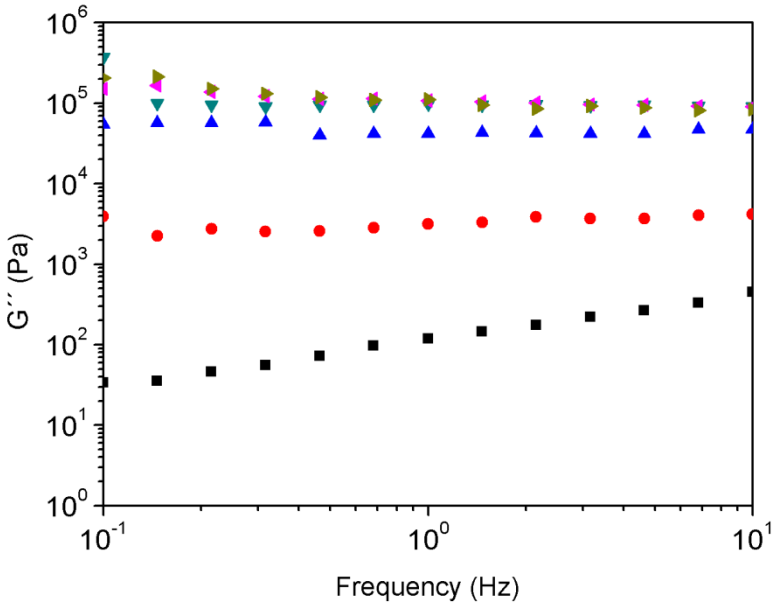

Figure 63. Frequency sweep results for 60wt % MR suspension of CI/PGMA particles (with higher molecular weight) at different magnetic fields. Variation of G´´ at different magnetic flux densities (0 mT ■, 67 mT ●, 144 mT ▲, 218 mT ▼, 292 mT ◀, 363 mT ▶)

In the presence of magnetic fields, the loss modulus is lower than the storage modulus. And the explanation of this fact was found in literature [47]. A nonzero G'' value represents the existence of free chains with one or two ends not connected to the surface of the geometry.

The values of viscoelastic moduli for MR suspensions containing 60 wt% of PGMA-coated particles were slightly lower compared to viscoelastic moduli of MR suspension containing 60 wt% of bare CI particles. However, the decreases were very little, nearly negligible. This outcome fully corresponds with the results of magnetic measurement. The controllably grafted PGMA layer almost did not affect the saturation magnetization therefore suspension containing such particles is able to interact to external magnetic field comparably to suspension of bare CI particles. Thus the coated layer on the surface of the particles almost did not affect the values of viscoelastic moduli of prepared MR suspensions.

11.11 Sedimentation stability – results

The sedimentation stability was examined for all three prepared MR suspensions. Graphical representation of the weight gain, which represented the settling particles, as a function of observation time is shown in the Figure 64. On the basis of the graphical results we can confidently claim that the use of core-shell CI/PGMA particles as a dispersed phase enhances the sedimentation stability of MR suspensions compared to suspensions of the same amount of bare CI particles. Improved sedimentation stability of suspensions containing CI/PGMA particles is due to reduced density of the particles, and due to presence of PGMA polymer chains which provide better interactions to the silicone oil. Therefore, increased friction between particles and carrier fluid, results in better resistance to gravitational settling of the particles.

The suspensions based on particles coated with higher molecular weight PGMA exhibit slightly better sedimentation stability compared to suspensions based on lower molecular weight PGMA particles, probably due to presence of more entangled polymer chains which provide better interactions and reduced density.

However, the difference in sedimentation stability between both coated variants is minor, probably due to fact that polymer chains are not fully radially oriented, therefore the length of polymer chains does not play that important role as was expected, so their surface activity to silicone oil is nearly similar and contribution to sedimentation improvement is probably due to reduced density.

Sedimentation stability of the suspensions was considerably improved with the use of CI/PGMA particles and the results indicate that prepared particles moved suspension one step closer to possible applications.

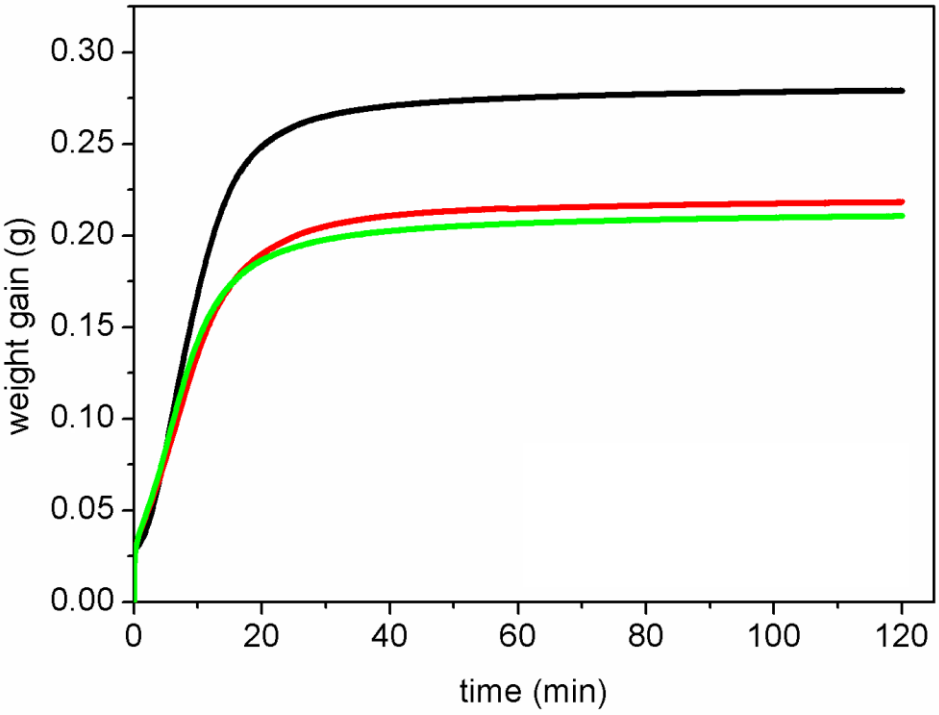

Figure 64. The time dependence of the weight gain of settled particles for 10 wt% MR suspensions of bare CI particles (–), CI/PGMA particles (with lower molecular weight) (–) and CI/PGMA particles (with higher molecular weight) (–) in the silicone oil

CONCLUSION

The aim of this thesis was to prepare new type of core-shell particles with enhanced properties for their effective utilization in magnetorheology. Considerable part of this thesis deals with preparation and characterization of the particles as well as the MR suspensions.

The core of the particles was commercially available CI (SL grade) which surface was covalently modified with PGMA *via* ATRP method. Modification of CI consisted from intermediate steps; functionalization of CI particles with APTES, amidation reaction with BIBB and specific ATRP polymerization. Within this study two types of CI/PGMA composite particles differing in polymer chains lengths were prepared.

Final molecular weights of grafted PGMA polymer chains and PDI´s were examined by NMR and GPC techniques. The size and morphology of bare CI particles as well as both variants of coated particles were observed with the help of SEM. Elemental analysis of polymer coatings was elucidated with EDS, which proved the presence of expected elements in the polymer chains. Success of coating process was also confirmed with FT-IR spectroscopy. Magnetic properties of CI particles and CI/PGMA structures were obtained from VSM measurement. Very slight decrease in saturation magnetizations was detected due to non-magnetic coating, namely 3.9% decrease for CI particles with grafted lower molecular weight PGMA and 5.3% decrease for CI particles with grafted higher molecular weight PGMA. Prepared particles also exhibited considerably enhanced chemical stability in acid environment. Moreover, controlled PGMA-coating greatly improved thermo-oxidative stability which was evaluated with the help of TGA.

Rheological behavior of MR suspensions containing 60 wt% of bare CI particles as well as both coated analogues was observed by a rotational rheometer at different magnetic flux densities. Experimental data in steady shear flow were fit with two constitutive rheological models. For MR suspensions Robertson-Stiff model better fits the experimental data than Bingham model. PGMA coating synthesized *via* ATRP slightly decreased the yield stress what is in accordance with results of saturation magnetization obtained from VSM. However, due to polymer coating the off-state viscosity even decreased at low shear rates. The small-strain oscillatory tests were carried out through strain sweeps and frequency sweeps. The results have shown that PGMA layer coated *via* ATRP has negligible effect on viscoelastic behavior, while the sedimentation stability of prepared MR suspensions was considerably enhanced.

BIBLIOGRAPHY

[1] J. DE VICENTE, D.J. KLINGENBERG and R. HIDALGO-ALVAREZ. Magnetorheological fluids: a review. *Soft Matter*. 2013, vol. 7, issue 8, s. 3701-. DOI: 10.1039/C0SM01221A.

[2] G. BOSSIS, S. LACIS, A. MEUNIER and O. VOLKOVA. Magnetorheological Fluids. 2002, vol .252, no. 1-3 s. 224-228. *Journal of magnetism and magnetic materials*. ISSN 0304-8853.

[3] S. GORODKIN, R. JAMES and W. KORDONSKI. Irreversible Effects in Magnetorheological Fluids. *Journal of Intelligent Material Systems and Structures*. 2011-11-29, vol. 22, issue 15, s. 1749-1754. DOI: 10.1177/1045389X11426180.

[4] X. QUAN, W. CHUAH, Y. SEO, H.J. CHOI. Core-Shell Structured Polystyrene Coated Carbonyl Iron Microspheres and Their Magnetorheology. 2014, vol. 50, no. 1 s. 1-4. ISSN: 0018-9464.

[5] M. SEDLACIK, V. PAVLINEK, P. SAHA, P. SVRCINOVA, P. FILIP and M. ZATLOUKAL. Core-shell Structured Polypyrrole-coated Magnetic Carbonyl Iron Microparticles and their Magnetorheology. s. 284-291. DOI: 10.1063/1.3604489.

[6] M. MACHOVSKY, M. MRLIK, V. PAVLINEK and V. BABAYAN. Novel synthesis of core–shell urchin-like ZnO coated carbonyl iron microparticles and their magnetorheological activity. *RSC Advances*. 2013, vol. 4, issue 2, s. 996. DOI: 10.1039/c3ra44982c.

[7] M. SEDLACIK, V. PAVLINEK, P. SAHA, P. SVRCINOVA and J. STEJSKAL. Rheological properties of magnetorheological suspensions based on core–shell structured polyaniline-coated carbonyl iron particles. *Smart Materials and Structures*. 2010-11-01, vol. 19, issue 11, s. 115008-. DOI: 10.1088/0964-1726/19/11/115008.

[8] S.Y. KIM, S.H. KWON, Y.D. LIU, J.S. LEE and Ch.Y. YOU. Core–shell-structured cross-linked poly(glycidyl methacrylate)-coated carbonyl iron microspheres and their magnetorheology. *Journal of Materials Science*. 2014, vol. 49, issue 3, s. 1345-1352. DOI: 10.1007/s10853-013-7818-3.

[9] J.S. CHOI, B.J. PARK, M.S. CHO and H.J. CHOI. Preparation and magnetorheological characteristics of polymer coated carbonyl iron suspensions. *Journal of Magnetism and Magnetic Materials*. 2006, vol. 304, issue 1, e374-e376. DOI: 10.1016/j.jmmm.2006.02.055.

[10] K. MATYJASZEWSKI. Atom Transfer Radical Polymerization (ATRP): Current Status and Future Perspectives. *Macromolecules*. 2012-05-22, vol. 45, issue 10, s. DOI: 10.1021/ma3001719.

[11] D.A. NIXON *et al.* LORD CORPORATION, Cary, N.C. Magnetorheological Materials Utilizing Surface-Modified Particles [patent]. United States. US005578238A, 5 ,578,238. Granted 1996-11-26.

[12] B.J. PARK, F.F. FANG and H.J. CHOI. Magnetorheology: materials and application. *Soft Matter*. 2010, vol. 6, issue 21, s. 5246-. DOI: 10.1039/c0sm00014k.

[13] M. SEDLACIK, V. PAVLINEK, R. VYROUBAL, P. PEER and P. FILIP. A dimorphic magnetorheological fluid with improved oxidation and chemical stability under oscillatory shear. *Smart Materials and Structures*. 2013-03-01, vol. 22, issue 3, s. 063520-. DOI: 10.1088/0964-1726/22/3/035011.

[14] J. RABINOW. NATIONAL BUREAU OF STANDARDS. *Magnetic fluid torque and force transmitting device* [patent]. United States. 192/21.5, US 2575360 A. Granted, 1951-11-20.

[15] R. ROSENFELD, VYSOKÁ ŠKOLA BÁŇSKÁ V OSTRAVĚ. Velikost částic práškového železa, vyrobeného z pentakarbonylu železa. J. Kubelík. Ostrava, 1968. XIV, 5. Sborník vědeckých prací. článek 480.

[16] M. SEDLACIK. Intelligent fluids - electro-rheological (ER) and magneto-rheological suspensions: Inteligentní tekutiny - elektroreologické (ER) a magnetoreologické (MR) suspenze: doctoral thesis summary. Zlín: Tomas Bata University, 2012. ISBN 978-80-7454-197-1.

[17] H. SHAOPAN, H. XIANDENG and Z. CHENGBIN. Carbonyl iron preparation method based on photochemical reaction [patent]. Germany. C01G49/16, CN20101120476. Granted 2010-07-21.

[18] V. NOVACEK. Technologie výroby magnetoreologických kapalin. Brno, 2009. Bachelor thesis. Brno University of Technology. Vedoucí práce Jakub Roupec.

[19] M.T. LOPEZ-LOPEZ, P. KUZHIR, S. LACIS, G. BOSSIS, F. GONZALEZ-CABALLERO and J.D. DURAN. Magnetorheology for suspensions of solid particles dispersed in ferrofluids. *Journal of Physics: Condensed Matter*. 2006-09-27, vol. 18, issue 38, S2803,S2813. DOI: 10.1088/09538984/18/38/S18.

[20] M.T. LOPEZ-LOPEZ, P. KUZHIR, A. MEUNIER and G. BOSSIS. Synthesis and magnetorheology of suspensions of submicron-sized cobalt particles with tunable particle size. *Journal of Physics: Condensed Matter*. 2010-08-18, vol. 22, issue 32, s. 324106-. DOI: 10.1088/0953-8984/22/32/324106.

[21] M.T. LOPEZ-LOPEZ, P. KUZHIR and G. BOSSIS. Magnetorheology of fiber suspensions. I. Experimental. *Journal of Rheology*. 2009, vol. 53, issue 1. DOI: 10.1122/1.3005402.

[22] S.P. RWEI, L.Y. WANG and P.W. YANG. Synthesis and Magnetorheology Study of Iron Oxide and Iron Cobalt Oxide Suspensions. *Journal of Nanomaterials*. 2013, vol. 2013, s. 1-7. DOI: 10.1155/2013/612894.

[23] M. SEDLACIK , V. PAVLINEK, P. PEER and P. FILIP. Tailoring the magnetic properties and magnetorheological behavior of spinel nanocrystalline cobalt ferrite by varying annealing temperature. *Dalton Transactions*. 2014, vol. 43, issue 18, s. 6919-. DOI: 10.1039/c4dt00166d.

[24] F.F. FANG, J.H. KIM and H.J. CHOI. Synthesis of core–shell structured PS/Fe_3O_4 microbeads and their magnetorheology. *Polymer*. 2009, vol. 50, issue 10, s. 2290-2293. DOI: 10.1016/j.polymer.2009.03.023.

[25] M. MRLIK, V. PAVLINEK, P. SAHA, P. SVRCINOVA, P. FILIP and M. ZATLOUKAL. Core-shell Structured Polypyrrole-coated Magnetic Carbonyl Iron Microparticles and their Magnetorheology. *Journal of Physics: Conference Series*. 2013-02-15, vol. 412, s. 284-291. DOI: 10.1088/1742-6596/412/1/012016.

[26] J.C. ULICNY and A.M. MANCE. Materials science and engineering: Evaluation of Electroless Nickel Surface Treatment for Iron Powder Used in MR Fluids. Lausanne: Elsevier Sequoia, 2004. ISSN: 0921-5093.

[27] P.P. PHULE and J.M. GINDER. Synthesis and Properties of Novel Magnetorheological Fluids Having Improved Stability and Redispersibility. *International Journal of Modern Physics*. 1999-06-30, vol. 13, 14n16, s. 2019-2027. DOI: 10.1142/S0217979299002095.

[28] A.G. OLABI, and A. GRUNWALD. Design and Application of Magneto-Rheological Fluid "MRF". Dublin, Ireland, 2006. 19 s. Journal paper. Dublin City University. School of Mechanical and Manufacturing Engineering.

[29] D. BICA, L. VEKAS, M. AVDEEV, V. MARINICA, V. SOCOLIUC, M. BALASOIU and V.M. GARAMUS. Sterically stabilized water based magnetic fluids: Synthesis, structure and properties. *Journal of Magnetism and Magnetic Materials*. 2007, vol. 311, issue 1, s. 17-21. DOI: 10.1016/j.jmmm.2006.11.158.

[30] J.H. PARK, B.D. CHIN and O. PARK. Rheological Properties and Stabilization of Magnetorheological Fluids in a Water-in-Oil Emulsion. *Journal of Colloid and Interface Science*. 2001, vol. 240, issue 1, s. 349-354. DOI: 10.1006/jcis.2001.7622.

[31] M.T. AVRAAM. MR-fluid brake design and its application to a portable muscular rehabilitation device. Bruxelles: Universit´e Libre de Bruxelles, November 2009. 152 s. Doctor thesis. Facultedes Sciences Appliquées. Department of Mechanical Engineering and Robotics.

[32] A. GOMEZ-RAMIREZ, M.T. LOPEZ-LOPEZ, F. GONZALEZ-CABALLERO and J.D. DURAN. Wall slip phenomena in concentrated ionic liquid-based magnetorheological fluids. *Rheologica Acta*. 2012, vol. 51, issue 9, s. 793-803. DOI: 10.1007/s00397-012-0639-5.

[33] TUNGHAI UNIVERSITY. Magnetic Properties [online]. Department of applied physics, 2009 [cit. 2014-04-08].

[34] J. BROZ. Moderní problémy feromagnetismu. 1. vyd. Praha: ČSAV, 1962. 189 s.

[35] Z. JANACEK and P. PONIZIL. Úvod do fyziky pevných látek. Vyd. 1. Brno: PC-DIR, 1995. Učební texty vysokých škol. ISBN 80-214-0700-X.

[36] V.S. RAMACHANDRAN. Handbook of analytical techniques in concrete science and technology: principles, techniques and applications. 2001, xiii, 964 s. ISBN 08-155-1437-9; Electronic ISBN: 978-0-8155-1738-2.

[37] K. SIMON. The Role of Different Rheological Models in Accuracy of Pressure Loss Prediction. 2004. vol. 16 s. 87-91. ISSN:0353-4529.

[38] A.Y. MALKIN. RUSSIAN ACADEMY OF SCIENCES. Rheology. Fundamentals. Moscow, Russia: *ChemTec Publishing*, 1994, 315 s. ISBN 1-895198-09-7

[39] V.C. KELESSIDIS and R. MAGLIONE. Modeling rheological behavior of bentonite suspensions as Casson and Robertson–Stiff fluids using Newtonian and true shear rates in Couette viscometry. *Powder Technology*. 2006, vol. 168, issue 3, s. 134-147. DOI: 10.1016/j.powtec.2006.07.011.

[40] M.J. YUN and W. ZHENG. Fractal Analysis of Robertson-Stiff Fluid Flow in Porous Media. *Chinese Physics Letters*. 2012-06-01, vol. 29, issue 6, s. 064706-. DOI: 10.1088/0256-307X/29/6/064706.

[41] P. FILIP, J. DAVID and R. PIVONKOVSKY. INSTITUTE OF HYDRODYNAMICS. *Applied Rheology: a Comprehensive Journal for the Study and Characterization of the Flow of Complex and Technologically Important Materials,*. Zürich: Kerschensteiner Verlag, 2013. ISSN 1430-6395; ISBN: 978-1-61804-026-8. Vol. 23, Issue 4, s. 220-227.

[42] M.H. LAUN, C. KORMANN and N. WILLENBACHER. Rheometry on magnetorhological (MR) fluids: Steady shear flow in stationary magnetic fields. Germany: *Rheol Acta*, 1996.

[43] E. MITSOULIS. NATIONAL TECHNICAL UNIVERSITY OF ATHENS. Flows of Viscoplastic Materials: Models and Computations. Greece*: Rheology Reviews*, 2007, s. 135-178. ISBN 0-9547414-6-3.

[44] M.T. BALHOFF, L.W. LAKE, P.M. BOMMER, R.E. LEWIS, M.J. WEBER and J.M. CALDERIN. Rheological and yield stress measurements of non-Newtonian fluids using a Marsch Funnel. *Journal of Petroleum Science and Engineering.* University of Texas at Austin: 1 University Station, 2011. ISSN 0920-4105.

[45] P. GRAD. IET engineering: Smart fluids that can change their viscosity in real time are enabling a new generation of actuators. Australia: Institution of Engineering and Technology, Dec. 2006, Volume:1, Issue: 9. ISSN 1750-9637. 34 - 37.

[46] B. MEISSNER and V. ZILVAR. Fyzika polymerů: Struktura a vlastnosti polymerních materiálů. Praha: STNL - Nakladatelství technické literatury Alfa, 1987, 308 s. ISBN 04-634-87.

[47] J. RAMOS, J. DE VICENTE and R. HIDALGO-ALVAREZ. Small-Amplitude Oscillatory Shear Magnetorheology of Inverse Ferrofluids. *Langmuir*. 2010-06-15, vol. 26, issue 12, s. 9334-9341. DOI: 10.1021/la100252g.

[48] J. DE VICENTE, F. VEREDA, J.P. SEGOVIA-GUTIÉRREZ, M. DEL PUERTO MORALES and R. HIDALGO-ÁLVAREZ. Effect of particle shape in magnetorheology. The Society of Rheology, Inc. Spain: Universidad de Granada, 2010, s. 27. DOI: 10.1122/1.3479045.

[49] M. MRLIK, M. ILCIKOVA, V. PAVLINEK, J. MOSNACEK, P. PEER and P. FILIP. Improved thermooxidation and sedimentation stability of covalently-coated carbonyl iron particles with cholesteryl groups and their influence on magnetorheology. *Journal of Colloid and Interface Science*. 2013, vol. 396, s. 146-151. DOI: 10.1016/j.jcis.2013.01.027.

[50] J. DE VICENTE, J.P. SEGOVIA-GUTIERREZ, E. ANDABLO-REYES, F. VEREDA, R. HIDALGO-ALVAREZ and N.M. WERELEY. Dynamic rheology of sphere- and rod-based magnetorheological fluids. *The Journal of Chemical Physics*. 2009, vol. 131, issue 19, s. 194902-. DOI: 10.1063/1.3259358.

[51] R.C. BELL, J.O. KARLI, A.N. VAVRECK, D.T. ZIMMERMAN, G.T. NGATU and N.M. WERELEY. Magnetorheology of submicron diameter iron microwires dispersed in silicone oil. *Smart Materials and Structures*. 2008-02-01, vol. 17, issue 1, s. 015028-. DOI: 10.1088/0964-1726/17/01/015028.

[52] J. VEREDA, J. DE VICENTE, J.P. SEGOVIA-GUTIERREZ and R. HIDALGO-ALVAREZ. On the effect of particle porosity and roughness in magnetorheology. *Journal of Applied Physics*. 2011, vol. 110, issue 6, s. 063520-. DOI: 10.1063/1.3633233.

[53] B. HU, A. FUCHS, S. HUSEYIN, F. GORDANINEJAD and C. EVRENSEL. *Polymer*. 2006, vol. 47, issue 22, s. 7653-7663. DOI: 10.1016/j.polymer.2006.08.069.

[54] H. JANOCHA. Adaptronics and smart structures: basics, materials, design, and applications. New York: Springer, c1999, xi, 438 p. ISBN 3-540-61484-2.

[55] M. OCALAN, and G.H. MCKINLEY. High-flux magnetorheology at elevated temperatures. *Rheologica Acta*. 2013, vol. 52, issue 7, s. 623-641. DOI: 10.1007/s00397-013-0708-4.

[56] Ch.H. HONG, Y.D. LIU and H.J. CHOI. Carbonyl iron suspension with halloysite additive and its magnetorheology. *Applied Clay Science*. 2013, 80-81, issue 1, s. 366-371. DOI: 10.1016/j.clay.2013.06.033.

[57] D.J. KLINGENBERG and J.C. ULICNY. Enhancing magnetorheology. *International Journal of Modern Physics B*. 2011-03-20, vol. 25, issue 07. DOI: 10.1142/S021797921105847X.

[58] J.C. ULICNY, M.P. BALOGH, N.M. POTTER and R.A. WALDO. Magnetorheological fluid durability test—Iron analysis. *Materials Science and Engineering: A*. 2007, vol. 443, 1-2, s. 16-24. DOI: 10.1016/j.msea.2006.06.050.

[59] K. KARAKOC, J.E. PARK and A. SULEMAN. Design Considerations for an Automotive Magnetorheological Brake. 2008, vol. 18, no. 8 s. 434-447. ISSN:0957-4158

[60] D.M. WANG, Y.F. HOU and Z. TIAN. A Novel High-torque Magnetorheological Brake with a Water Cooling Method for Heat Dissipation. 2013, vol. 22, no. 2. ISSN:0964-1726

[61] M. YU, X.M. DONG, S.B. CHOI and C.R. LIAO. Human Simulated Intelligent Control of Vehicle Suspension Systém with MR dampers. 2009, vol. 319, no. 3 s. 753-767. ISSN:0022-460X.

[62] S.K. MANGAL and G.H. KUMAR. Experimental and Numerical Studies of Magnetorheological (MR) Damper. *Chinese Journal of Engineering*. 2014, vol. 2014, issue 7. DOI: 10.1155/2014/915694.

[63] Q.P. HA, M.T. NGUYEN, J. LI and N.M. KWOK. Smart Structures With Current-Driven MR Dampers: Modeling and Second-Order Sliding Mode Control. *IEEE/ASME Transactions on Mechatronics*. 2013, vol. 18, issue 6, s. 1702-1712. DOI: 10.1109/TMECH.2013.2280282.

[64] Z.Q. CHEN, X.Y. WANG, J.M. KO, Y.Q. NI, B.F. SPENCER, G. YANG and S.Ch. LIU. MR damping system on Donting Lake cable-stayed brigde. s. 229-235. DOI: 10.1117/12.498072.

[65] B.M. KAVLICOGLU, F. GORDANINEJAD and X. WANG. Study of a magnetorheological grease clutch. *Smart Materials and Structures*. 2013-12-01, vol. 22, issue 12, s. 125030-. DOI: 10.1088/0964-1726/22/12/125030.

[66] E. KOSTAMO, M. FOCCHI, E. GUGLIELMINO, J. KOSTAMO, C. SEMINI, J. BUCHLI, M. PIETOLA and D. CALDWELL. Magnetorheologically Damped Compliant Foot for Legged Robotic Application: Modeling and Second-Order

Sliding Mode Control.*Journal of Mechanical Design*. 2014-02-01, vol. 136, issue 2, s. 021003-. DOI: 10.1115/1.4025966.

[67] E. ASADI, A. HOYLE and S. ARZANPOUR. Design of a Magnetorheological Damper-Based Haptic Interface for Rehabilitation Applications. *Journal of Intelligent Material Systems and Structures*. 2011-10-04, vol. 22, issue 11, s. 1269-1277. DOI: 10.1177/1045389X11418863.

[68] 2005 IEEE International Conference on Robotics and Biomimetics: Shatin, N.T. China, 5-9 July 2005. IEEE, c2006. ISBN 0780393155.

[69] A. SILVA, E. SILVA, A. CARRICO and E.T. EGITO. A Promising Device for Targeting Drugs Into the Human Body. *Current Pharmaceutical Design*. 2007-04-01, vol. 13, issue 11, s. 1179-1185. DOI: 10.2174/138161207780618993.

[70] J. SUTRISNO, A. FUCHS, H. SAHIN, F. GORDANINEJAD. Surface Coated Iron Particles Via Atom Transfer Radical Polymerization for the Thermal-oxidatively Stable High Viscosity Magnetorheological Fluid. 2012, vol. 128, no. 1 s. 470-480. ISSN:0021-8995.

[71] P.F. CANAMERO, J.L. DE LA FUENTE, E.L. MADRUGA and M. FERNANDEZ-GARCIA. Atom Transfer Radical Polymerization of Glycidyl Methacrylate: A Functional Monomer. *Macromolecular Chemistry and Physics*. 2004-11-03, vol. 205, issue 16, s. 2221-2228. DOI: 10.1002/macp.200400186.

[72] T. WILLIAMS. Gel permeation chromatography: A review. *Journal of Materials Science*. 1970, vol. 5, issue 9. DOI: 10.1007/BF00562169.

[73] R.D. WILLIS and T.L. CONNER. *Guidelines for the application of sem/edx analytical techniques for fine and coarse pm samples*. U.S. Environmental Protection Agency, Washington, DC, EPA/600/R-02/070 (NTIS PB2004-100988), 2003.

[74] B. VAN EERDENBRUGH and L.S. TAYLOR. Application of mid-IR spectroscopy for the characterization of pharmaceutical systems.*International Journal of Pharmaceutics*. 2011, vol. 417, 1-2, s. 3-16. DOI: 10.1016/j.ijpharm.2010.12.011.

[75] UNIVERZITA PALACKÉHO V OLOMOUCI. Fyzikální princip měření magnetického pole & SQUID & MPMS XL magnetometer [online]. 2009.

[76] K. CHEN, Y. TIAN, L. SHAN and X. ZHANG. The rheological properties of magnetic field excited magnetic powders sheared between two parallel plates. *Smart Materials and Structures*. 2013-11-01, vol. 22, issue 11, s. 115036-. DOI: 10.1088/0964-1726/22/11/115036.

[77] W.C. WANG, Q. ZHANG, B.B. ZHANG, D.N. LI, X.Q. DONG, L. ZHANG and J. CHANG. Preparation of monodisperse, superparamagnetic, luminescent, and multifunctional PGMA microspheres with amino-groups. *Chinese Science Bulletin*. 2008, Vol. 53, Issue 8, s. 1165-1170. DOI: 10.1007/s11434-007-0512-6.

[78] M.A. ABSHINOVA, N.E. KAZANTSEVA, P. SAHA, I. SAPURINA, J. KOVAROVA and J. STEJSKAL. The enhancement of the oxidation resistance of carbonyl iron by polyaniline coating and consequent changes in electromagnetic properties. *Polymer Degradation and Stability*. 2008, vol. 93, issue 10, s. 1826-1831. DOI: 10.1016/j.polymdegradstab.2008.07.008.

[79] J.M. GINDER and L.C. DAVIS. Shear stresses in magnetorheological fluids: Role of magnetic saturation. *Applied Physics Letters*. 1994, vol. 65, issue 26, s. 3410-. DOI: 10.1063/1.112408.

[80] J. CLARACQ, J. SARRAZIN and J.P. MONTFORT. Viscoelastic properties of magnetorheological fluids. *Rheologica Acta*. 2004-2-1, vol. 43, issue 1, s. 38-49. DOI: 10.1007/s00397-003-0318-7.

[81] P. COUSSOT. Rheometry of pastes, suspensions, and granular materials: applications in industry and environment. Hoboken, N.J.: *Wiley*, 2005. ISBN 0471653691.

LIST OF ABBREVIATIONS

MR	Magnetorheological.
CI	Carbonyl Iron.
PGMA	Poly(glycidyl methacrylate).
ATRP	Atom Transfer Radical Polymerization.
CI/PGMA	Poly(glycidyl methacrylate)-coated carbonyl iron particles.
PDI	Polydispersity index.
US	United States.
vol%	Volume percent.
μm	Micrometer.
M_S	Saturation magnetization.
CVD	Chemical Vapor Deposition.
°C	Celsius unit.
$Fe(CO)_5$	Pentacarbonyl iron.
Fe	Iron *(Ferrum)*.
CO	Carbon monoxide.
Fe_3O_4	Iron(II,III) oxide, (magnetite).
Fe^{2+}, Fe^{3+}	Ferrous and ferric ionts.
FF	Ferrofluids.
$CoFe_2O_3$	Cobalt ferrite.
PS	Polystyrene.
CI/PS	Polystyrene-coated carbonyl iron particles.
emu	The designation “emu” is not a unit.
g	Gram.
CI/PPy	Polypyrrole-coated carbonyl iron particles.

PANI	Polyaniline.
CI/PANI	Polyaniline-coated carbonyl iron particles.
Ni	Nickel *(Niccolum)*.
CI/Ni	Nickel-coated carbonyl iron particles.
PMMA	Poly(methyl methacrylate).
m	Magnetic moment.
I	Electric current.
H	Magnetic field strength.
SI	International System of Units *(Systéme International d´Unités)*.
B	Magnetic induction (magnetic flux density).
G	Gauss (unit).
Wb	Weber (unit).
Oe	Oersted (unit).
π	Ludolphine number.
m	Meter.
A	Ampere (unit).
M	Mass magnetization.
kg	Kilogram.
J	Joule (unit).
T	Thermodynamic temperature.
μ	Permeability.
H	Henry (unit).
μ_0	Permeability of free space.
μ_r	Relative magnetic permeability.
χ	Magnetic susceptibility.
K	Kelvin (unit).

T_C	Curie temperature.
B-H	Relation between magnetic flux density and magnetic field strength.
B_r	Remanence.
H_c	Coercitivity.
μ_i	Initial permeability.
τ	Shear stress.
η	Dynamic viscosity.
$\dot{\gamma}$	Shear rate.
Pa	Pascal (unit).
Φ	Volume fraction.
η_C	Viscosity of carrier fluid.
Φ_m	Maximum volume fraction.
$[\eta]$	Intrinsic viscosity.
τ_0	Yield stress.
μ_P	Plastic viscosity.
K	Consistency index.
n	Flow behavior index.
μ	Consistency factor.
C	Initial shear rate.
3P	Three-parameter.
2P	Two-parameter.
PP	Parallel-plate.
CP	Cone-plate.
ω	Angular frequency.
r	Radius of the geometry.

h	Height of the position between the plates.
$\Delta\tau(H)$	Shear stress increase.
$\eta_r\ (H)$	Relative viscosity.
$\tau(0)$	Shear stress measured for a given shear rate in off-state.
$\eta(0)$	Viscosity measured for a given shear rate in off-state.
$\tau(H)$	Shear stress measured for a given shear rate at imposed magnetic field strength.
$\eta(H)$	Viscosity measured for a given shear rate at imposed magnetic field strength.
const.	Constant.
LVE	Linear viscoleastic.
NLVE	Nonlinear viscoelastic.
VP	Viscoplastic.
N	Newtonian.
$G´$	Storage modulus.
$G´´$	Loss modulus.
i	Imaginary unit.
G^*	Complex shear modulus.
LVR	Linear Viscoelasticity Region.
δ	Loss angle (damping factor).
tan	Tangent.
nm	Nanometer.
wt%	Weight percent.
etc.	Et cetera (and other things).
i.e.	That's.
ms	Millisecond.

FEM	Finite Element Method.
p.a.	Analytical grade *(pro analysi)*.
GMA	Glycidyl methacrylate.
M	Molar concentration.
HCl	Hydrochloric acid.
mL	Milliliter.
rpm	Rotations per minute.
mbar	Millibar.
APTES	(3-Aminopropyl)triethoxysilane.
$–NH_2$	Amino group.
BIBB	α-Bromoisobutyryl bromide (2-Bromo-2-methylpropionyl bromide).
–Br	Bromide group.
–NH–CO–	Amide linkage.
HBr	Hydrogen bromide.
THF	Tetrahydrofuran.
NaOH	Sodium hydroxide.
SF	Schlenk flask.
CI/APTES	Silane-treated CI particles.
CI/BIBB	Initiator-treated CI particles.
Et_3N	Triethyleneamine.
CuBr	Cuprous bromide.
PMDETA	*N,N,N ',N'',N''*-pentamethyldiethylenetriamine.
GPC	Gel Permeation Chromatography.
NMR	Nuclear Magnetic Resonance.
USA	United States of America.
$CDCl_3$	Deuterated chloroform.

SEC	Size Exclusion Chromatography.
ppm	Parts-per-million (10^{-6}).
SEM	Scanning Electron Microscopy.
kV	Kilovolt.
BSE	Backscattered electron.
SE	Secondary electron.
EDS	Energy-Dispersive Spectroscopy.
Na	Sodium *(Natrium)*.
U	Uranium *(Uranium)*.
FT-IR	Fourier transform infrared spectroscopy.
IR	Infrared.
ATR	Attenuated Total Reflection.
mid-IR	Mid-infrared.
VSM	Vibrating-Sample Magnetometer.
kOe	Kilooersted.
TGA	Thermogravimetric analysis.
mm	Millimeter.
mT	Millitesla.
Hz	Hertz (unit).
h	Hour.
mol	Mole.
$\bar{M}_n$	Number average molecular weight.
PSD	Particle Size Distribution.
C	Carbon *(Carboneum)*.
O	Oxygen *(Oxygenium)*.

N	Nitrogen *(Nitrogenium)*.
Br	Bromine *(Bromum)*.
–C=O	Carbonyl group.
C–O–C	Bond of methacrylate.
k	Boltzmann constant.
H_2O	Water.
$[Fe(H_2O)_6]Cl_2$	Hexaaquairon(II) chloride.
H_2	Hydrogen (molecule).
FeO	Iron(II) oxide.
Fe_2O_3	Iron(III) oxide.
B_C	Critical magnetic flux density.
γ_C	Critical strain.

LIST OF FIGURES

LIST OF TABLES